AD NUMBER
AD380951
CLASSIFICATION CHANGES
TO: **unclassified**
FROM: **confidential**
LIMITATION CHANGES
TO: **Approved for public release, distribution unlimited**
FROM: **Distribution authorized to U.S. Gov't. agencies and their contractors; Critical Technology; JAN 1967. Other requests shall be referred to Air Force Rocket Propulsion Laboratory, Attn: RPPR-STINFO, Edwards AFB, CA 93523.**
AUTHORITY
31 Jan 1979, per document marking, DoDD 5200.10; AFRPL ltr, 5 Feb 1986

SECURITY MARKING

The classified or limited status of this report applies to each page, unless otherwise marked.
Separate page printouts MUST be marked accordingly.

THIS DOCUMENT CONTAINS INFORMATION AFFECTING THE NATIONAL DEFENSE OF THE UNITED STATES WITHIN THE MEANING OF THE ESPIONAGE LAWS, TITLE 18, U.S.C., SECTIONS 793 AND 794. THE TRANSMISSION OR THE REVELATION OF ITS CONTENTS IN ANY MANNER TO AN UNAUTHORIZED PERSON IS PROHIBITED BY LAW.

NOTICE: When government or other drawings, specifications or other data are used for any purpose other than in connection with a definitely related government procurement operation, the U. S. Government thereby incurs no responsibility, nor any obligation whatsoever; and the fact that the Government may have formulated, furnished, or in any way supplied the said drawings, specifications, or other data is not to be regarded by implication or otherwise as in any manner licensing the holder or any other person or corporation, or conveying any rights or permission to manufacture, use or sell any patented invention that may in any way be related thereto.

CONFIDENTIAL

AFRPL-TR-67-89

(TITLE - UNCLASSIFIED)

EVALUATION OF AN ADVANCED NON-REGENERATIVELY COOLED ROCKET THRUST CHAMBER CONCEPT

R. J. TAYLOR

THE MARQUARDT CORPORATION

TECHNICAL REPORT AFRPL-TR-67-89

JANUARY 1967

AIR FORCE ROCKET PROPULSION LABORATORY
RESEARCH AND TECHNOLOGY DIVISION
AIR FORCE SYSTEMS COMMAND
EDWARDS AIR FORCE BASE, CALIFORNIA

CONFIDENTIAL

NOTICES

"When U. S. Government drawings, specifications, or other data are used for any purpose other than a definitely related Government procurement operation, the Government thereby incurs no responsibility nor any obligation whatsoever, and the fact that the Government may have formulated, furnished, or in any way supplied the said drawings, specifications, or other data, is not to be regarded by implication or otherwise, or in any manner licensing the holder or any other person or corporation, or conveying any rights or permission to manufacture, use, or sell any patented invention that may in any way be related thereto."

THE Marquardt CORPORATION VAN NUYS, CALIFORNIA

Copy No. [redacted]

(UNCLASSIFIED TITLE)

EVALUATION OF AN ADVANCED NON-REGENERATIVELY COOLED ROCKET THRUST CHAMBER CONCEPT

R. J. Taylor

THE Marquardt CORPORATION VAN NUYS, CALIFORNIA

FOREWORD

(This Foreword is Unclassified)

This report was prepared by The Marquardt Corporation under USAF Contract No. AF 04(611)-10917. This contract was initiated under Project 3058, Purchase Request Number 3058522. The work was administered under the direction of the Air Force Rocket Propulsion Laboratory, Research and Technology Division with Mr. Michael Powell/RPRR as the Air Force Project Engineer.

The work at The Marquardt Corporation was conducted in the ASTRO Division and was under the direction of Mr. B. A. Webb, Program Manager, and Mr. R. J. Taylor, Project Engineer.

This report, and the studies and investigations leading to its preparation resulted from the efforts of a large team of engineers and scientists associated with The Marquardt Corporation. It is impractical to list the names of all these persons, but the efforts of R. A. Bjorklund, J. F. Dolowy, Jr., P. E. Elkins, K. Marnoch, A. R. Nagy, and R. E. Pecsar should be noted with acknowledgment intended for all participants.

This report covers work conducted from 1 June 1965 to 31 October 1966. The Phase I efforts (subscale chamber evaluation) were previously reported in a summary report, AFRPL-TR-66-69 (Marquardt Report No. 25,189). This report covers primarily the Phase II efforts on fullscale chamber evaluation. For cross-reference identification, the Marquardt Corporation report number for this report is 25,211. This report was submitted by the author in January, 1967.

This report contains no classified information extracted from other classified documents except from the Phase I Summary Report.

This technical report has been reviewed and is approved.

Michael Powell
USAF Project Engineer

THE Marquardt CORPORATION VAN NUYS, CALIFORNIA

ABSTRACT

(This Abstract is Unclassified)

(U) Subscale (100 lb) and fullscale (5000 lb) rocket thrust chambers of an advanced nonregeneratively cooled concept were designed, fabricated, and tested for durability at 500 psi chamber pressure, using N_2O_4/0.5 N_2O_4-0.5 UDMH propellants. The concept employs a silicon carbide-coated graphite thrust-chamber liner prestressed in compression by a refractory metal outer shell. The subscale units were successfully tested for continuous and intermittent firing durations exceeding 600 seconds. In the subscale tests, the inner SiC coatings were cracked through the nozzle region, but did not oxidize or erode. In both fullscale rocket thrust chamber tests, the SiC coating fractured catastrophically during the initial 5-second test, leaving the graphite substrate unprotected. Test results and failure analyses indicate that a practical size/configuration limit was exceeded for this structural design concept in progressing from the 1.75-inch diameter chambers to the 6.0-inch diameter chambers. Since the silicon carbide is highly efficient from the environmental resistance aspect, new design concepts should be developed to circumvent the critical size limitation.

TABLE OF CONTENTS

LIST OF ILLUSTRATIONS

LIST OF ILLUSTRATIONS
(Cont'd)

LIST OF TABLES

NOMENCLATURE

A	-	area, in^2
c_p	-	specific heat, Btu/lb - ^oF
C^*	-	characteristic velocity, ft/sec
D	-	diameter, inches
E	-	modulus of elasticity, psi
F	-	allowable strength, psi
h	-	heat transfer coefficient, Btu/ft^2-hr-^oF
k	-	thermal conductivity, Btu-ft/ft^2-hr-^oF; spring rate, psi/inch
K	-	shape constant, N.D.
L^*	-	characteristic length (chamber volume/nozzle throat area), inches
L	-	length, inches
N	-	number of nodes in buckled shell
O/F	-	mixture ratio, oxidizer/fuel flow rates
P	-	pressure, psi
r, R	-	radius, inches
t	-	thickness, inches
T	-	temperature, ^oF or ^oR
ΔT	-	temperature difference, ^oF
W	-	weight flow, lb/sec
$\dot{w}$	-	mass flow, lb/sec

Greek Symbols

α - coefficient of thermal expansion, in/in/^{o}F

β - Biot's modulus, N. D.

Δ, δ - deflection, inches

ϵ - strain, inches

η - efficiency, percent

ν - Poisson's ratio, N. D.

σ - stress, psi

Subscripts

a - ambient

c - chamber or compression

cr - critical

f - fuel

g - gas

i - inward

G - Graphite

o - outward

ox - oxidizer

r - radius

SiC - silicon carbide

t - total or tension

Ta-10W - 10% tungsten-90% tantalum alloy

th - thermal

I

INTRODUCTION

(U) Rocket propulsion systems needed for spacecraft, ballistic missiles, and air-launched missiles of the future, using advanced propellants, require nonregeneratively-cooled thrust chambers with improved capability, flexibility, and reliability. Advanced thrust chambers are needed which can demonstrate improved performance with high-energy propellants operating at higher chamber pressures for longer firing durations and with multiple restart capability. Future applications of new thrust chamber concepts also demand emphasis on additional factors, including low cost, low weight, simplicity, reproducibility, and decreased development time.

(U) Research in the area of high-temperature, corrosion-resistant, and thermal-shock-resistant materials has resulted in several promising materials which may enable thrust chambers to fulfill the desired characteristics. One of the most promising materials to become available for applications to such advanced thrust chambers is a silicon carbide (SiC) coated graphite composite developed at Marquardt. Before this program began, the outstanding performance of this composite thrust-chamber material had been repeatedly demonstrated at Marquardt with N_2O_4/0.5 N_2H_4-0.5 UDMH propellants. Cumulative firing durations up to 18-1/2 minutes had been achieved at a chamber pressure of 100 psia. The vapor-deposited silicon carbide coating is highly erosion- and oxidation-resistant, and had proved to be an extremely effective protective coating for the graphite substructure.

(U) Previous work at Marquardt, under a Company-sponsored Independent Research Program, resulted in the evolution of a combined heat sink/radiation cooled, prestressed rocket thrust chamber concept capable of 500 psi chamber-pressure operation using high-energy propellants. The design concept incorporates a graphite thrust-chamber liner coated with vapor-deposited silicon carbide.

The entire liner is prestressed in compression to accommodate all of the predicted chamber-pressure loads, including any ignition spike, or thermal shock loadings encountered under startup and restart conditions.

(U) Evidence of the potential of this nonregeneratively cooled thrust-chamber approach for extending liquid rocket thrust chamber technology to higher chamber pressure and longer firing duration with associated restart capability was thus very convincing. Consequently, the present program was conducted to demonstrate the concept capability for long-duration (600 sec) multiple restart operation at 500 psi chamber pressure using N_2O_4/ 0.5 N_2H_4-0.5 UDMH propellants. The program consists of two phases: analysis, design and evaluation testing of subscale (100-lb thrust) chambers, and the design and fabrication of fullscale (5000-lb thrust) chambers for testing at AFRPL. The summary report (AFRPL-TR-66-69) covered the Phase I subscale thrust-chamber evaluation program, and this report covers the Phase II fullscale chamber efforts.

(U) The thrust chamber differs very little from well-proven designs. It uses a one-piece, silicon carbide-coated graphite thrust chamber liner backed up by a tantalum alloy sleeve. The shrink-fitted sleeve puts the graphite under a compressive preload, thereby allowing it to carry all predicted chamber-pressure loads, including those associated with ignition pressure spikes, and thermal shock stresses due to rapid heating, despite the inherently low tensile properties of graphite. Prior to the initiation of the program, this particular design concept had been verified experimentally by thermal cycling and pressure spike tests in a laboratory engine, and it had seen application in two different size thrust chambers (1.1 and 3.0 inch inside diameter) which were fabricated and tested. The 1.1-inch diameter chamber was hydrostatically tested at room temperature to more than 5000 psi, and was also successfully tested to a modified Gemini OAMS duty cycle at an O/F ratio of 1.6 nominal and using N_2O_4/MMH propellants at a chamber pressure of 125 psi with no measurable throat erosion.

(U) Two of the 3.0-inch diameter chambers were previously tested at a chamber pressure of 500 psi for short times with a slurry-type propellant which produced higher heat fluxes and more severe erosion problems than are experienced with the N_2O_4 - 50/50 combination used in the present program. The results of those tests demonstrated the structural integrity and capability of the design concept for high-pressure operation. The work reported in the summary report further demonstrated the capability of this design concept. Phase I of this program consisted of three major tasks:

1. Subscale chamber analysis and design study which included materials, heat transfer and structural analyses to provide the design data for the subscale chambers.

2. Subscale chamber design and fabrication incorporating selected design variations including chamber-shell material and thickness, liner coating thickness, and liner contour.

3. Hot-firing test evaluations of six subscale chambers with a goal of 10-minute continuous or intermittent operation with up to 5 restarts. Propellants were N_2O_4/0.5 N_2H_4-0.5 UDMH at a design mixture ratio of 2.0 and a chamber pressure of 500 psia.

(U) The results of the subscale chamber evaluation of Phase I are summarized in the following paragraphs.

(U) The design of the subscale chambers was based on the results of extensive materials, heat transfer, and structural analyses. The basic subscale design had a 1.75-inch diameter by 3.58-inch long combustion chamber with a 0.414-inch diameter throat, exiting to sea-level pressure. The chamber L^* was $\approx$40. The chamber diameter was fixed by the size of the injector face selected for use in the test program, and the chamber throat size was dictated by the propellant flow rates achievable with the test facility and injector. The chamber liner consisted of Carbone 2239

graphite (1/4-inch thick wall) coated with 0.010 to 0.050-inch thickness of Marquardt RM-005 vapor-deposited silicon carbide on all surfaces. The compression shells were constructed of three different refractory metal alloys: Ta-10W, TZM, and 1/2 Ti Moly. Nominal shell thicknesses ranged from 0.080 to 0.200 inches. Commercially available silicide coatings were used on all shells.

(U) In order to achieve full, even contact and a prescribed interierence fit (ranging from 0.002 - 0.014 inches) when assembled, both the cylindrical outer surface of the SiC-coated liner and the internal surface of the encasing shell were machined to very close tolerances. The assembly was accomplished by heating the coated shells in air to between 2000° and 3000°F and rapidly inserting the coated graphite liner. A total of seven subscale thrust chamber assemblies were produced for testing.

(U) The testing of the completed subscale thrust-chamber assemblies was accomplished in the Marquardt rocket research facility using a standard 8 on 8 Apollo-type injector with no fuel film cooling. The chamber-to-injector sealing was accomplished with a pyrolytic graphite washer to minimize heat soak into the injector. Calibrations were first conducted on a heat-sink copper chamber to establish required propellant flow rates, line pressures, etc., for high combustion efficiency at an O/F of 2.0.

(U) Six subscale chamber assemblies were utilized in a highly successful test program to demonstrate 10-minute duration with up to 5 restarts at 500 psi chamber pressure. Individual test runs ranging in duration from 12 to 601 seconds were conducted without damage or evidence of erosion of the chamber liner or throat. One chamber was fired for consecutive runs of 2 three-minute, and 4 one-minute bursts with restarts after 15 to 45 seconds, with no detrimental effects. A chamber which had accumulated 601 seconds on a continuous run was refired at a later date for an additional 132 seconds without measurable throat erosion.

(U) Exterior surface temperatures were, in all cases, below predicted levels and varied little with combustion efficiency or gas composition at the wall. However, even at high C^* efficiencies, no effect on liner coating performance was noted. The SiC coating on the inner chamber liner surface, however, cracked in every instance, either before or during firing. Nevertheless, numerous test-firings on cracked liners failed to reveal any detrimental effects. The cracks were so minute that they could not be detected without a dye penetrant test. The major problem associated with the subscale test program, as it turned out, was the reliability of the high temperature injector-to-chamber seal. Although effective sealing was accomplished for a number of tests, the short-duration runs were, in most instances, terminated by a seal failure. Consequently, considerable effort and emphasis was placed on improving the sealing scheme.

(U) It appeared from the results of the subscale tests that the ultimate capability of this chamber concept and the SiC liner coating had not yet been approached. Consequently, a high degree of confidence existed in the probability of successfully constructing and test firing the fullscale thrust chambers under Phase II. The results of the Phase II efforts are discussed in Sections IV, V, and VI of this report.

II

SUMMARY

(U) This report presents the results of Phase II of a two-phase program to design, fabricate and evaluate an advanced nonregeneratively cooled rocket thrust chamber concept for 500 psi, multiple restart, long firing duration with N_2O_4/0.5 N_2H_4-0.5 UDMH propellants. The specific design concept under evaluation is that of a prestressed composite wall chamber composed of a contoured SiC coated graphite liner encased in a cylindrical refractory metal shell. Phase I analytical and experimental efforts on the subscale chambers (100-pound thrust) were completed in December, 1965 and reported in Reference 1. For continuity, a review of these efforts are also presented in Section III of this report.

(U) The Phase II effort was to design and fabricate two 5000-lb thrust chambers for delivery to the AFRPL, Edwards AFB, California, for evaluation testing with the noted liquid propellants. The goal of the test program was to achieve a firing duration of 600 seconds with up to 5 restarts at a chamber pressure of 500 psi. This goal was not reached, as both of the fullscale thrust chamber assemblies were tested for only 5 seconds each. During both tests, the inner SiC coating was lost by a progressive failure mode of mechanical breakup, detachment from the graphite substrate, and subsequent expulsion downstream.

(U) The design of the fullscale thrust chambers was based on a scale-up of the subscale chambers which had performed so successfully in the Phase I firing evaluations. To match the existing Air Force test hardware, the basic fullscale design had a 6.046-inch chamber diameter transisting to a 2.90-inch throat diameter. The first chamber had an exit cone designed for exhaust to 13.2 psia ambient pressure. This cone was not used in the second assembly, since full contained expansion was not required. The chamber liner consisted of Carbone 2239 graphite (contoured from 1/2-inch to 2.1-inch wall thickness) coated with 0.010 to 0.090-inch thickness of Marquardt RM-005 vapor deposited SiC on all surfaces. A 0.20-inch thick Ta-10W cylindrical flanged compression shell was used to provide the liner preload. Sylcor R512 was used as an oxidation protection coating on the shell and on the Ta-10W exit cone.

(U) Testing of both 5,000-lb thrust chambers was performed by the Air Force at Test Area 1-46, AFRPL, Edwards, California. An AF multielement injector was used, and the firings were horizontal. The firing schedule

for both assemblies was to start with a 5-second run, inspect, and then retest for longer times. In both instances, the thrust chambers were unsuitable for further test after the initial 5-second runs, since the majority of the inner SiC coating had been lost by mechanical breakup, leaving the graphite substrate unprotected.

(U) Both the 100 and 5000-lb thrust chambers experienced extensive cracking of the SiC coating. In the subscale chambers this cracking did not result in dislocation of the coating, which may be attributed to several factors: tensile failure with sufficient outward radial motion to relieve stresses throughout the coating cross-section, a small radius of curvature which allows a net outboard bending moment rather than a critical compressive-shear condition, and a high allowable ΔT for thermal shock failure.

(U) In the case of the fullscale chambers, coating failure appears to be of a compressive-shear type initiated by a critical tensile stress (thermally induced) at the SiC-graphite interface. This fracture pattern results in the destructive dislocation of fragments, leading to the eventual loss of most of the coating. The factors contributing to such a failure are: (1) A large radius of curvature resulting in a much lower allowable ΔT for thermal shock failure and a high compressive-shear loading existing after the tensile crack initiation. (2) A relatively smaller outward bending moment. (3) A statistical brittle material strength reduction with the larger coating surface area and volume. (4) A possibly more severe wall heating condition with the highly efficient fullscale injector. (5) Reduced stability of the large diameter SiC liner to compressive buckling type loads.

(U) The size factor combined with the tension-compression stress distribution makes the design of a continuous chamber liner of this size impractical with SiC. This is an empirical conclusion based on failure analysis and could not reasonably be predicted through analysis alone because of the many uncertainties involved. It is also concluded that SiC may be used for the liner of such a chamber by designing a segmented chamber such that the size factor is minimized. Further analysis and laboratory effort is required to optimize the composite wall chamber concept.

III

REVIEW OF SUBSCALE CHAMBER EVALUATIONS

(U) During the initial phase of this program, subscale chambers were designed, fabricated and hot firing tested as reported in Reference 1. Since much of the analysis and results of the subscale chamber evaluations formed the bases for decisions relative to the fullscale chambers of Phase II, a review of Phase I is presented in this report section.

A. SUBSCALE CHAMBER ANALYSIS, DESIGN AND FABRICATION

1. Materials Survey

(U) Based on the design concept of a prestressed chamber composed of a SiC coated graphite liner enclosed in a refractory metal shell, a thorough survey was made of each of the component materials applicable to the composite motor. The study was broken down into essentially four areas:

1. Shell materials based on the refractory metals or refractory metal alloys.
2. Liner materials of a graphite compatible with SiC.
3. Liner coating of SiC.
4. Shell coating compatible with the respective shell material and the environmental requirements.

Generally, the properties of interest of the candidate chamber materials were specific heat, thermal conductivity, thermal expansion, modulus of elasticity, tensile and compressive strengths, creep and rupture strengths and in the case of the coatings, oxidation, heat, and erosion resistance. In addition to the physical, thermal, and mechanical properties, other material factors such as cost, availability, and fabrication techniques were also considered since under the tight schedule of the program, availability and/or fabrication technique could be the key factor in chamber fabrication.

a. Shell Materials

(U) Assuming a chamber shell temperature of 2800-3200°F for

at least ten minutes and a prestressed condition with minimum creep, it is necessary to use an alloy based on the refractory metals Ta, Mo, Cb, or W to maintain design stress loads. Preliminary analysis of the refractory metal alloys indicated that Cb alloys did not have sufficient creep strength nor tensile strength to maintain the fine balance of stress-interference necessary for the chamber liner. On the other hand W is particularly heavy, difficult in many cases to fabricate into shaped parts, and brittle. The alloys of Ta and Mo however, are quite compatible with the requirements of stress and creep resistance of the composite chambers. Table I shows typical 3000°F tensile properties of the candidate Ta and Mo alloys, Ta-10W and TZM.

TABLE I

TENSILE PROPERTIES OF Ta-10W AND TZM AT 3000°F

Alloy	Ultimate Tensile Strength	0.2% Yield Strength	Elongation	Modulus of Elasticity
Ta-10W	20 Ksi	14 Ksi	33%	5.5×10^6 psi
TZM	16 Ksi	9 Ksi	25%	12×10^6 p

Figures 1 and 2 show the creep strength of Ta-10W and TZM. Generally, the creep resistance of the two alloys in the temperature range of interest is about the same, however the dropoff of TZM is much greater than Ta-10W. Below 2800°F the creep resistance of TZM is considerably better than Ta-10W, however TZM also lacks a degree of toughness rendering the material somewhat brittle. However for the requirements of the composite chambers, bend ductility and notch test data indicated that TZM was potentially applicable. As a consequence, Phase I chamber shells were fabricated using both Ta-10W and TZM. Since real data were lacking on TZM in this particular application, further use of the alloy (Phase II) was made contingent upon its performance in the Phase I tests.

(U) A prime consideration in the utilization of the refractory metal shell was the method of fabrication. Essentially three techniques were studied:

1. Machine the shell from solid rod.

2. Spin form the shell from a plate or tube.

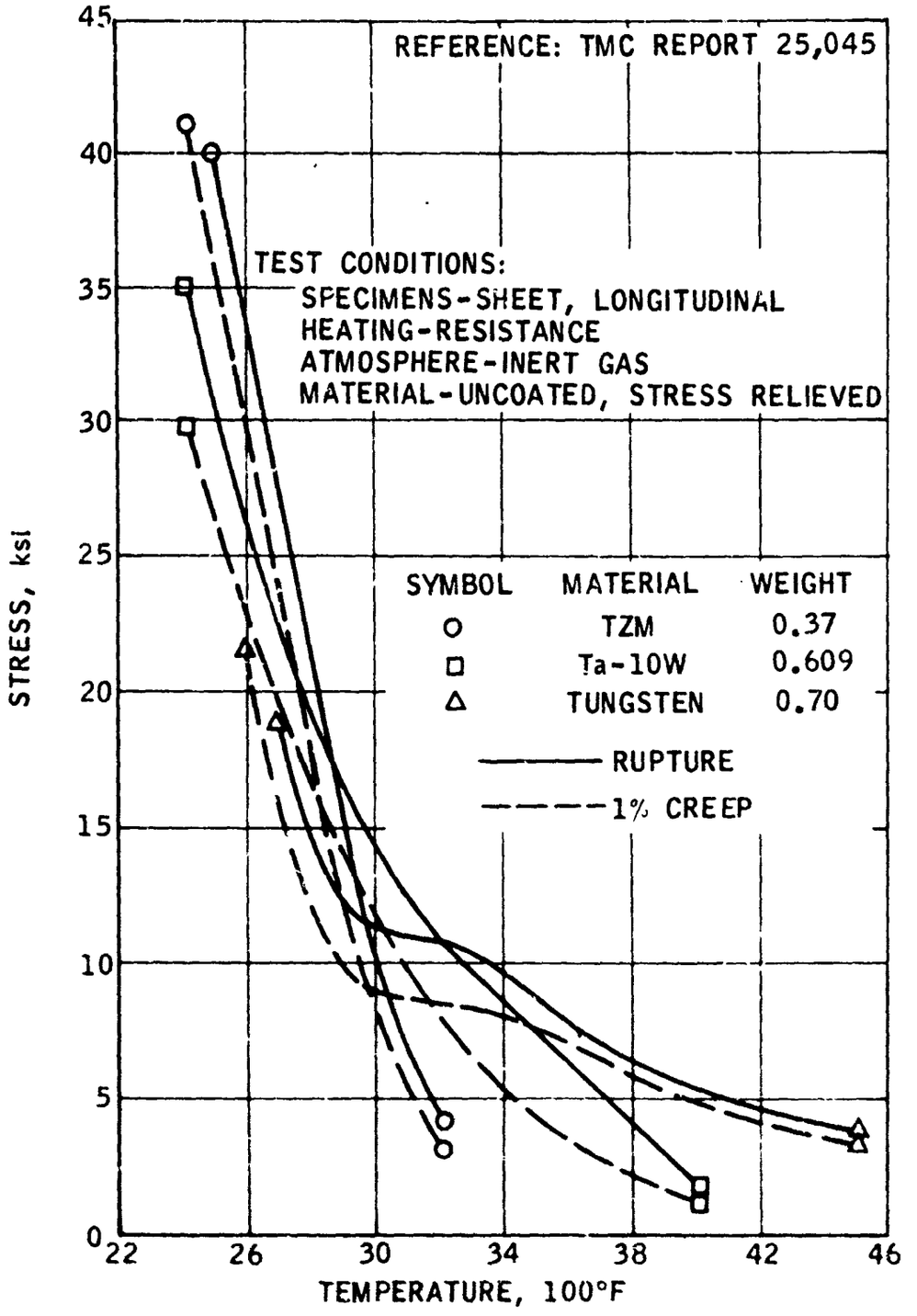

Figure 1
10 MINUTE RUPTURE AND CREEP STRENGTH
OF REFRACTORY METALS

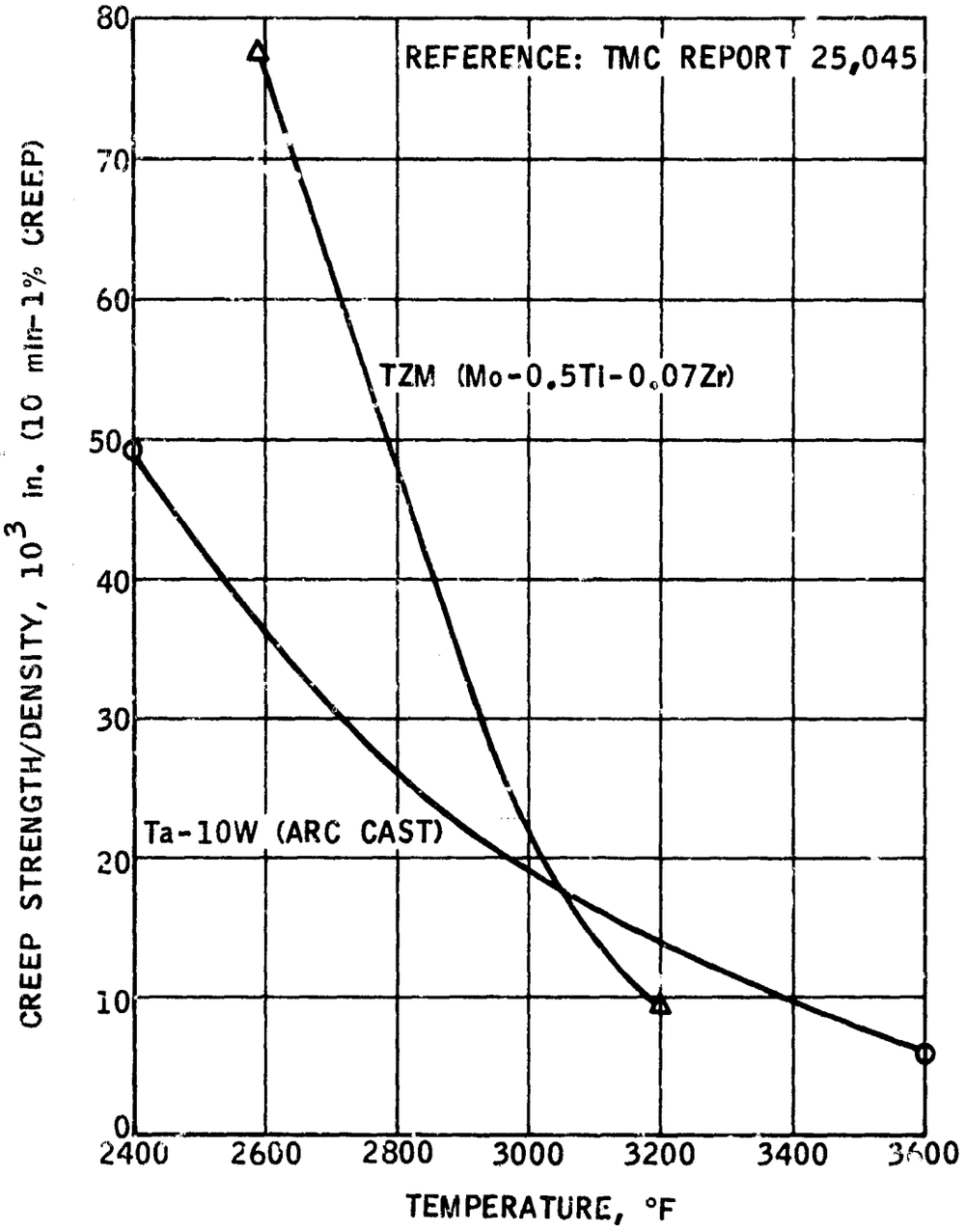

Figure 2

10 MINUTE - 1% CREEP STRENGTH-TO-DENSITY RATIO FOR TZM AND Ta-10W

3. Roll form from a sheet and electron beam weld a longitudinal seam.

For the Phase I shell it was found that the deciding criterion in fabrication was based on availability of stock and the most expeditious fabrication technique.

b. Graphite Liner

(U) A preliminary analysis of the applicable graphites for use as the thrust chamber liner indicated that four grades of graphites had sufficient mechanical strengths and compatibility with SiC. The graphites evaluated were National Carbon RVC, Carbone 2239 and P5890, and Great Lakes Carbon MHLM-85. To match the graphite to the requirements of the thrust chamber duty cycle and the SiC coating, the graphite selection criteria was based mainly on:

1. Tensile and compressive strengths. For the anticipated stress cycle of the composite chamber the maximum possible tensile and compressive strength were desired.

2. Isotropy. Since the liner coating is isotropic β SiC the graphite must be isotropic.

3. Thermal expansion to match SiC.

4. Thermal conductivity as high as possible to minimize thermal stresses, and excessive coating temperatures.

(U) Table II lists the significant properties of the four grades of graphite. The properties of SiC are included for comparison. Although RVC and MHLM-85 have modulus and thermal conductivity values comparable to 2239 and P5890, they have a marked degree of anistropty. This difference in properties by virtue of the grain alignment is incompatible with β SiC, particularly for large shapes. Although P5890 has somewhat higher mechanical strength, grade 2239 appeared to offer the best compromise in expansion compatibility while retaining a high mechanical strength. All of the chamber liners for the Phase I chamber were machined from 3 3/4 inch diameter x 5 1/4 inch long Carbone No. 2239 moulded graphite rounds.

TABLE II

GRAPHITE PROPERTIES *

Graphite Grade	Modulus 10^6 psi w.g.	a.g.	Compressive Str. psi w.g.	a.g.	Tensile Str. psi w.g.	a.g.	Linear Expansion/°C w.g. R.T.	a.g.	Thermal Conductivity cal/gm-cm°C w.g. R.T.	a.g.	3000°F
RVC	1.77	1.38	11,160	10,940	2700	1300	3.7	4.5	0.268	0.236	0.07
MHLM-85	1.5	1.5	6,000	5,800	1800	1500	2.8	2.7	0.4		0.08
2239	1.4		15,000		3200		4.0		0.32		0.08
F5890	1.45		22,000		4000		4.2		0.32		0.08
SiC	20-60		150,000 - 300,000		10,000 - 20,000		3.8		0.4		0.04

* All room temperature data except where noted.

c. Coatings

1. Shell Coatings

(U) Selection of the oxidation protection coating for the chamber shells was based on a 10 minute firing time, a 2800-3200°F shell temperature, and a static air environment. Essentially, four coating systems were found applicable to the chamber materials: tin-aluminide or R512 on Ta-10W; Durak B on TZM; and hafnium-tantalum on Ta-10W and TZM. In view of the temperature range and the limited methods of application, the added cost, time, and complexity of the Hf-Ta coating was not considered justified. The tin-aluminide coating is very applicable to the shell environmental conditions, having protected tantalum base alloys for well over one hour at 3000°F in static air. The major problem however, in the tin-aluminide coating was the 3-6 week delivery of a coated part. For the two remaining coatings, R512 on Ta-10W and Durak B on TZM, both

are commercially available and have been extensively tested under static air and dynamic combustion product environments. R512 coatings have been established as reliable for well over one hour at 3200°F and Durak B for the same time period at 3000°F. Durak B is a disilicide coating applied by the Chromizing Corporation in Los Angeles. Sylcor R512 is a fused silicide supplied by Sylcor Division of Sylvania in Hicksville, Long Island. All subscale chamber shells were coated with either Durak B or Sylcor R512.

2. Liner Coating - RM-005 Silicon Carbide

(U) The ASTRO Division of Marquardt had previously developed, under a Company-sponsored research program, the highly successful RM-005 coating. This silicon carbide coating, which can be applied to a variety of substrates, to any desired thickness by chemical vapor deposition, is an extremely hard, tightly bonded, dense refractory coating with outstanding oxidation, erosion, and thermal shock resistance. The outstanding performance of this coating has been demonstrated in laboratory tests and in numerous rocket firings. Both long runs and a wide variety of pulsing runs have shown that RM-005 is superior to any other insert material tested. Early tests sometimes encountered failures due to differential thermal expansion of the coating and graphite, but study of the thermal expansion characteristics of a large number of graphites, including their anisotropy, resulted in the choice of a graphite which is well matched with the RM-005 coating. A graphite surface conditioning also strengthens the bond between the coating and the graphite. Concurrently, additives to the silicon carbide were found which improved its formation of a thin highly viscous surface oxide coating when exposed to oxidizing conditions, and also its compatibility with other refractory substrates. The potential of the coating system, as presently formulated, exceeded the severity of conditions in liquid thrust chambers so far tested.

(U) The choice of an RM-005 coated graphite thrust chamber liner was based on extensive analysis, laboratory testing, and liquid rocket engine testing of a wide variety of material systems. Silicon carbide is reported to decompose or sublime at temperatures between 4350° and 4900°F at atmospheric pressure. However, a phase diagram constructed from data taken at pressures of 35 atmospheres (~ 500 psi) shows a peritectic decomposition occurring at 5100°F into a two-phase liquid plus solid carbon region. This evidence would indicate that appreciable decomposition and/or sublimation of the RM-005 coating at chamber pressures of 500 psi would not be expected at temperatures below about

5000°F. Therefore, since a steady-state heat transfer analysis of the subscale chamber design indicated an effective wall temperature well below this point, no loss of coating due to thermal decomposition or sublimation was anticipated, and in fact, none occurred. In addition, the RM-005 coating had been tested under near vacuum conditions at temperatures exceeding 4000°F for 2 hours without measurable loss of material. Therefore, vacuum operation is not expected to present a problem, even though it was not evaluated in this program in actual test firings.

(U) The limiting factor in the life of the silicon carbide coating was expected to be the rate of consumption of the silicon carbide surface, due to the formation and subsequent loss of the oxidation product, SiO_2. Silicon carbide oxidizes only slowly and by a diffusion-controlled process up to temperatures of 3100°F. Beyond this temperature at atmospheric pressure, the rate increases due to volatilization of SiO and if shear forces are present, through erosion of the viscous SiO_2. These considerations would lead one to predict high coating erosion rates at the higher heat flux conditions anticipated at a chamber pressure of 500 psi. However, a number of factors tend to minimize this effect. At higher chamber pressures, the volatilization of the SiO_2 film should be suppressed. In addition, the endothermic nature of the chemical reactions, along with the blowing effect caused by the gas evolution, may reduce the net rate of heat transfer to the wall. Nevertheless, the rate of oxygen diffusion through the liquid SiO_2 film, whose thickness is partially determined by the shear forces created by the combustion gas, can be an important consideration. Fortunately, the quantities of oxidizing species in the $N_2O_4/0.5\ N_2H_4$-0.5 UDMH combustion environment are low in comparison with an air environment, and thus the oxidizer partial pressure at the coating surface is less severe, resulting in lower comparative oxidation rates. This observation has been experimentally verified in silicon carbide oxidation tests in air, oxyacetylene torch, and rocket exhaust environments. Figure 3 gives an indication of the time-temperature oxidation protection afforded a substrate by the RM-005 SiC coating. Torch oxidation represents a severe test of the coating durability. Longer times at higher temperatures can be accommodated by SiC if the atmosphere is less oxidizing.

d. Material Property Design Data

(U) After selection of the individual component materials for the composite subscale thrust chambers, the pertinent thermal, physical

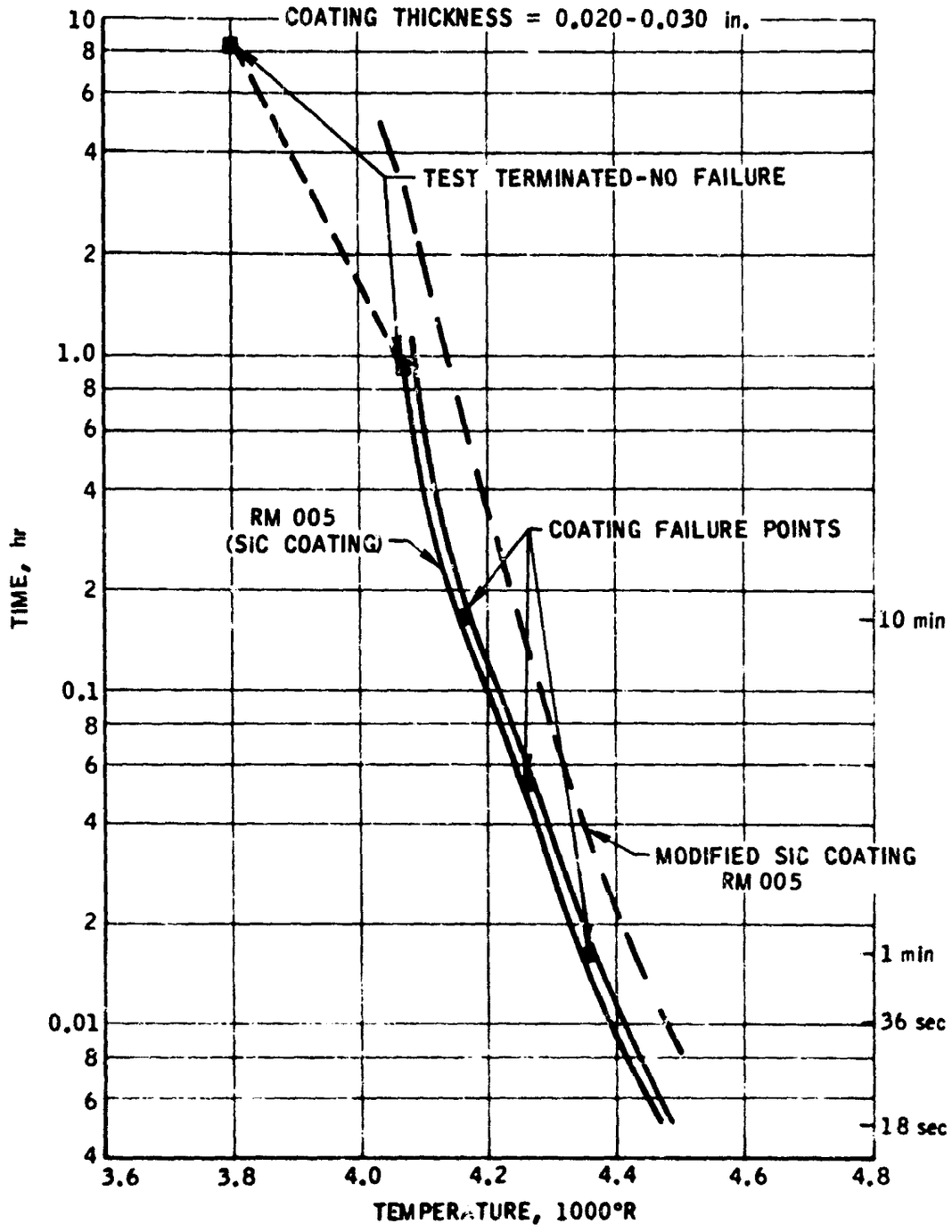

Figure 3

TORCH OXIDATION TEST RESULTS
SiC COATING ON GRAPHITE

R-15,154C

and mechanical property data were surveyed for use in the thermal and structural analyses. These data were presented in Reference 1 (pages 20-31).

2. Heat Transfer Analysis

(U) In order to determine the magnitudes of the temperatures and the temperature differences throughout the subscale chamber assemblies, a number of heat transfer calculations were performed. Starting with the original contour from Figure 4 and the basic concept of a four layer wall (SiC-Graphite-SiC-Refractory metal), a "thermal analyzer" routine was written to determine the transient and steady-state temperatures in the chamber walls. A description of the "thermal analyzer" heat transfer calculation method was given in Appendix I of Reference 1.

(U) For this thermal analysis, the subscale chambers were described by a two-dimensional model because of axial symmetry. In the cylindrical part of the chamber, the structure was separated into differential volumes bounded by two radial planes and two concentric cylinders. The throat section was somewhat more complicated because of the convergent and divergent conical sections. An analysis was made for the determination of the geometric proportions of the thermal resistances and capacitances of the differential volumes. From the geometry of the chamber, a thermal circuit was developed which contains 77 nodes and 141 resistors. The node positions in the subscale chamber are shown in Figure 5.

(U) After the geometrical resistance values had been computed the first IBM 7040 computer runs were made. This initial subscale chamber configuration had a chamber diameter of 1.75 inches, an inner SiC shell 0.030 inches thick, a graphite substrate 0.250 inches thick, an outer SiC shell 0.020 inches thick, all contained in a 0.100 inch thick Ta-10W shell coated inside and out with Sylcor R-512 (0.001 to 0.002 inches thick). The thermal-physical properties of these materials needed for the analysis, were taken from the material property data presented in Section III-A of Reference 1.

(U) The thermal analysis model and routine were written in such a manner as to accommodate different thicknesses of materials, different materials thermal properties and material thermal conductivity variations with temperature. In this manner the effects of different materials and

BASIC INTERNAL LINES

L* = 50

EXPANSION RATIO = 5.41

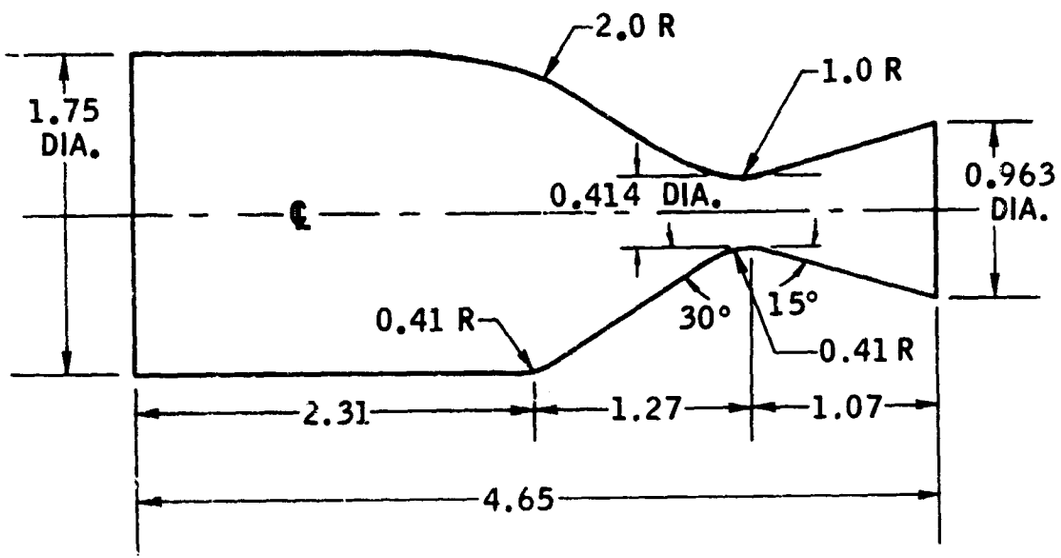

LOWER HALF - ORIGINAL CONTOUR
UPPER HALF - REVISED CONTOUR

Figure 4

SUBSCALE THRUST CHAMBER

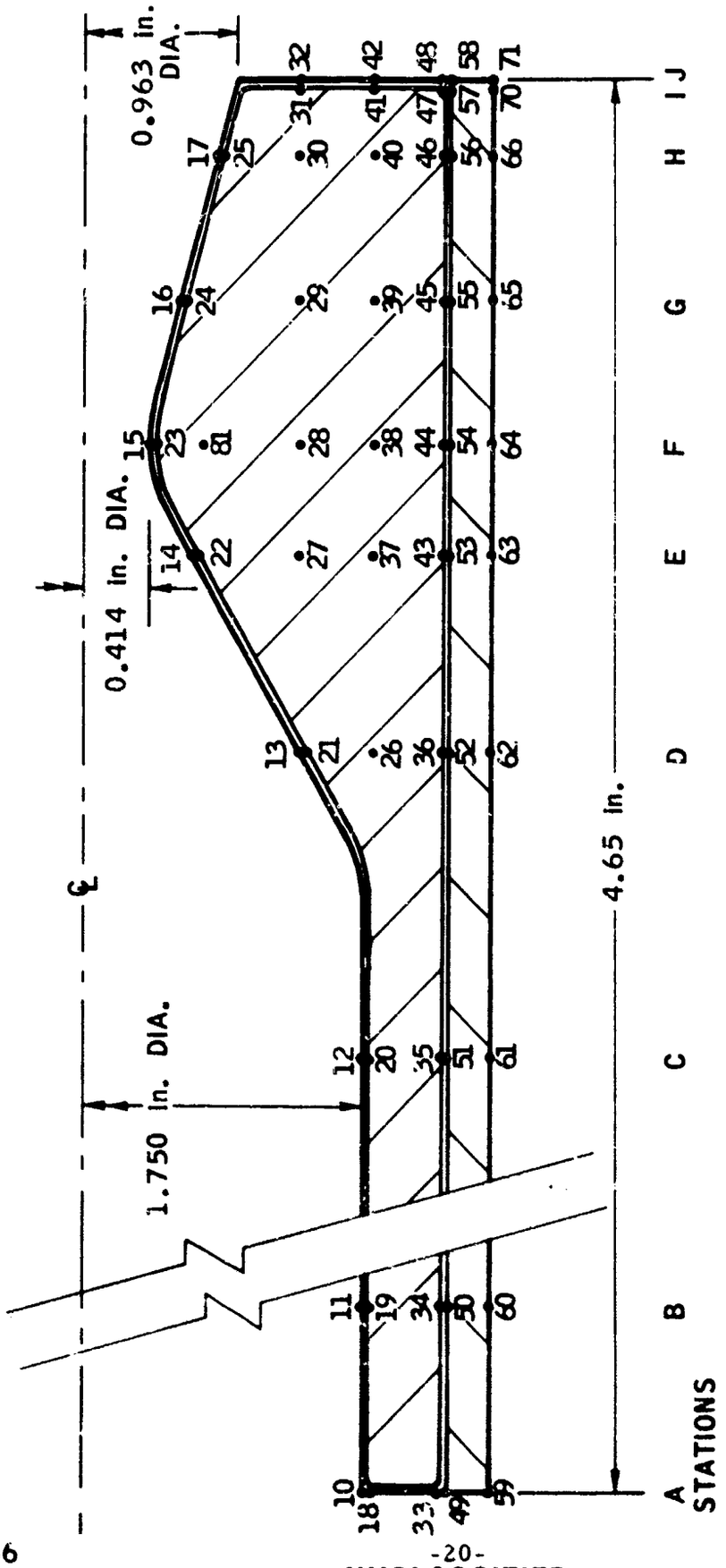

Figure 5

SUBSCALE THRUST CHAMBER

NODE POSITIONS IN THERMAL ANALYZER PROGRAM

different thicknesses of materials in the wall can be determined, and from the computed temperatures and temperature gradients, a realistic structural analysis can be made. These, in combination, can determine the most efficient materials and proportions thereof, for the chamber design conditions. Steady-state conditions were run first in order to determine maximum shell temperatures. From this information, the refractory metal shells were rough sized and the long lead time materials ordered. Transient temperatures were computed later.

(U) Operation of the thermal analyzer routine on the IBM 7040 first required a number of trial runs in order to set the number of iterations for meaningful results and to properly select the dampening parameters for temperature convergence. The first results of the computation were for Thermal Model 1-A which used 97% theoretical gas temperature and the Bartz equation (Reference 2) to compute the convective heat transfer coefficient from the hot gas to the wall. The indicated wall temperature approached a value of 4900°F for this upper boundary case as shown in Table III. Experience has shown the Bartz heat transfer coefficient to be up to 100% higher than the experimental value at the throat, attributed principally to the injector spray pattern. Consequently, it was necessary to select heating conditions that would more closely approximate the actual chamber wall temperatures.

(U) After establishing the maximum possible temperatures with Thermal Model 1-A, three more computations were made to determine the effect of: (1) higher thermal conductivity of graphite, (2) reduction in Bartz heat transfer coefficient, and (3) a reduction in effective gas temperature. The increased conductivity of graphite in this composite structure was found to have a very minor effect on any of the temperatures since both the original and higher values (from different references) were relatively low. Maximum throat wall temperature was lowered about 250°F by a 1/3 reduction in the Bartz hot gas convective heat transfer coefficient. Reducing the effective gas temperature was 80% effective in reducing the throat wall temperature (i.e. a 1000°F drop in effective gas temperature lowers the wall by 800°F). The Thermal Model reflecting this reduction is designated 1-C, and the computed temperatures at the node points of Figure 5 are given in Table IV.

(U) For Model 1-C the cooling effect was assumed to result in an "effective" gas temperature 1000°F lower than the theoretical gas temperature. This assumption was taken at this stage in lieu of experimental heat transfer data. The Bartz equation was used to predict the convective heat

TABLE III STEADY-STATE THERMAL ANALYSIS

SUBSCALE NON R/C ROCKET THRUST CHAMBER EVALUATION

TEMPERATURES* AT NODE POINTS THERMAL MODEL NO. 1-A

Effective Gas Temperature 5340°F(97 % Theoretical)

Bartz Heat Transfer

Station	Node Pt.	Temp. °F	Station	Node Pt.	Temp. °F
A	10	2912	F	15	4926
	18	2837		23	4811
	33	2715	(Throat)	31	4426
	49	2709		39	3612
	59	2693		38	3508
				44	3005
B	11	(temps		54	2959
	19	still		64	2911
	34	oscillating)			
	50		G	16	4775
	60			24	4620
				29	3545
C	12	3354		39	3210
	20	3272		45	2915
	35	3035		55	2872
	51	2995		65	2826
	61	2950			
			H	17	4342
D	13	4050		25	4196
	21	3908		30	3303
	26	3484		40	2880
	36	3122		46	2606
	52	3067		56	2573
	62	3014		66	2453
E	14	4911	I	31	3047
	22	4774		41	2817
	27	3724		47	2552
	37	3395		57	2519
	43	3060		70	-
	53	3009			
	63	2959	J	32	3034
				42	2774
				48	2534
				58	2501
				71	-

* Some temperatures listed had not yet converged and are as much as 300°F off.

TABLE IV STEADY-STATE THERMAL ANALYSIS

SUBSCALE NON R/C ROCKET THRUST CHAMBER EVALUATION

TEMPERATURES AT NODE POINTS — THERMAL MODEL NO. 1-C

Effective Gas Temperature 4340°F

Station	Node Pt.	Temp. °F	Station	Node Pt.	Temp. °F
A	10	2376	F	15	4083
	18	2341		23	3941
	33	2264	(Throat)	81	3725
	49	2264		28	3202
	59	2257		38	2990
				44	2807
B	11	2691		54	2775
	19	2639		64	2739
	34	2512			
	50	2496	G	16	3958
	60	2471		24	3854
				29	3167
C	12	2875		39	2954
	20	2819		45	2776
	35	2670		55	2738
	51	2646		65	2701
	61	2617			
			H	17	3686
D	13	3469		25	3546
	21	3371		30	3044
	26	3087		40	2847
	36	2845		46	2776
	52	2811		56	2649
	62	2772		66	2618
E	14	4049	I	31	2892
	22	3953		41	2731
	27	3271		47	2578
	37	3054		57	2573
	43	2823		70	2554
	53	2800			
	63	2762	J	32	2840
				42	2690
				48	2558
				58	2548
				71	2531

transfer rate from the gas to the wall. This calculation method assumes fully developed, turbulent flow. Since these conditions may not exist in the chamber and depending upon the influence of the propellant injection process, the actual heat transfer rates could be at variance with those predicted. Test results show that even the reduced temperatures of Model 1-C were higher than the actual observed temperatures in the subscale tests.

3. Structural Analysis and Design

(U) The thrust chamber structure is composed basically of a contoured inner liner and a cylindrical outer shell. The liner is of graphite, machined to the desired chamber-nozzle shape, and completely coated with SiC. Its function is to contain the combustion gases with an unchanging inner contour. Since SiC and graphite have low tensile strengths, it is the function of the thin cylindrical outer shell to hold the thrust chamber liner in place and under an initial preload to prevent liner failure under combined thermal and pressure loads. In designing a structure of this type there are many variables which must be evaluated to achieve a reliable composite rocket thrust chamber.

(U) First, the range of temperature must be determined as an aid to selecting the correct proportions of materials in the composite. However, before a realistic heat-transfer analysis can be made, an initial chamber configuration must be selected. Choice of the initial configuration was made by assuming an inner SiC coating thickness of 0.030 inches, different thicknesses of graphite, an outer SiC coating thickness of 0.020 inches, and different thicknesses for the outer Ta-10W shell. Hand calculations were made (one-dimensional heat-transfer analysis) which showed the temperatures to be in reasonable ranges for the materials capabilities at approximate stress loadings. From this point the heat transfer analysis was conducted as described in the previous section, to define more accurately the wall temperatures and temperature differences.

(U) The initial structural analysis included defining the loading conditions that could occur and selecting those that would affect the design of the subscale thrust chamber. These loading conditions were taken in two basic categories; those without chamber pressure, and those with chamber pressure. In the first group, without pressure loads, are those due to chamber-liner prestress and thermal conditions at:

1. ambient temperature

2. maximum temperature (immediately after hot firing)

3. transient temperatures (cool-down after hot firing)

In the second group, with pressure loads, are those due to chamber pressure, prestress and thermal condition at:

4. ambient temperature (pressure leak test)

5. transient temperatures (during heat-up)

6. maximum temperature (steady-state operation)

7. transient temperature from an above ambient temperature start (restart before full cool-down)

(U) The composition of the thrust chamber wall structure was next studied to ascertain which loading conditions would be critical for the various sections of the composite wall. The sketch on the following page shows the composition of the wall cross-section and identifies the radial planes for the analysis.

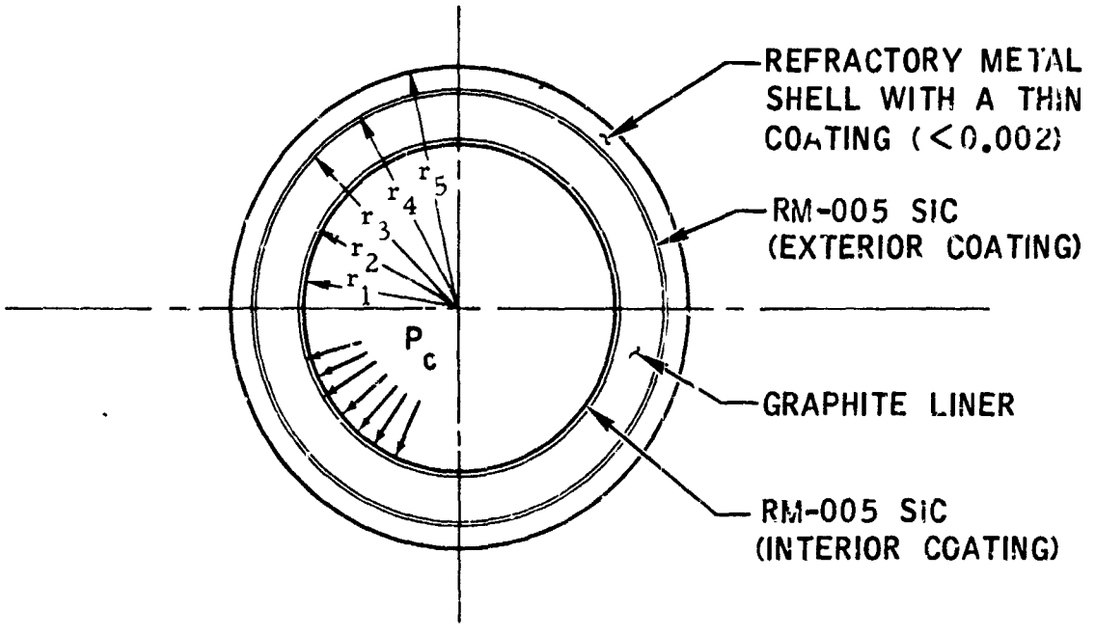

Radii r_3, r_4, and r_5 are constant (straight cylindrical) along the full chamber length but r_1 and r_2 change through the nozzle throat section. The initial r_4 of the refractory metal shell is smaller than the r_4 of the SiC coated liner, so that when assembled, the liner is put into compression by the shell and the shell is put into tension by the liner. The amount of initial interference can be selected from a considerable range since the shells can be heated to $\sim 3000^{\circ}F$ before liner insertion, which results in a radial expansion of about 0.014 inches for a Ta-10W shell. The interference extremes effects on the chamber components are as follows: with minimum, or zero interference, the coated liner may fracture in tension due to a combined pressure and thermal loads. With maximum interference, the graphite or silicon carbide of the liner could fail in compression and the outer refractory metal shell would be highly loaded in tension, thus subjecting it to high-temperature creep and subsequent loss of interference prestress. In between these extremes is an optimum value for each chamber configuration for a particular service condition and lifetime.

(U) Returning to the assessment of loading-condition effects on the composite structure, it was found that two loading conditions would probably provide maximum stress loads on the critical sections. These were loading conditions 5 and 6 above. Condition 5 produces a maximum differential temperature (Δ T) through the inner SiC coating and the graphite liner which results in maximum thermal stresses in these components. Condition 6 produces maximum temperatures on the entire thrust chamber structure in conjunction with full pressure loading, under which conditions the refractory metal and the SiC have their least strength. Although spike pressure loads were not a design requirement for these chambers a high initial overpressure can be accommodated because of the prestress interference values used.

(U) Possible methods of analysis were surveyed for this composite structure under the combination of pressure, thermal and initial prestress loads. Any sophisticated structural analysis method required a rather precise knowledge of all material properties (thermal, mechanical and physical) over the temperature range of operation. This particular design utilizes relatively brittle materials in the liner, having thickness (volume) strength effects which are only generally known, and material properties such as Poissor's ratio (ν) and modulus of elasticity (E) whose variation with temperature is only approximately known. Consequently, it was evident that a highly sophisticated analytical method was not practical in this instance, and thus the following design-analysis method was used.

1. Conventional linear analysis formulae for stress and deflection were used, such as those from Timoshenko (Reference 3) and Roark (Reference 4) for pressure and thermal loading of thick and thin walled cylinders.

2. The results of sophisticated analyses in the literature were applied to indicate maximum probable combined stresses and deflections. For example, the work of Chang and Chu (Reference 5) describes the stress distribution in a metal tube which is subjected to a very high radial temperature variation and internal pressure.

3. Different effective prestress conditions were applied to the subscale chambers either by a change in design interference, shell thickness or shell material. Pre-test and post-test dimensional and conditional inspections could then be performed to verify the design analyses.

(U) The method of analysis used was based on the principle of compatible deformations. The input variables were the material properties from report section IIIA in Reference 1 (static and creep strengths, modulii of elasticity, thermal expansion coefficients, Poisson's ratios), the material thicknesses, the amount of prestress, the chamber pressure and the temperature distribution. For the structural analysis and design of the subscale chambers, the thermal analyses of the report section above provided the necessary temperature distributions and magnitudes. The temperatures of Thermal Model 1-C were used for the chamber design. Figure 6 presents the two temperature distributions, through the throat section, that were used for design. The lower line (15 seconds after start-up) corresponds to load condition 5 in that it is a condition of maximum ΔT through the inner SiC coating (node 15-23) and the graphite substrate (node 23-44). The upper line shows the maximum wall temperatures for steady-state operation, corresponding to load condition 6.

(U) Before the chamber wall composition was selected, which produced the temperatures of Thermal Model 1-C, the effect of graphite liner thickness and Ta-10W shell thickness variations were evaluated. Shell thicknesses of 0.10 inch and 0.20 inch in a total wall thickness up to 1.00 inch were assumed at the nozzle throat section. The variation of inside and outside wall temperatures were calculated which showed that the inside wall temperature is relatively insensitive to the thickness of graphite or shell metal surrounding it. The outer shell temperature, however, is almost inversely proportional to the amount of graphite between it and the chamber hot-wall.

(U) Since Ta-10W and TZM are highly strength-temperature affected in the over 2500°F range, it was considered to be most advantageous to select a graphite thickness that would result in shell material temperature below 3000°F. The basic subscale thrust chamber configuration that satisfied this requirement and resulted in a generally efficient and readily fabricated structure was as follows. A liner would be machined from No. 2239 graphite with a nominal chamber section thick-

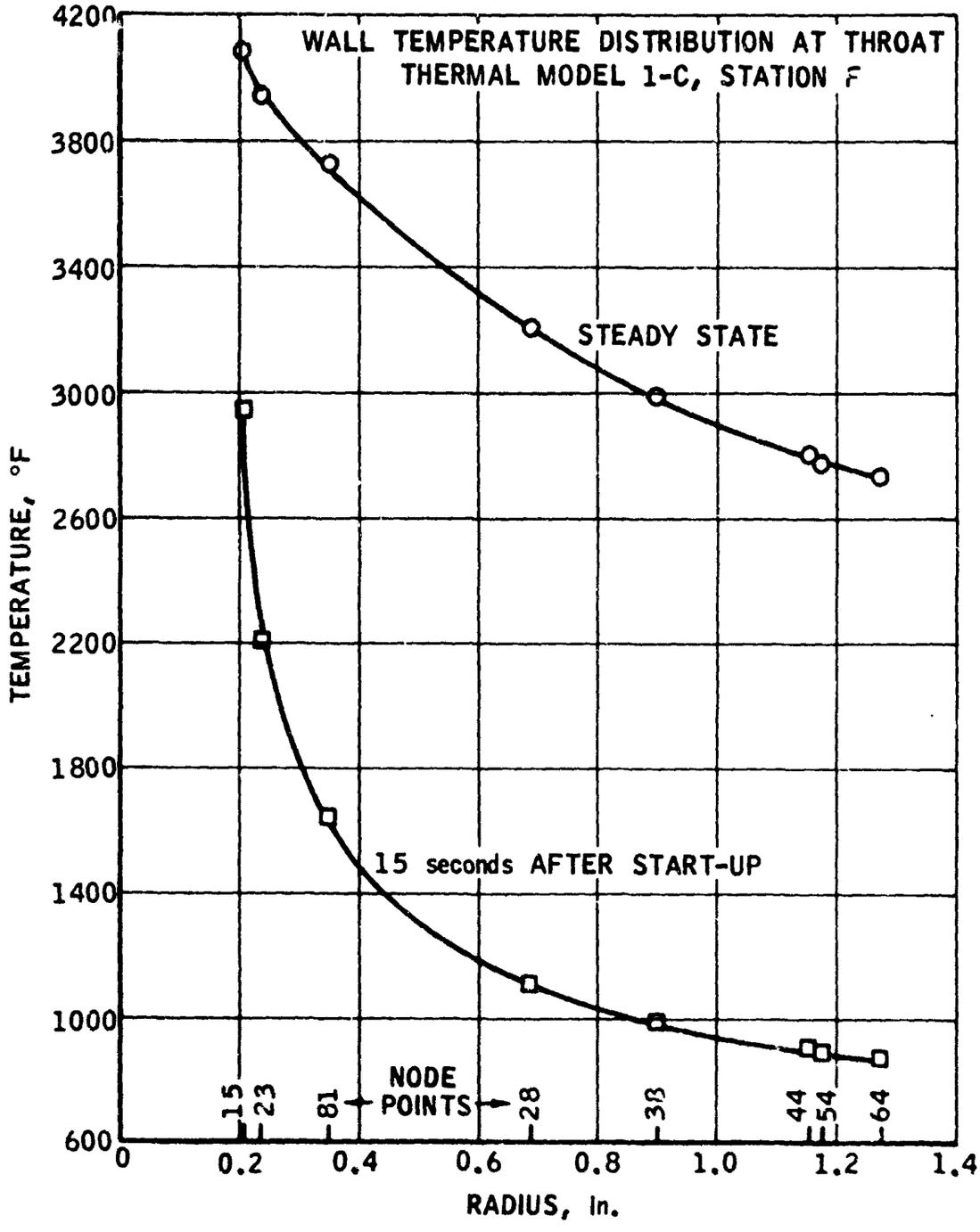

Figure 6

SUBSCALE CHAMBER TEMPERATURES

ness of 0.25 inches with a straight cylindrical outer diameter. This liner would be completely coated on all surfaces with vapor deposited SiC. The design thickness of the inner coating was 0.030 inches and the outer was 0.010 to 0.020 inches. The outer shell was to be cylindrical 0.100 inch thick Ta-10W for maximum creep resistance at 3000°F and low temperature shock tolerance.

(U) Different shell materials, thicknesses, and initial radial interference values would also be incorporated in subsequent assemblies. Also, liners would be fabricated with thicker SiC coatings in the event that the 0.030 thickness should be eroded before the desired 10 minutes of thrust chamber operation was completed. The molybdenum alloy, TZM, was the other candidate material for the shell. Compared with Ta-10W, TZM is less expensive, less dense, and has a higher creep strength-to-density ratio at temperatures below 3050°F (Figure 2, page 12). It was recognized to have a possible low temperature brittleness problem, but in view of the potential gains, the fabrication and test evaluation of molybdenum shelled chambers was considered necessary.

(U) Table V presents a tabular summary of the composition of the subscale chambers, the condition before and after assembly, and after test. The relative shell stiffnesses (resistance to radial elastic deformation) for the shells at room temperature and at 3000°F are as follows, where the 0.100 inch thick Ta-10W shell at room temperature equals a stiffness of 1.0. TZM and $\frac{1}{2}$ Ti-Mo have the same stiffness.

Temperature	0.080 Ta-10W	0.100 Ta-10W	0.100 TZM	0.200 TZM
80°F	0.80	1.00	1.50	2.77
3000°F	0.15	0.18	0.40	0.74

Radial interference values of 0.002-0.003 inches were used for the molybdenum alloy shell assemblies, and 0.004-0.007 inches for the Ta-10W shell assemblies. All assemblies were calculated to have positive margins of safety under load conditions 5 and 6 (transient heat-up and steady-state). As noted in Table V the only chamber failure that occurred during test was with the 0.200 inch thick TZM walled assembly. None of the other liner-shell assemblies experienced any type of structural failure or measurable permanent deformation as a result of the hot-firing tests.

TABLE V SUBSCALE CHAMBER ASSEMBLIES

Assy No.	Shell No.	Liner No.	Shell Dimensions: Matl.	t (in.)	Coating & t	Liner Dimensions SiC Coating t (in.): Inside	Outside	Throat Dia (in.): Before Test	After Test	Liner Condition: Before Assy	After Assy	After Test	Test Cond.: No.	P_c psia	Time sec	NOTES
001	X7295-3 S/N 001	X20212-7 S/N 002	Ta-10W	0.100	R512 0.001-0.002	0.051	0.009	0.4125		No Cracks	Siezed during assy-no good		--	--	--	
002	X7295-3 S/N 002	X20212-7 S/N 001	Ta-10W	0.100	R512 0.001-0.002	0.051	0.010	0.413	0.413	Five ln cracks in throat	Cracks propogated ln & circ	New circ cracks - I.D. near injector end.	12	476	24.5	Cooling water off. Springs relaxed.
													13	436	36.9	Run 15 min after #12-cooling water on. P.G. seal split.
003	X7295-5 S/N 003	X20212-5 S/N 004	TZM	0.100	Durak "B" 0.001	0.039	0.010	0.412		No Cracks	Hot press assy failed		--	--	--	
004	X7295-5 S/N 004	X20212-5 S/N 001	TZM	0.200	Durak "B" 0.001	0.040	0.010	0.412		No dye check performed	ln & circ cracks conv & throat		--	--	--	Liner leaked and was removed. New assy is designated 004-A
004-A	X7295-5 S/N 004	X20221-3 S/N 005	TZM	0.200	Durak "B" 0.001	0.038	0.010	0.416		No Cracks	1 ln crack in throat	Brittle fracture of liner & shell.	22	477	1.4	Assembly failed at start of test. Pressure & thermal shock on thick TZM shell.
005	X7295-1 S/N 005	X20221-3 S/N 007	Ta-10W	0.100	R512 0.001-0.002	0.059	0.010	0.404	0.403	No Cracks	No Cracks	Numerous hairline cracks thru conv, throat & div inner surface.	15	499	601	Leaked after test cool down. P_c was steady during test.
								0.403	0.403			Fwd seal area failure.	23	530	132	Small area leak - P.G. seal and SiC coating.
006	X7295-7 S/N 006	X20221-3 S/N 007	Ta-10W	0.060	R512 0.001-0.002	0.037	0.010	0.417	0.417	No Cracks	No Cracks	Numerous hairline cracks thru contoured inner surface of nozzle.	16	482	180	Off 45 no dimensional
													"	465	180	Off 30 change of P.G.
													"	455	60	Off 15 seal or SiC
													"	460	60	Off 15 coated chamber
													"	455	60	Off 15
													"	460	60	
007	X7295-7 S/N 007	X20221-3 S/N 006	Ta-10W	0.060	R512 0.001-0.002	0.040	0.009	0.411	0.411	No Cracks	No Cracks	Numerous hairline cracks in conv throat sect + short cracks near fwd fa[illegible]	14	439 Max	273	P_c was low due to leaks past P.G. seal. Unburned propellants leaked out, requiring shut down for safety.
008	X7295-5 S/N 008	X20[illegible]-7 S/N [illegible]	Ta-10W	0.100	Durak "B" 0.001	0.038	0.010	0.410	0.410	Excess porosity I.D.	2 ln & 1 circ cracks	No further cracking was evident	9	489	26.0	Shell was broken trying to remove insert prior to new assy.
													10	502	18.2	
													11	495	12.6	
009	X7295-5 S/N 009	---	Ta-10W	0.100	Durak "B"	--	--	--	--				--	--	--	Shell cracked during coating

ln - [illegible] (axial)
circ - circumferential
conv - convergent
div - divergent
t - thickness
P.G. - Pyrolytic Graphite
P_c - chamber pressure
SiC - Silicon Carbide

(U) In an effort to substantiate and possibly refine the method of coated liner-shell prestress analysis, critical inspections were made of all components before and after assembly and after test. However, because of normal production tolerances and the small dimensional changes being assessed, it was not possible to supplement the original analytical procedure. The method of compatible deformations and the load and material properties inputs used had proven to be a useful analytical procedure for the design of the subscale thrust chambers.

(U) The assembly of the original SiC-coated liners into the refractory metal shells did, in each case, precipitate some longitudinal and circumferential cracking of the inner SiC coating in the convergent section of the nozzle. This was most severe with a liner that was cracked before assembly, but also occurred with a liner that had no discernable cracks before assembly. SiC coated graphite nozzles have been previously used successfully with cracks in the inner coating so it was believed that these composite chambers might also be tested successfully. The action of the inner coating during operation tends to close up the cracks due to constrained expansion, and when the SiC reaches a high enough temperature, the cracks could glass over and effectively seal. Thus, it was not known how detrimental the cracks might be until the first attempts were made to pressure check an injector-chamber assembly.

(U) Pressure checking showed a noticeable leak at the ends of the shell-liner interface which is radially outside of the injector-chamber seal on the forward face of the SiC coated graphite liner. This meant that the chamber pressure had found a path either through the graphite or along the graphite SiC interface.

(U) After this discovery of the pressure leak path, two approaches to the solution of the problem were taken. First, the possibility of sealing the cracks internally or at the ends of the liner-shell interface was evaluated. A number of low and high temperature melting compounds and brazes were applied to determine their ability to wet and adhere to the SiC coating. A first successful pressure check was made with an assembly that had epoxy in the local end areas of the liner-chamber interface. The leak rate of this chamber, when assembled with the injector, was only 1 psi per minute at a chamber pressure of 500 psi. After the first test run, B_2O_3 was melted into the same area where the epoxy had burned out. Neither of these materials provided the necessary seal for a long duration test run.

(U) Concurrently, an analysis of the causes of cracking and potential solutions was undertaken. As the cracks seem to emanate from the transition radii in the throat and the nozzle-chamber entrance, both of which were originally 0.41 inches, it is possible that these radii were too sharp for the stresses that are introduced during assembly. There is an additional factor of discontinuity and potential stress intensification at these two points since the SiC coating tends to be less thick at these points where the flow direction changes rather sharply. Design changes were made which greatly increased these radii and provided a much smoother transition from the large chamber diameter to the small throat diameter.

(U) An analysis of the stresses induced in the liner during assembly shows that they are somewhat different than those for which it was designed and to which it is subjected in actual operation. The basic difference is the thermal stresses caused by the manner of heating. The assembly of liner and shell is effected by heating the shell inductively to greater than 2000°F and then inserting the cold liner into the shell in one to two seconds. The liner is thereby subjected to external heating rather than internal for which it was designed. Basically, external heat on a cylinder causes longitudinal and circumferential tensile stresses at the inner surface and similar compressive stresses at the outer surface.

(U) Reviewing the properties of SiC, it is noted that the tensile strength is only one fourth to one tenth of the compressive strength. This is one of the basic reasons for investigating this composite prestressed design; to keep the inner SiC liner, as well as the graphite, in compression or low tension at all times. Preliminary analysis of the stresses at assembly had assumed that the shell compression (cool down) would act coincidentally with the liner heat up such that no liner cracking problem was anticipated.

(U) The new contour SiC coated graphite liners were effective in reducing the local discontinuity stresses which had caused or contributed to cracking of the inside coating upon assembly into the refractory metal shell. Four of these new liner-shell assemblies were made and only one crack was generated in one assembly (S/N 004 A). Assemblies number 005, 006, and 007 were crack free. To illustrate the change made in the internal contour, two coated liners were sectioned and photographed. Figure 7 shows the original contour on the left and the revised contour on the right.

ORIGINAL AND REVISED CONTOURS

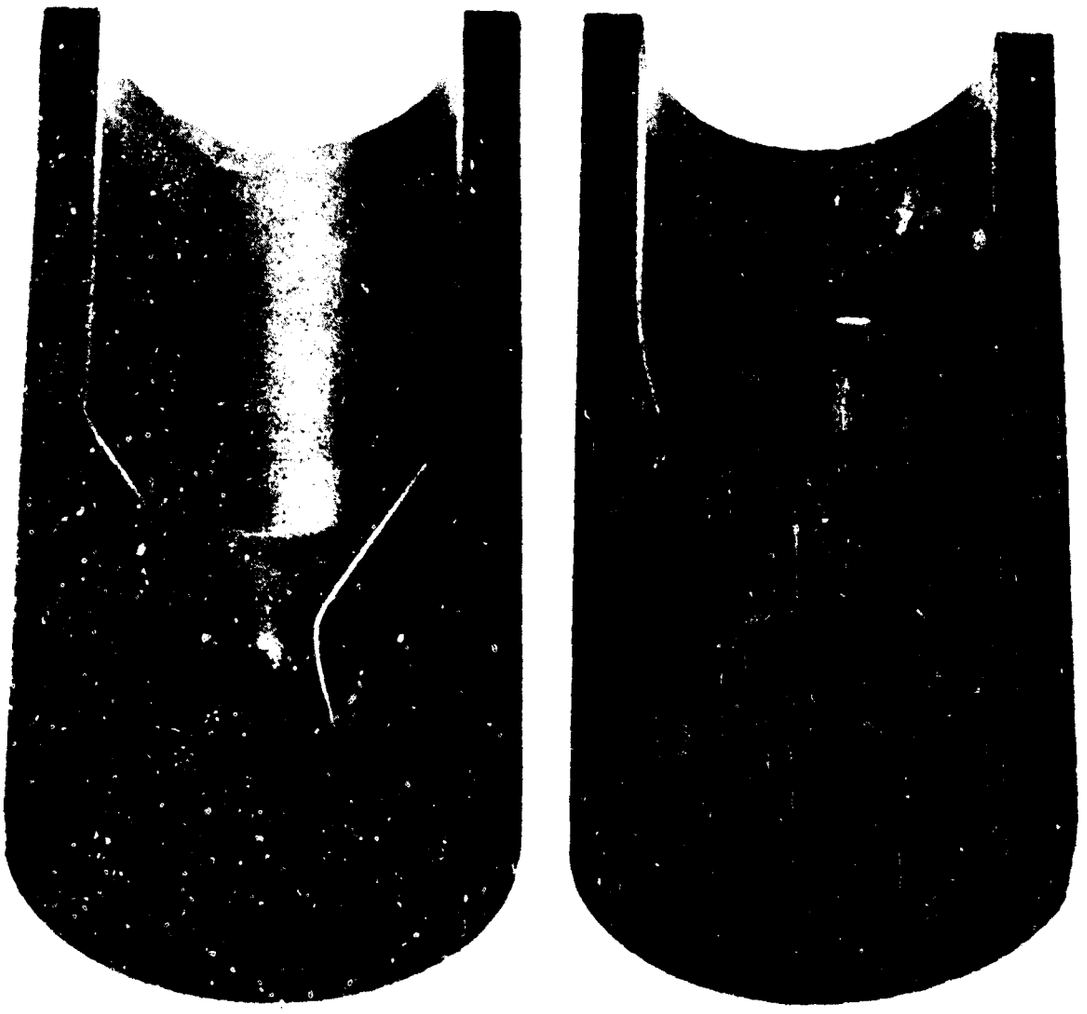

Figure 7

SECTIONED SiC COATED GRAPHITE LINERS

4. Subscale Chamber Fabrication

(U) All subscale chamber liners were fabricated by machining No. 2239 graphite to the subsurface chamber-nozzle contours shown in Figure 7. The RM-005 silicon carbide coating was then vapor deposited onto the graphite substrate. The outer diameter and the end surfaces of the SiC were then ground to a very smooth finish and precise dimensions.

(U) The outer shells were fabricated by rough machining a tube from solid bar stock of Ta-10W, TZM, or 1/2 Ti-Moly. The outside and ends of the shells were machine finished and the inner diameter was ground to a fine finish and a precise dimension for the desired prestress. The shells were then coated with thin oxidation protective coatings. After inspection and smoothing of irregularities in the coating surface, the chambers and liners were ready for assembly.

(U) Insertion of the chamber liners into the shells was accomplished by inductively heating the shells to high temperatures and then rapidly plunging the liners into the expanded shells. Needless to say, alignment of the shell and the respective liner was critical, as was the heating of the shells to a sufficiently high temperature. After the liner-shell assembly was allowed to cool, the unit was then pressure-checked and dye-checked to determine if it was still crack-free and sound. In all, seven liners and shells were successfully assembled.

B. SUBSCALE CHAMBER TESTING

1. Test Facility

(U) All test firings of the subscale thrust chambers were conducted on Pad F of the Aerothermo Laboratory (ATL) test cell complex in the Air Force-Marquardt Test Facility (AF-MJL-VN) at Van Nuys, California. The experimental rocket engines were mounted vertically on a specially constructed support stand for firing down into the exhaust duct. A close-up photograph of a typical test cell installation is shown in Figure 8.

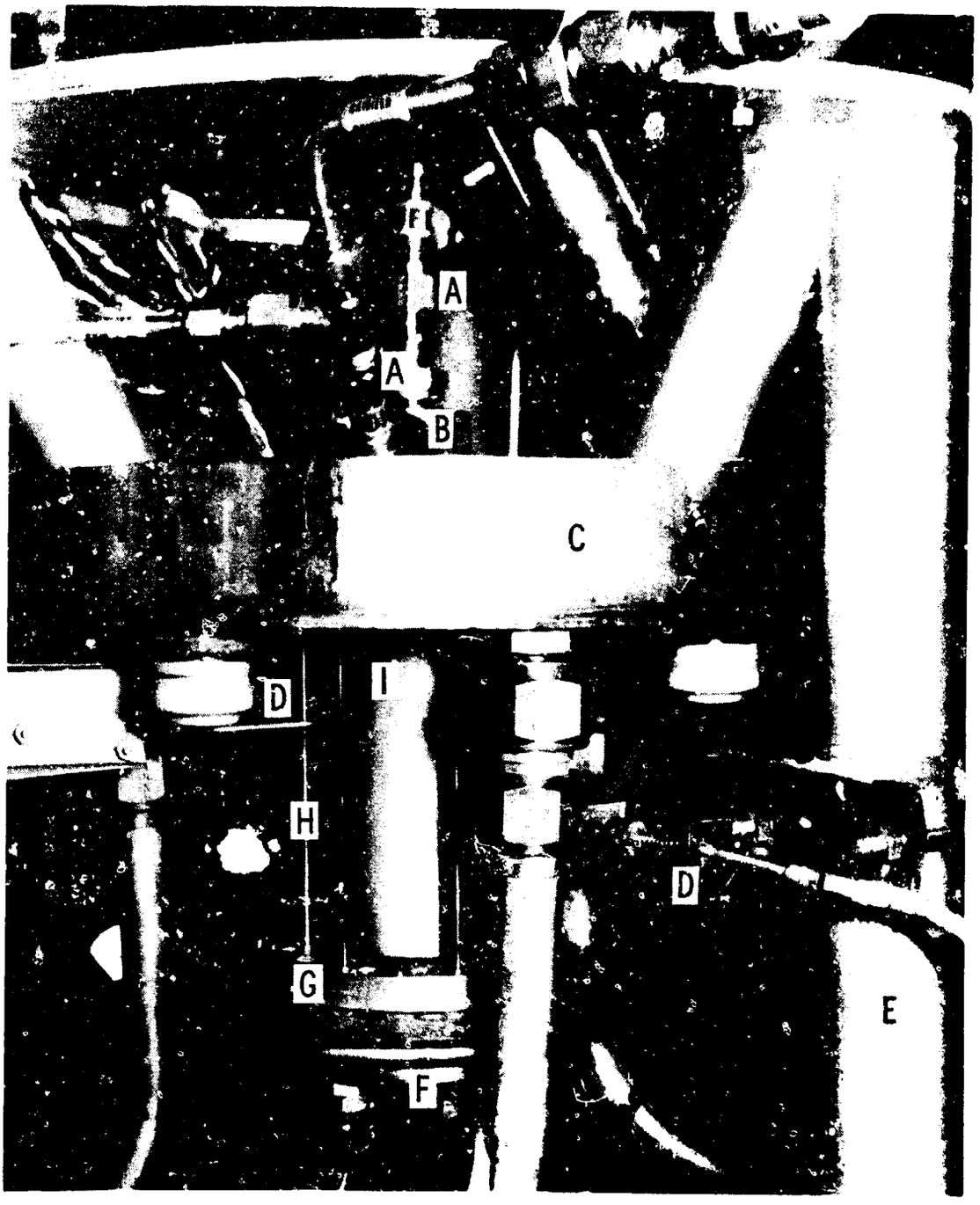

A - PROPELLANTS LINES
B - INJECTOR (8 ON 8)
C - INJECTOR COOLANT SPLASH PAN
D - SPRING LOADED T/C
E - SUPPORT STAND
F - SPRING PLATE
G - END PLATE (TZM)
H - WATER COOLED TIE BOLTS (6)
I - CHAMBER ASSEMBLY

Figure 2

SUBSCALE EXPERIMENTAL THRUST CHAMBER
TEST CELL INSTALLATION

R-21,5[illegible]
Neg. T3336-7

2. Test Results

a. Combustion Performance

(U) As the intent of the subject contract was the development of nonregeneratively cooled thrust chambers, only the combustion performance was computed. No effort was made to determine nozzle performance or to design an optimum nozzle with reduced losses due to separation and boundary layer effects. Based on a theoretical specific impulse of 263 seconds at and O/F of 2.0 and a total propellant flow of 0.400 pps, the nominal thrust level of 100 lbs was achieved. The maximum theoretical gas temperature is reached at an O/F of 2.0, thus providing a critical test of the durability of the SiC coated graphite chambers. In order to evaluate the combustion performance during the test operations, a theoretical determination of the characteristic velocity (C*) as a function of chamber pressure and total propellant flow rate was made for the $N_2O_4/0.5\ N_2H_4$- 0.5 UDMH propellant system. In this computation shifting equilibrium of combustion products was assumed up to the nozzle throat with frozen conditions present in the diverging portion of the nozzle. The results of this computation are shown in Figure 9.

(C) Upon comparing the experimental combustion performance results from Table VI with the analytical computation a discrepancy in η_{c^*} varying from 1% to 20% was found. There are a number of reasons for this as will now be described. A principal loss in combustion efficiency is due to the propellants injection pattern. In the initial mode of injection used in Runs 1-16, a central core of unreacted oxidizer was created. This uncombusted oxidizer produced little net thrust generation and thus contributed to poor combustion performance. That this reason is essentially correct is verified from two observations. First, when the fuel flow rate was maintained constant but the oxidizer flow rate decreased to a lower O/F ratio, as in Runs 10-12, the combustion efficiency increased on the order of ten percent. Second, cold flow tests of the injector head with water flowing from the inner and outer orifices separately and in combination indicated a tendency for the spray from the outer orifices to sheet and converge on the centerline unless interrupted by an impinging stream of sufficient momentum from the inner orifices. Based on these observations it may be concluded that the average combustion efficiency of 80%-85% for this injection mode is not a fundamental limit but rather is due to nonoptimal injection stream impingement.

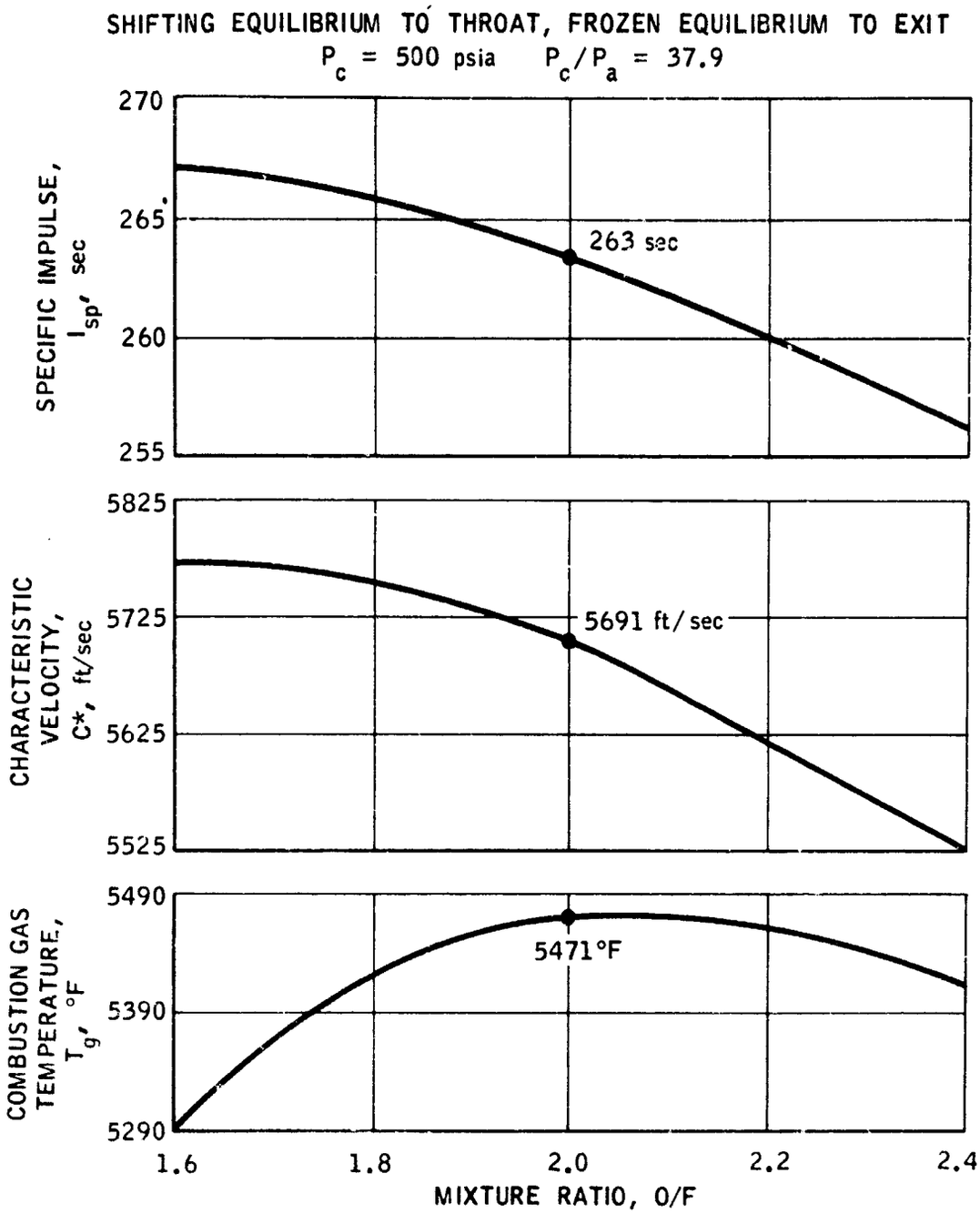

Figure 9

THEORETICAL PERFORMANCE OF N_2O_4/0.5 N_2H_4 - 0.5 UDMH

R-19,282

TABLE VI RUN SUMMARY

SUBSCALE NON-REGENERATIVELY COOLED THRUST CHAMBERS

Run No.	Duration sec	Duration min.	Seal Leak	P_c psia	T_4 °F	T_5 °F	T_6 °F	w_{ox} lb/sec.	w_f lb/sec.	w_t lb/sec.	O/F	C* ft/sec.	η_c* %	COMMENTS
1 & 2	0	--	--	--	--	--	--	--	--	--	--	--	--	Oxidizer valve did not open.
3	3	0.05	no	427	207	309	338	0.250	0.127	0.377	1.97	4944	87	Good run. No damage to copper chamber.
4	6	0.10	no	443	338	495	516	0.262	0.130	0.392	2.01	4909	86	Good run. No damage. P_c too low.
5	0	--	--	--	--	--	--	--	--	--	--	--	--	Fuel valve did not open.
6	3	0.05	no	424	220	340	360	0.284	0.132	0.416	2.15	4430	78.8	O/F too high. Poor performance.
7	0	--	--	--	--	--	--	--	--	--	--	--	--	Fuel valve did not open.
8	16.2	0.27	no	484	1065	1590	1425	0.292	0.141	0.433	2.07	4856	85	Good run. Acceptable conditions. No damage.
9	26.0	0.43	yes	489	--	--	--	(0.316)	0.158	(0.474)	(2.0)①	(4480)	(79)	w_{ox} & T_{wall} instrumentation was inoperative. ① O/F = 2.0 assumed. Fire at chamber seal.
10	18.2	0.30	yes	502	510	780	647	0.246	0.150	0.396	1.64	5500	95.5	O/F too low. Fire at chamber seal.
11	12.6	0.21	yes	495	433	643	600	0.270	0.151	0.421	1.79	5130	89.3	O/F still too low. Fire at chamber seal.
12	24.5	0.41	yes	476	714	844	982	0.238	0.150	0.388	1.59	5320	92.4	O/F too low. Cavitating venturi in oxidizer line not cavitated. Fire at chamber seal.
13	36.9	0.62	yes	436	805	972	1062	0.305	0.151	0.456	2.02	4170	73.5	O/F good. Cavitating venturi in oxidizer line OK. Low P_c because of seal leak.
14	273.0	4.55	yes	439	1740	2120	1830	0.289	0.157	0.446	1.84	3970	69.2	Chamber seal leaking fuel. Run stopped because area contaminated with fuel vapor.
15	601.8	10.03	no	499	1904	1960	1060	0.288	0.151	0.439	1.91	4700	82.2	Good run. No seal leakage. No damage.
16	180	3	no	482	1990	1990	1500	0.292	0.152	0.444	1.92	4800	84.0	Good run. No seal leakage.
	180	3	no	465	2010	2010	1560	0.296	0.148	0.444	2.0	4640	81.5	Restart after 45 seconds.
	60	1	no	460	1860	1890	1390	0.294	0.149	0.443	1.98	4550	80.0	Restart after 30 seconds.
	60	1	no	460	1860	1920	1410	0.296	0.149	0.445	1.99	4580	80.5	Restart after 15 seconds
	60	1	no	455	1910	1860	1420	0.296	0.147	0.443	2.01	4550	80.0	Restart after 15 seconds.
	60	1	no	460	1890	1870	1370	0.296	0.147	0.443	2.01	4600	80.8	Restart after 15 seconds.
17	1.03	0.067	no	520	--	709	--	0.256	0.125	0.381	2.05	5619	98.8	Copper reference chamber - Fuel valve stuck open from contamination fouling.
18	4.05	0.067	no	532	--	777	290	0.263	0.120	0.383	2.19	5575	99.2	Copper reference chamber - lost fuel flow turbine meter - possible injector fuel orifice plugging from contamination fouling.
19	4.05	0.067	no	400	--	338	284	0.265	0.120	0.385	2.21	4080	72.7	
20	4.05	0.067	no	467	--	390	284	0.265	0.122	0.387	2.17	4660	82.9	
21	4.05	0.067	no	555	--	948	451	0.265	0.125	0.390	2.12	5380	95.2	
22	1.38	0.023	no	477	234	175	175	0.270	0.1260	0.396	2.14	5250	93.2	Thrust chamber blew apart shortly after ignition - possible thermal shock.
23	132.0	2.2	no	528	1460	1790	2020	0.273	0.1325	0.406	2.05	5580	95.0	Good run. Seal leak caused shutdown.

Runs 1 through 8 and 17 through 21 used a copper heat sink chamber.

(C) In addition to the above specific reasons, two other generally applicable reasons for poor combustion performance exist. During Runs 9-14, before the chamber-injector sealing technique was perfected, the seal developed a sufficient leak so as to reduce the level of the chamber pressure. This resulted in a significant loss in C* at higher O/F ratios, as evidenced by the data for Runs 13-14. The extent of this effect, however, was quite variable and impossible to quantitatively evaluate. A second consideration, for Runs 1-13 and 17-22 of short duration, is the heat losses to the chamber walls during transient operation. Computations made for engines of 100 lbs thrust level indicate that this correction is of the order of 4%-5% during transient wall heat-up, reducing to 1%-2% following attainment of steady-state wall temperatures. The decrease in heat loss to the chamber walls as a long time run progressed was manifested by a slightly increasing chamber pressure until steady-state wall temperatures were reached. This was evident from the chamber pressure traces recorded during Runs 14, 15, and 16. The low η_{C^*} of the initial short test runs can thus be attributed partly to transient heat losses and the unknown rate and composition of gas leaking by the seal, but was due mainly to the incomplete mixing of oxidizer and fuel.

(C) For the later propellant injection mode the fuel and oxidizer were oriented in the normal positions of fuel through the outer orifices and oxidizer through the inner orifices. A general high level of combustion performance was exhibited with this injector in Runs 17-23, with the possible exception of Runs 19 and 20 when temporary injector fouling was suspicioned. C* efficiencies of 93% to 99% were achieved during these runs, indicating excellent propellant mixing and reaction with this injection mode.

b. Chamber Performance

(U) A total of seven chambers were tested under this program. One of these was a copper chamber which was used for test instrumentation and injector operation checkout runs. The other six were subscale thrust chambers. A description of chamber performance during the significant test runs is presented below to supplement the summary of data previously presented in Table V and Table VI.

(U) The pertinent dimensions, pre-test and post-test conditions of all subscale chamber assemblies were given in Table V. Table VI presents a summary of all test run conditions. For cross reference, the test run number, chamber pressure and test time are listed in each table. During the subscale chamber tests, outer wall temperatures were measured at three stations with spring loaded contact thermocouples. T_4 was located at the throat plane, T_5 was at the chamber-to-convergent intersection plane, and T_6 was located on the cylindrical section of the combustion chamber. Figure 8 is a close-up photograph of a typical test cell installation. Spring loaded T/C (D) on the left side of the photograph measured T_6. The one on the right side measured T_5. T_4 was attached to the rear leg of the support stand and is not visible in this photograph.

(U) Test Runs No. 1-8: Significant results were obtained during Runs No. 3, 4, and 8 of this series with the copper heat-sink chamber. Run times were 3, 6, and 16 seconds respectively. The variables recorded were the head temperature, fuel flow, oxidizer flow, chamber pressure, fuel upstream pressure, oxidizer upstream pressure, fuel temperature, oxidizer temperature, and three chamber wall temperatures.

(C) For the 3-second run, P_c was 429 psia, W_f was 0.127 pps, W_{ox} was 0.250 pps with an O/F of 1.97, yielding a C* efficiency of 87%.[1] The wall temperature reached a maximum of 350°F. As no damage was noted to the chamber or injector, a 6-second run was made with P_c = 443 psia, W_f = 0.130 pps, W_{ox} = 0.262 pps and an O/F = 2.01. The resultant C* efficiency was 86%. In this run the maximum wall temperature was 525°F.

(C) As the chamber pressure was below the desired level, the upstream pressures were increased and a longer run was attempted for 16 seconds. In this run, P_c = 484 psia, W_f = 0.141 pps, W_{ox} = 0.292 pps, yielding O/F = 2.07 and C* efficiency of 85%. The maximum wall temperature was 1500°F. At the conclusion of the run, a blue salt deposit was on all the metal surfaces, believed to be copper nitrate. The throat area actually decreased during the runs, but only slightly.

(U) Test Run No. 9: After the system had been checked out with the copper heat sink chamber, the first subscale chamber was readied for test firing. This chamber assembly (S/N 008) was composed of a SiC coated graphite inner liner, contoured to a chamber-nozzle shape, with

[1] C* efficiencies were not corrected for heat loss.

a 0.10-inch thick, 1/2 Ti-Moly shell shrunk onto the liner. The molybdenum alloy shell was Durak "B" coated for oxidation protection. For the first run, leak pressure seals were made at the ends of the liner-shell interface with epoxy.

(U) The duration of Run No. 9 was 26 seconds. The run was terminated at that time to prevent possible damage to external hardware because flames were observed at the seal. Evidently the epoxy burned out and allowed a small amount of hot gas to pass from the chamber through the liner cracks and then out the end of the liner-shell interface. The chamber pressure remained constant at 489 psia, and although instrumentation malfunctions during this run prevented an accurate calculation of O/F ratio and the performance parameters, an approximate calculation showed them to be in the desired range. A post-run dye check of the SiC liner did not show any cracks that had not been previously evident.

(U) Test Runs No. 10 and 11: After sealing the interface with B_2O_3, the same chamber (S/N 008) was again readied for test. Flowmeters, transducers, and the associated recording devices were checked and recertified for operations. During test Run No. 10, the chamber pressure was constant at 502 psia for the 18.2-second duration, when a similar fire occurred, and the run was terminated. After about 15 minutes, Run No. 11 was made without touching the chamber or resealing the leaks in any way. This run was terminated after 12.6 seconds because of fire in the same location. The length of this run without crack-sealing indicates that the path for leaking gasflow is a rather tortuous one. Most probably, the gas was leaking from a crack in the inner SiC convergent section along the graphite-SiC convergent section along the graphite-SiC interface to a point under the shell where the SiC is also cracked, and from there out to the end of the chamber. This also indicates that the graphite substrate is not cracked, since that would be a straight-through, fast-leak path.

(U) Test Runs No. 12 and 13: were conducted with subscale chamber assembly S/N 002. Pyrex glass and then silver-solder had been melted into the liner-shell interface in a final attempt to seal the internal leaks. The sealing effort was not very successful. Both Runs 12 and 13 had to be terminated after only 24.5 and 36.9 seconds, respectively, because flame appeared at the seal area.

(U) Test Run No. 14: was conducted with chamber No. 007, which had an 0.080-inch thick Ta-10W shell over a revised contour liner. Belleville spring washers were used in this assembly for the first time, to supply a 6000-lb end load to the P.G. seal. All previous tests had been run with die springs providing the seal load. This test was terminated after 4.55 minutes because the chamber seal was leaking, however, no external burning was visible. Even though this was the most successful test up to that time, it was evident from an inspection of the P.G. seal and the chamber pressure decay during the test that the end load was still not sufficient to prevent an initial pressure leak and subsequent erosion of the seal. The seal face of the SiC-coated liner was discolored by the leaks and consequent uneven heating but was not eroded. Some very slight microcracking of the inner SiC liner near the seal end was disclosed by a post-test dye check. Since this did not occur in any of the subsequent chamber tests, it was evidently caused by the uneven heating due to the local seal leak areas. The propellant injection pattern inside this chamber was also unusual in that there were definite streaks deep into the chamber where mixing was inadequate. Since this was the only run in which these marks appeared, the seal leaks must have passed a majority of one propellant and very little of the other. Consequently, for this run it was impossible to calculate the chamber gas conditions with any degree of accuracy.

(C) Test Run No. 15: was conducted with chamber No. 005, another new contour-type liner in a 0.100-inch thick Ta-10W shell. Heavier Belleville washers were used to produce an end load of about 14,000 lb. This test was programmed and run for 601 seconds without interruption or loss of pressure. A pressure check and dye check of the chamber after test showed a pattern of hairline cracks through the nozzle region, and an escaping pressure path like all those previously tested. The most likely conclusion is that the cracking occurred on cooldown after the test, since there were no leaks before or during the test. C* efficiency during this test varied from 82% to 86% at an O/F ratio of 1.91. P_c was steady at 499 psia. This was the longest run time of the test series and from all indications, the chamber could have run for a much longer time, since there was no oxidation or erosion of the inner SiC-coated liner. The measured wall temperatures for this run are shown in Figure 10. The temperature change shown for T_4 and T_6 at 300 to 340 seconds could not be reconciled with any recorded data or observations.

THE Marquardt CORPORATION VAN NUYS CALIFORNIA

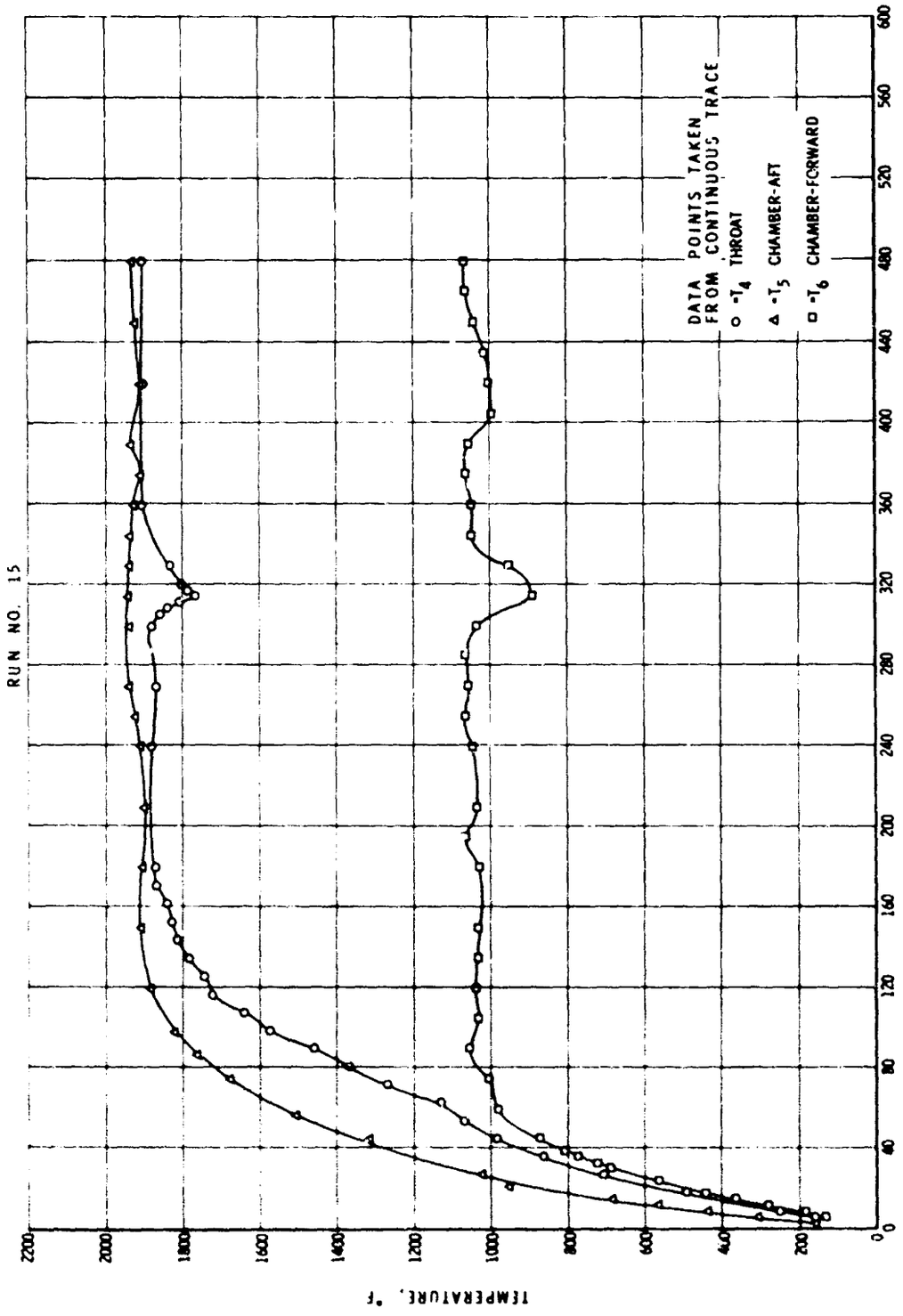

Figure 10
OUTER WALL THRUST CHAMBER TEMPERATURES

R-21,873

(C) Test Run No. 16: using chamber assembly number 006, was the last run to be made with the first injector. The Ta-10W shell was 0.080-inch thick, and there were some cracks in the thin SiC coating at the outer edge of the seal face which had occurred during assembly. The pre-test pressure check showed no leakage, so the test was run with the following sequence; 180-sec run, off 45 sec, 180-sec run, off 30 sec, 60 sec on, 15 sec off, 60 sec on, 15 sec off, 60 sec on, 15 sec off, 60 sec on, run terminated. Propellant flows, C*, and chamber pressure varied during the run with O/F ratios from 1.92 to 2.01, P_c in the range of 482 to 455 psia, and C* efficiencies from 84.0% to 80.0%. P_c changes were due only to slight propellant flow rate changes. The measured wall temperatures for this run are shown in Figure 11.

(C) Test Runs No. 17-21: All of the remaining tests were run with the second injector, which had better performance characteristics at an O/F = 2 than the one used for the previous tests. The first five runs (No. 17-21) were short-time (4 seconds) tests with the copper heat-sink chamber to checkout the injector and propellant flow parameters. High combustion efficiencies (η_{c^*} = 95% - 99%) were achieved during three of these runs, but there was a problem with contaminants in the injector fuel valve and orifices which caused a loss of pressure and low combustion efficiency in Runs 19 and 20. The injector head was cleaned and flushed after Run 20, which disclosed some small metal chips in the fuel distribution passages. These were evidently causing a partial flow blockage which disrupted the fuel-oxidizer impingement pattern. Test Run 21 with the copper heat-sink chamber showed high pressure and 95% η_{c^*}, so the injector was considered qualified for subscale chamber testing.

(U) Test Run No. 22: was run on a heavy wall (0.20-inch) TZM shell chamber (S/N 004-A). The test run on this chamber resulted in the only catastrophic failure of the entire test series. Almost immediately after ignition, flames were visible on both sides along the length of the test chamber. Actually, chamber pressure was recorded for 1.4 seconds and reached a maximum of 477 psia. The thick-wall TZM chamber was found to have shattered (brittle failure) along eight axial lines into approximately equal-size pieces, as well as having broken along some uneven circumferential planes. The fact that the TZM shell broke into eight pieces (which corresponds to the number of injection doublets), as well as the fact that there was no indication of overpressure or hard-start during this or any other run, suggests that the failure was due to thermal

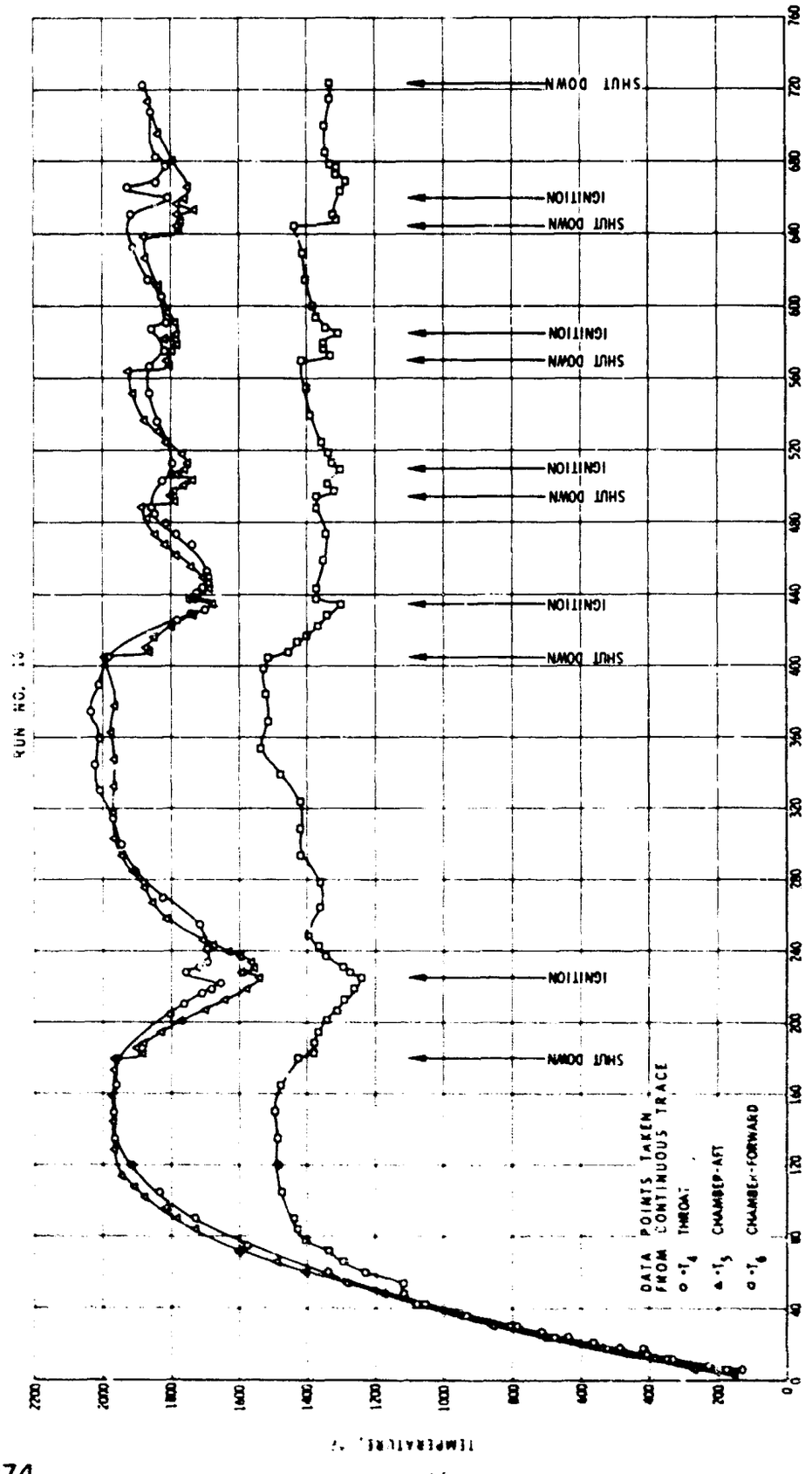

Figure 11
OUTER WALL THRUST CHAMBER TEMPERATURES

shock. The wall of this chamber shell was twice as thick as the 1/2-Ti-Mo shell of chamber No. 008, which had been tested three times with no damage to the shell. A stress analysis of this shell, using the temperatures from the transient thermal analysis, did not indicate stresses of a magnitude sufficient to cause this type failure ($\sigma_{th} \approx 10,000$ psi), so it was probably a combined effect of uneven heating and initial shock loading on the stiff, brittle shell.

(U) One other possible cause of failure was the quality of the material in this particular shell. However, a metallurgical examination of the fractured TZM shell showed no reason to suspect the material quality. Therefore, based on the mode of failure and the knowledge that the Phase II full-scale chambers would require thick shells because of their large diameter, this molybdenum-based alloy was judged potentially unreliable in this application. The tantalum alloys were given primary consideration as the structural material for the full-scale chamber shells.

(U) Test Run No. 23: was conducted with chamber assembly S/N 005. This thrust chamber was tested previously for 10 minutes steady-state at a chamber pressure of ~ 500 psia. As recorded in Table V, numerous hairline cracks had developed in the SiC coating of the nozzle section during test Run No. 15. It was felt that any further testing of this chamber assembly would be a severe test of the chamber concept under the worst possible starting conditions, and as such should prove the potential usefulness of a cracked, inner SiC coating. Without any rework or crack-sealing attempts, this chamber was installed in the test cell as shown in Figure 8, and tested at the conditions shown for Run No. 23 in Table VI. For more than two minutes, the chamber performed perfectly and the exterior temperatures appeared to be about the same as that visually noted during the previous long-time tests. The chamber pressure was steady until a leak occurred at the chamber-to-P.G. seal face. With the appearance of flames at the seal joint, the test run was terminated. The measured wall temperatures for this run are shown in Figure 12. A post-run inspection of subscale thrust chamber No. 005 showed no further cracking of the inner SiC coating, no measurable change in the nozzle throat diameter, and no visible deterioration of the SiC coating in the throat area. Recorded outer wall temperatures were no higher than during previous runs, although there was an indicated change in the area of maximum temperature, possibly due to the different injection mode.

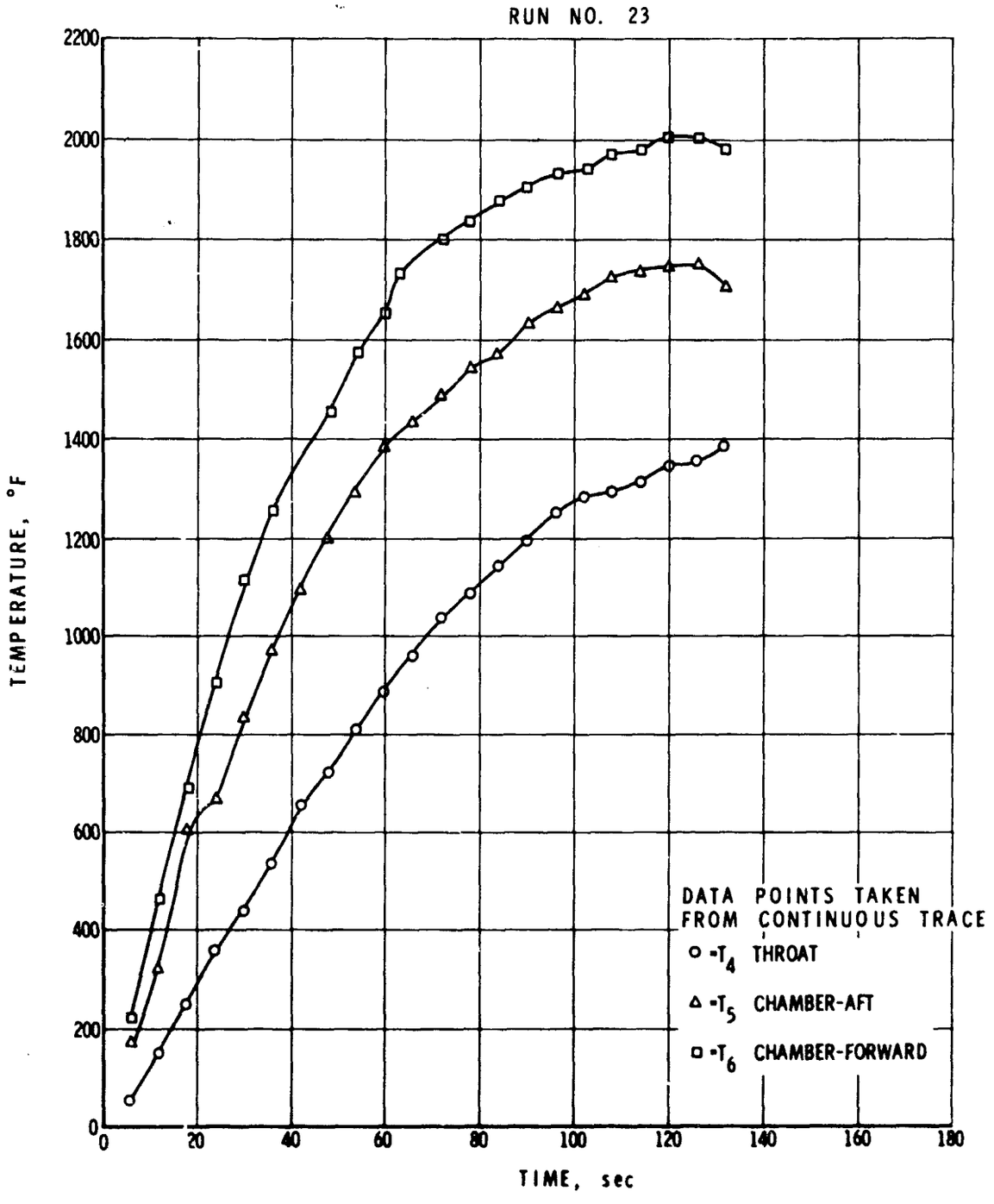

Figure 12

OUTER WALL THRUST CHAMBER TEMPERATURES

(C) Since the η_{c^*} was 95% during this run, and there was no damage to the SiC coating in the throat area or appreciable difference in shell temperature, it appeared that the limit of the Marquardt RM-005 SiC coating had not yet been reached and that all subscale chamber tests, with both injectors, were valid evaluations of the prestressed coated-liner concept.

3. Analytical - Experimental Comparison of Wall Temperatures

(C) As previously mentioned, the measured temperatures along the shell surface during test were considerably lower than those predicted from the analytical model. A number of possible reasons exit for this deviation but the most likely conclusion is that the entire chamber was operating cooler than predicted, due to boundary layer and flow profile effects along the internal wall. It appears conclusively that even though a high combustion efficiency (95% C*) was obtained, fully developed turbulent flow was not present at the wall and so the gas side heat transfer coefficient was lower than used in the analysis. The comparison between analytical and experimental results indicate that the analytical predictions are best viewed as the upper bound to be used for design consideration. The degree to which the experimental results approach this bound will be dependent upon the flow profiles and gas condition along the chamber wall.

(U) During actual testing two injector patterns were operational. In the first condition (Runs 1-16) fuel was directed through the inner 0.035 inch orifices toward the chamber wall with oxidizer flowing out the 0.030 inch orifices toward the centerline. This mode of operation resulted in low local O/F ratios at the chamber wall, thus inhibiting oxidation of the SiC coating. However, this also resulted in some unreacted oxidizer in the central core with a loss of combustion efficiency and gas temperature. The Rupe Number was 0.25 and the resulting momentum angle was 0°. As a consequence of this the wall temperatures, wall O/F and heat flux at the throat were low. In the injector used during the later tests the propellant injection points were reversed with the oxidizer flowing through the 0.035 inch diameter orifices and the fuel through the 0.030 inch diameter orifices. This mode, with a Rupe Number of 0.65, produced high local O/F ratios at the wall and higher combustion efficiences. The resulting momentum angle was 8° outward and was expected to produce a more severe environment for the SiC coating. However, the test with this injector produced no oxidation or erosion of the coating, even in the throat area.

(U) An interesting possibility for improved subscale chamber performance has been suggested by the test results. During some of the initial test runs, O/F ratios in the range of 1.6 were unintentionally obtained and the C* efficiencies were high. This indicates that by proper design and development the orifice sizes and direction could be adjusted to yield low local O/F ratios at the wall and high combustion efficiency. This would eliminate the unreacted oxidizer in the center of the chamber and provide for greater stream impingement and reaction. While a low local O/F at the wall has not been proven a requisite in the present study, such a condition should prove desirable for sustained operation. Also, in the event that higher chamber pressure operation is desired, the lower local O/F ratios should also produce a reduced heat flux in the critical throat region, thus improving coating durability.

IV

FULLSCALE THRUST CHAMBER DESIGN & FABRICATION

A. 5000 LB THRUST CHAMBER DESIGN

(U) The basic design criterion for the fullscale chambers were as follows:

Propellants	N_2O_4/0.5 N_2H_4 - 0.5 UDMH
Mixture ratio, MR	2.0
Chamber pressure, P_c	500 psia
Thrust level	5000 lb at P_{amb} = 13.2 psia
Chamber diameter	6.046 inches
Throat diameter	2.90 inches
Exit diameter	6.76 inches
Exit cone half angle	15°
Propellants flow rate, $\dot{w}$	18.66 lb/sec @ η_{c^*} = 100%
	19.44 lb/sec @ η_{c^*} = 96%
Operation time	10 min. (continuous or with up to 5 restarts)

(U) Like the subscale chambers, the fullscale chambers were composed of a SiC-coated graphite liner encased in a Ta-10W shell. The chamber-to-chamber extension seal was made on the forward flange of the shell. This was a basic change from the subscale thrust chambers in which the seal was made at the liner face. This new sealing method was expected to result in a more crack-tolerant design. Any cracking of the SiC coating which might occur would not result in a pressure-leak path to the outside of the composite motor.

(U) In the design of the first fullscale assembly, shown in Figure 13, a detachable thin-wall Ta-10W exit cone-flange assembly was used to expand the gas to ambient pressure (13.2 psia). The SiC-coated graphite liner extended to a point 2.75 inches downstream of the throat. The overall coated liner length was 8.12 inches, which was set by the maximum length of moulded Carbone 2239 graphite available in the necessary large-diameter size. An Air Force-furnished chamber extension section was used to provide a large L^* (>50).

(U) The selection of materials for this thrust chamber was based on the analyses and evaluations of the Phase I subscale chambers as reported in Section III above. The Marquardt RM-005 silicon carbide provides the high-temperature oxidation and erosion resistance to contain the high-

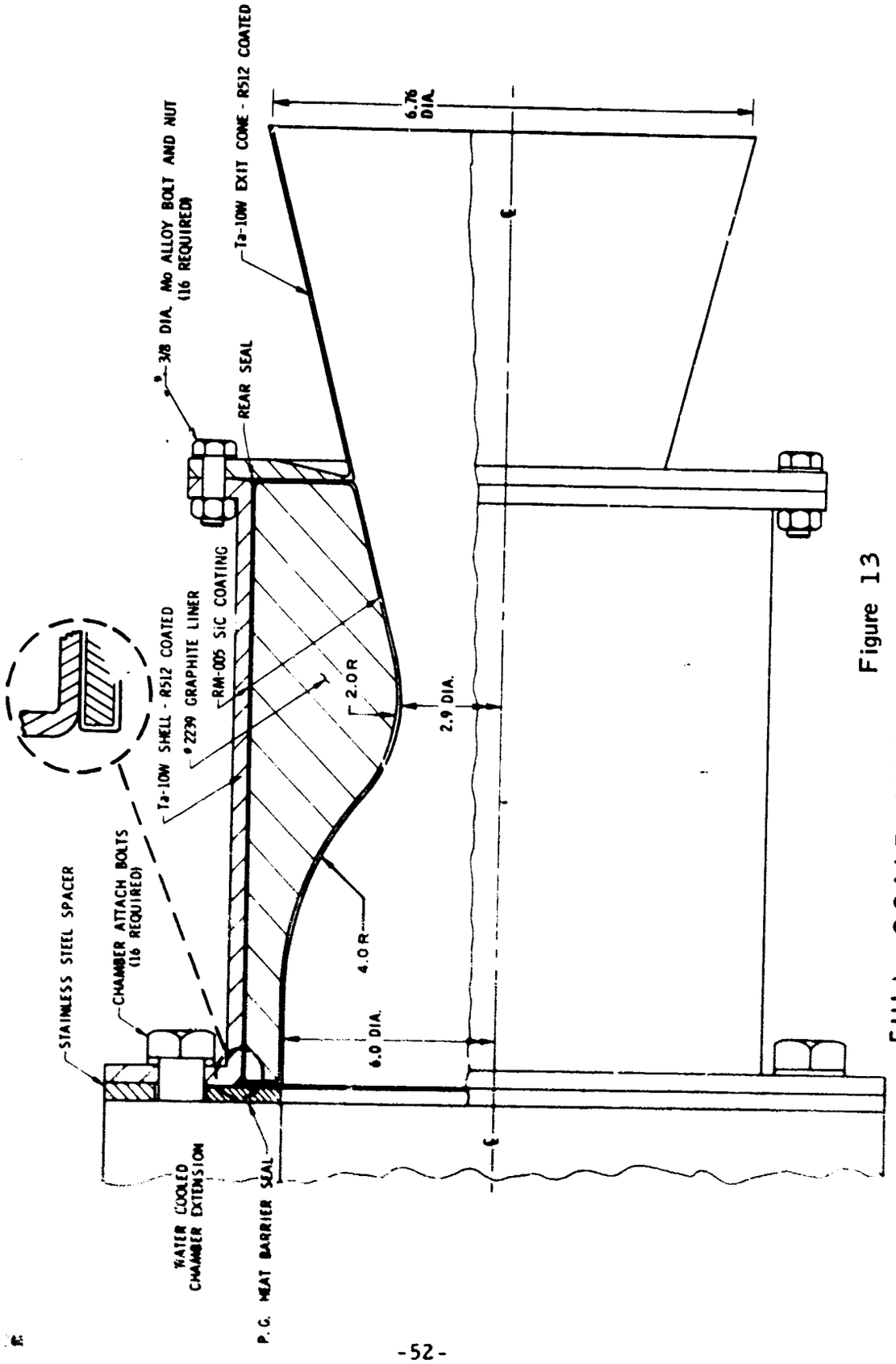

Figure 13
FULL SCALE (5000 POUND) THRUST CHAMBER

pressure combustor gases and retain the internal nozzle contour. The Carbone 2239 graphite provides an appropriate substrate for efficient deposition of the SiC coating, and also provides a heat-sink temperature-reducing medium to allow for effective use of a radiating, refractory-metal outer shell. Ta-10W metal for the outer shell provides a readily workable, ductile case which can be designed to provide the necessary prestress to the coated liner. Smoothly finished pyrolytic graphite proved to be a satisfactory high-temperature, high-pressure seal material when compressed between two equally smooth metal surfaces. These were the basic materials for the thrust-chamber construction as suggested by the results of the subscale thrust-chamber evaluations. The Phase II effort then consisted of: (1) analytically determining the correct proportions of materials, (2) purchasing materials, (3) developing fabrication methods, (4) assembling two motors for hot-firing tests by the Air Force at AFRPL, Edwards, California, and (5) evaluating the test results.

1. Design Analysis

(U) Starting with the basic configuration of a SiC-coated graphite liner encased in a Ta-10W shell, the design was set by considering the materials properties at the expected environmental conditions. Initially, a nominal RM-005 SiC thickness of 0.030 to 0.035 inch was selected, based principally on the following facts:

a) In the subscale tests the SiC coating did not oxidize or erode, so a thick coating was not required for in-firing coating thickness reduction.

b) SiC is basically a brittle, refractory material and is subject to a Weibull-type strength reduction with increasing thickness or volume under stress, thus thin sections can operate at higher stress levels than thick sections.

(U) The wall thickness of the graphite liner was set at 0.50 inches in order to provide a temperature drop, from inner to outer walls, that would allow the Ta-10W shell to operate at a temperature where its creep strength was still sufficient to provide a prestress to the coated liner after 10 minutes of operation.

(U) Based on a deflection analysis of the thrust chamber composite wall (method of compatible deformations), a Ta-10W wall thickness of 0.20 inches was found to be the minimum that would provide the desired

initial prestress to the inner SiC coating and still hold the liner in compression after 10 minutes of operation. In this analysis one of the major differences between the subscale and fullscale chambers was found to be the necessity for the materials of construction to have relatively close thermal expansions. Ta-10W has a higher α than the graphite and the SiC and thus tends to expand away from the liner and relieve the prestress. The molybdenum alloys that could also be used for the shell have an α lower than Ta-10W, but still higher than SiC and graphite. This effect was relatively inconsequential in the small chambers, but was a definite factor in the design of the large-diameter chambers. At the shell wall design temperature of 3000°F, the radius change (δ_r) due to free expansion would be about 0.010 inch greater for the Ta-10W shell than for the graphite liner. Of course the graphite would expand somewhat more than a consistent 3000°F temperature would indicate, since the inner part of the wall is at a higher temperature than the outer wall. However, it was believed necessary to design to a sufficient initial prestress interference to meet the goal of 10-minute operation.

(U) The initial fullscale chamber design was made considering the following facts primarily:

a. The Ta-10W shell was the pressure-retaining case, and as such would be subjected to the 500 psi chamber pressure when the shell had expanded away from the liner. Under this pressure load, at the 3000°F operating temperature, the shell would undergo an elastic, circumferential strain that would result in a radial deflection of 0.0035 inch.

b. If the Ta-10W case were to operate at this temperature and pressure level for ten minutes, it would creep plastically 0.3%. This would result in a radial deformation of 0.011 inch, unrecoverable. (Ref. 6, pg 956)

c. The difference in thermal expansion between the liner and shell would tend to unload the shell up to 0.010 inch, radially.

d. If the microcracking of the SiC coating should occur as it did in the subscale chambers, an inner SiC coating that was not loaded in compression would tend

to open up and allow the hot combustion gases to reach the graphite substructure. SiC has a lower coefficient of expansion than graphite, which is another tendency toward crack expansion at steady-state temperatures. With open cracks, the possibilities of graphite oxidation and even gas flow along the graphite-SiC interface are enhanced. This could undermine the support for the inner SiC coating and reduce the restart capability of the thrust chamber.

e. The analysis of as-assembled stresses in the SiC coating of the liner and in the Ta-10W shell showed them to be quite high with a high initial interference. However, due to initial uncertainties in the analytical procedure, the decision was made to attempt an assembly with a high radial prestress value that would accommodate the pressure, creep and thermal deflections noted above. If this could be accomplished, the thrust-chamber assembly would be theoretically capable of meeting the service life requirements within the design boundary conditions. It was anticipated that microcracking of the SiC coating would occur, with its attendant stress relief, thereby allowing the composite thrust chamber to perform as designed.

(U) As discussed later, in the fabrication section of this report, the initial assembly was not satisfactory, due to the high interference loads. However, the inner SiC coating failure did lend credence to the analytical procedure that had predicted high stresses in this thrust-chamber component. For the subsequent assemblies, the initial stress in the coating was reduced first by starting with less radial interference and additionally by increasing the coating thickness.

(U) Before making the design interference load and coating thickness changes, the original design was re-evaluated to find out what improvements could be made, and to review the selection of the original proportion of materials through the composite wall. Consideration was given to all recognizable factors affecting the selection of component thicknesses in the design. Starting with the RM-005 SiC coating on the inner surface, the following points were noted:

a. The assembly loads put the coating in compression. A very thin or highly loaded coating would tend to fail in a buckling instability mode.

b. The chamber concept requires a radiation, heat-sink-cooling type of operation (non-regeneratively cooled). There is a temperature drop through the entire wall composition. The ΔT through any homogeneous material section creates a stress which is directly proportional to the material thickness. Thus, a thicker SiC coating would have higher thermal stresses, which are additive to other circumferential and axial stresses caused by configuration, pressure, and preload. Also, it can accommodate less stress because of its lower strength with increased thickness. Thus, a thick SiC coating would tend to crack easier than a thin one, while providing a more stable structure for compressive buckling loads.

c. The SiC coating had not been oxidized or eroded in the subscale tests, so a thin coating would be sufficient for surface protection. Heat flux to the wall is theoretically less in a large-diameter chamber than a small one for the same gas conditions and mass flow per unit area, although injector effects could change this locally.

d. Thus, the SiC coating should have a thickness great enough to resist buckling, yet thin enough to retain high strength and resist the thermally induced stresses.

(U) For the graphite substrate, the following points were reviewed:

a. Its function is to provide support for the SiC coating and a temperature drop from inner to outer wall so the Ta-10W wall can run cooler.

b. If it were thicker, it would drive the temperature of the SiC coating up while reducing the shell temperature.

The SiC could be damaged by excessive heat. Thicker graphite would compress more under the initial prestress ($\epsilon = \sigma t/E$) thus providing less strain to the liner and shell. This would tend to be a desirable condition since a high radial interference could be used which would not highly stress the shell or liner coating, yet would provide a spring-type radial growth to take up some of the expansion difference between liner and shell.

c. With the theoretical lower heat flux in the large thrust chambers, a nominal 0.5 inch thickness of graphite was selected for the chamber section, compared to 0.25 inch for the subscale chamber section. The graphite thickness at the throat is a function of the required nozzle contour and is not subject to any design change possibilities. Minor changes in graphite thickness would have equally minor effects on the temperature and stress patterns, except as noted; thus the original design thickness was deemed satisfactory.

(U) Since the graphite and SiC were necessary, complementary items (required substrate for deposition of SiC), the major design variation possibilities were in the selection of material and configuration for the outer shell.

a. Ta-10W was the prime contender from among the refractory metals due to its fabricability, low-temperature ductility, high creep strength at operating temperature, and successful use in the subscale chambers. It was felt that the expansion difference would be overcome by a high initial radial interference. Refractory metals are expensive, heavy, not available in unusual shapes such as large tubes, and difficult to form from available stock. Fabricarion, then, was a primary consideration.

b. The effect of a design thickness increase of the shell is to increase the shell stiffness and the SiC coating stress, while lowering the initial and operating shell stresses. Additional thermal blockage with higher overall composite wall temperatures, and a heavier thrust chamber are other consequences of a thick shell wall.

c. Ideally, from a weight and low initial SiC compressive stress standpoint, a very thin shell wall would be desirable. However, since it must also react the interference loads and the chamber pressure, it must be thick enough to resist these loads without excessive deformation or internal stress.

(U) At this point, an obvious question is, how can the basic design be changed to reduce the loads on the shell such that it can be made thinner. The interference load could be lowered only if the shell material had a lower coefficient of expansion. Otherwise, the shell would expand away from contact with the liner at steady-state temperatures, leading to the possibility of fracture of the graphite substrate, particularly with a hot restart. The pressure load (from chamber pressure) could be removed from the shell surface by making the seal at the forward edge of the SiC-coated liner, instead of on the shell flange.

(U) However, since this was intended to be a light weight design, changing the seal area was not possible because of the leak possibilities and the stress and expansion state of the shell; i.e., if a crack should develop across the forward SiC seal face, it would be a straight-through leak path to the outside ambient pressure. Also, the end loads required for pressure sealing of the P.G. seal are carried through the shell. This would create a high axial stress and strain in the thin Ta-10W shell. During operation, the shell would expand (axially) more than the SiC-coated graphite liners, thereby removing the preload and allowing the seal to leak. This type of seal can only work with external loading that does not expand more than the coated liner, such as the cooled end-to-end bolts used in the subscale tests. With these design and operation conditions imposed, it was not possible to change the pressure sealing method.

(U) Since the shell load pattern could not be modified, it had to be designed to resist the anticipated loads. The initial interference stresses are relieved by expansion during operation, so they are secondary to the selection of wall thickness. Axial shell load, due to chamber pressure, is also a secondary consideration since it results in a low stress. The primary factors were the elastic (recoverable) and plastic creep (non-recoverable) expansion due to pressure-induced hoop stresses at operating temperature. The 0.2-inch wall thickness was seen to be a reasonable value as determined by the original boundary conditions.

(U) Then, in order for subsequent assemblies to be produced for test, some compromises would have to be made in the liner configuration which would reduce the as-assembled compression stress in the SiC coating. The possible variations were to increase the thickness of the coating or lower the initial design interference. The first composite wall chamber for test was assembled with a nominal 0.010-inch radial interference in the nozzle area, tapering in the chamber area to 0.007 inch at the forward edge. The SiC coating was intended to be 0.030 to 0.035-inch thick, but was actually deposited to only 0.026-inch thick. Thus, it was more highly stressed and more susceptible to compressive buckling instability than had been intended. It was recognized that restart capability had probably been compromised, but if the Ta-10W shell should actually operate at as low a temperature as the subscale chamber shells, even this capability loss would be minimal.

(U) After the hot-firing test of the No. 1 chamber assembly had resulted in almost total loss of the inner SiC coating by mechanical breakup, a second liner was designed and fabricated. In this unit, the SiC coating thickness was increased to 0.090 inch, and the interference values remained about the same as for the No. 1 test chamber. The method of computing the initial interference-induced stresses is presented in the following section. An analyses of test results and design effects is presented in the final section of this report.

2. Deflection and Stress Comparison of Composite Wall Chambers

(U) Reviewing the basics of this concept, it should be noted that the SiC is deposited as a continuous coating, completely surrounding the graphite substrate. The outer SiC surface has a larger diameter than the inner diameter of the Ta-10W shell. Assembly is made by thermally expanding the shell and inserting the cold, SiC-coated graphite liner. At ambient temperature this produces an effective P_o at the Ta-10W-to-SiC interface which deflects the shell outward from its unassembled equilibrium position and the SiC-coated graphite inward from its unassembled equilibrium position. The assembled equilibrium position of the interface depends on the relative deformation resistances of the individual or combined chamber components. The following paragraphs describe the method of compatible deformations that was used to compute the as-assembled deflections and stresses in both the sub- and full-scale thrust chambers.

1. The Ta-10W shell is free to move outward (no external restraint) and its deflection under an internal load is thus resisted only by the stiffness of its cylindrical shell. The radial deflection for this component under a uniform internal load P_o is:

$$\delta = \frac{P_o r^2}{Et}$$ (circumferential strain only: no end load present)

2. The inner SiC coating (cylindrical section) is similarly free to move inward under an external load. The radial deflection for this component under a uniform external load P_i is:

$$\delta = \frac{P_i r^2}{Et}$$

These deflections can be calculated on the basis of unit pressure loadings, δ/P, the reciprocal of which will be a reasonable approximation of the spring rate, k, for that component.

3. Between the inner and outer shells there is a cylinder of graphite which is "thick-walled" at the nozzle section, transisting to almost "thin-walled" at the combustion-chamber section. Where it is thin-walled, the equations above would describe its free motion (no external or internal restraint) to external or internal pressure loads. The Lamé equations for thick-walled cylinders can be used to describe the free motion of the thick-walled sections, where the deflections of the inner and outer surfaces are not the same.

Deflection of thick-wall cylinder:

due to external pressure, P.

$$\delta_{r_o} = P \frac{r_o}{E} \left(\frac{r_o^2 \quad r_i^2}{r_o^2 - r_i^2} - \nu \right)$$

$$\delta_{r_i} = P \frac{r_i}{E} \left(\frac{2 r_o^2}{r_o^2 - r_i^2} \right)$$

due to internal pressure, P.

$$\delta_{r_o} = P \frac{r_o}{E} \left(\frac{2 r_i^2}{r_o^2 - r_i^2} \right)$$

$$\delta_{r_i} = P \frac{r_i}{E} \left(\frac{r_o^2 \quad r_i^2}{r_o^2 - r_i^2} + \nu \right)$$

(U) The relative deflections per unit radial pressure load, and the spring rates of the individual components can thus be calculated, but a realistic analysis of the composite deflections and stresses requires something more. Specifically, the graphite is not free to move under load, either radially inward or outward. The inner SiC coating restricts its inward motion and the outer Ta-10W shell restricts its outward motion. There is also a very thin, < 0.010 inch outer coating of SiC on the graphite, but the effect of this is small and is neglected in this analysis.)

(U) The equilibrium position of the shell-liner interface can be calculated by knowing the relative deformation resistances and finite deformations of the inner and outer structures at that position. For a two-cylinder system the analysis is statically determinate by use of the equations noted above. The three-cylinder system used here is statically indeterminate and requires an iterative calculation process to approximate the stresses and deflections of the individual components. Since there are definite variations in the properties of materials used in these thrust chambers and incomplete determination of these variations, it was felt that an approximate analysis method would be adequate. It was assumed that sufficient characterization of the individual component deflections and stresses in both subscale and fullscale chambers could be made as follows:

1. The individual component deflections per unit load could be calculated for unrestrained cylinders at the throat, and through a chamber station. (δ/P).

2. The spring rate for each component could be calculated. ($k = 1 \div \delta/P$). In the thick graphite sections there are four δ/P values and four k values. Two each at the inner surface and at the outer surface because of different response to internal and external loads.

3. Since the Ta-10W shells are shrunk onto the SiC-coated liners, the problem is to find the combined resistance of the graphite and SiC. Initially it was assumed that the spring rate of the SiC plus an average of the graphite spring rates (due to external load) could be added for direct comparison with the shell rate. This would determine the proportions of initial interference absorbed by the shell and by the coated liner, with the SiC and graphite acting as parallel springs.

$$\left(\%\text{ of interference to shell} = \frac{k_{SiC}\ k_G}{k_{SiC}\ k_G\ k_{Ta\text{-}10W}} \times 100\right)$$

4. After the determination of the relative deflections of the Ta-10W outer shell and the SiC plus graphite inner liner, the tensile stresses (σ_t) in the shell are calculated from the δ/P and $\sigma_t = \frac{Pr}{t}$ relationships.

5. Next, approximations of the deflection and compressive stress in the SiC coating are made by assuming the SiC reacts all of the inward radial deflection (δ_{r_i}). This would provide the theoretical maximum interference load that could be transmitted to the inner SiC coating if the graphite were incompressible, i.e. if it transmitted the load without being internally deformed. From this an unachievable maximum compressive stress in the SiC is calculated.

$$\left(\sigma_c = \frac{Pr}{t}\right) \text{ where } P = P_i = \frac{\delta r_i}{(\delta/P)_{SiC}}$$

6. The calculations above are based on thin wall hoop stress and deflection formulas which disregard radial strain through the wall, except in the thick wall graphite at the throat sections. When the equivalent P_o to move the graphite through the distance, δ_{r_i}, was calculated, in most cases it was found to be small in relation to the equivalent P_o on the Ta-10W shell and the P_i on the SiC coating. Thus, even though it would take a very low load to move an unsupported graphite cylinder through the required distance, the graphite is actually transmitting much higher loads between the inner and outer cylinders. In the process of transferring these loads the graphite must be compressed radially.

7. As it is being compressed radially, the graphite is essentially reducing the initial prestress interference. i.e. interference that is absorbed by radial strain in the graphite is not transmitted to the SiC or Ta-10W. Thus the approximate interative process begins with certain additional assumptions as to the stressed condition of the graphite. First, the linear compressive strain ϵ_G (radial) in the graphite is computed by assuming the graphite is loaded by an intermediate percentage of the average of P_o and P_i less the effective P_o to deflect the graphite through the distance δ_{r_o}. The compressive strain from this calculation is subtracted from the

initial interference, Δ. New values for P_o and P_i are then calculated and compared with the assumed pressure difference compressing the graphite. This iterative process is continued until the assumed and calculated pressure values converge and the actual radial strain in the graphite is determined. At this point the radial displacements and strains through the composite wall are known and the acting P_o and P_i can be calculated. With these more realistic pressures, hoop tension and compression values in the Ta-10W shell and the SiC liner can be calculated with the assurance that they are reasonably correct.

(U) The results of these calculations are shown in Table VII for three subscale configurations and both fullscale thrust chambers. The material properties used in conjunction with the dimensions shown in the table were as follows:

Young's modulus at room temperature:

$$E_{Ta\text{-}10W} = 20.6 \times 10^6 \text{ psi}$$

$$E_{Graphite} = 1.0 \times 10^6 \text{ psi}$$

$$E_{SiC} = 30.0 \times 10^6 \text{ psi}$$

Poisson's ratio:

$$\text{Graphite} = 0.50$$

The modulus of 30×10^6 psi for SiC is based on some previous tests of RM-005 SiC coated retangular graphite bars in bending. Silicon carbide is generally reported as having a modulus of about 60×10^6 psi. The precise effect of a E_{SiC} change of this magnitude has not been calculated, but it would have the following general effect. The SiC coating would be twice as stiff (resistant to deformation) as it was calculated to be. This would change the deflection pattern such that more of the initial radial interference would be transferred to the Ta-10W outer shell and less to the inner SiC coating. The effect of a higher SiC modulus of elasticity would be to significantly lower the as-assembled compressive stress in the liner.

TABLE VII

COMPOSITE WALL THRUST CHAMBERS - DEFLECTION AND STRESS COMPARISON

	SUBSCALE CHAMBERS						FULLSCALE CHAMBERS			
	BASIC DESIGN		S/N 005		S/N 006		ASSY NO. 1		ASSY NO. 2	
	CHAMBER	THROAT	CHAMBER	THROAT	CHAMBER	THROAT	CHAMBER	THROAT	CHAMBER	THROAT
Component Dimensions (inches)										
RM-005 SiC coating thickness, t_{SiC}	0.010	0.011	0.055	0.055	0.037	0.037	0.026	0.026	0.090	0.090
Ta-10W shell thickness, $t_{Ta\text{-}10W}$	0.100	0.100	0.100	0.100	0.080	0.080	0.200	0.200	0.200	0.200
SiC inner radius, r_1	0.875	0.206	0.875	0.202	0.875	0.208	3.027	1.450	3.023	1.450
SiC outer radius, r_2	0.905	0.236	0.930	0.257	0.912	0.245	3.053	1.476	3.113	1.540
Graphite outer radius, r_3	1.165	1.165	1.165	1.165	1.165	1.165	3.548	3.552	3.546	3.550
Ta-10W inner radius, r_4	1.175	1.175	175	1.175	1.175	1.175	3.555	3.562	3.556	3.560
Ta-10W outer radius, r_5	1.275	1.275	.275	1.275	1.255	1.255	3.755	3.762	3.756	3.760
Liner-Shell Radial Interference, Δ	0.005	0.005	0.005	0.005	0.005	0.005	0.008	0.010	0.006	0.010
Stiffness, δ/P (10^{-6} in./psi) | Spring Rate, $k=(P/\delta)$ (10^6 psi/in.)										
Ta-10W shell	0.729 | 1.37	0 .. | 1.37	0.729 | 1.37	0.729 | 1.37	0.895 | 1.17	0.895 | 1.17	3.24 | 0.309	3.24 | 0.309	3.24 | 0.309	3.24 | 0.309
SiC coating	0.681 | 1.335	0.54 | 18.5	0.493 | 2.03	0.032 | 31.3	0.718 | 1.39	0.046 | 21.8	11.85 | 0.084	2.75 | 0.364	3.69 | 0.287	0.828 | 1.21
Graphite - "thin wall"	4.12 | 0.243		4.66 | 0.215		4.25 | 0.235		22.0 | 0.045		25.6 | 0.039	
outer r, due to external P		0.684 | 1.46		0.785 | 1.42		0.694 | 1.44		3.26 | 0.307		3.42 | 0.293
inner r, due to external P		0.491 | 2.04		0.540 | 1.85		0.512 | 1.95		3.57 | 0.280		3.79 | 0.264
outer r, due to internal P		0.099		0.118		0.106		1.46		1.64
inner r, due to internal P		0.374		0.411		0.390		2.83		3.02
δ to Ta-10W shell, percent	50.1%	93.7%	62.3%	96.0%	58.2%	95.2%	29.5%	68.1%	51.3%	82.9%
Deflection, δ_{r_a} (inches)	0.0025	0.0047	0.0031	0.0048	0.0029	0.0048	0.00236	0.00681	0.00308	0.00829
Deflection, δ_{r_i} (inches)	0.0025	0.0003	0.0019	0.0002	0.0021	0.0002	0.00564	0.00319	0.00292	0.00171
Equivalent P_a on Ta-10W shell (psi)	1440	6410	4280	6580	3400	5320	730	2100	950	2560
Equivalent σ_t in Ta-10W shell (psi)	(42, 100)	(78, 800)	(52, 400)	(80, 500)	(51, 700)	(64, 500)	(13, 200)	(38, 400)	(17, 300)	(46, 800)
Equivalent P_i on liner (psi)	2840	5550	3860	6260	2910	4400	470	1160	840	2070
Equivalent σ_r in SiC coating (psi)	(84, 200)	(40, 900)	(63, 300)	(26, 200)	(70, 500)	(26, 900)	(55, 000)	(65, 400)	(28, 600)	(34, 400)
Equivalent P_a to deflect graphite δ_{r_a} (psi)	600	630	420	370	490	390	260	890	110	450
Compressive pressure on graphite, P_G (psi)	2200	2660	3070	2870	2050	2600	340	640	750	1300
Graphite strain, ϵ_G (in.)	0.00059	0.00249	0.00075	0.00263	0.00054	0.00242	0.00017	0.00134	0.00032	0.00262
Effective radial interference, Δ_i (in.)	0.00461	0.00251	0.00425	0.00237	0.00446	0.00258	0.00783	0.00866	0.00567	0.00738
Deflection, δ_{r_a} (in.)	0.00221	0.00235	0.00264	0.00228	0.00259	0.002456	0.00231	0.00590	0.00290	0.00611
Deflection, δ_{r_i} (in.)	0.00220	0.00016	0.00161	0.00009	0.00187	0.000124	0.00552	0.00276	0.00277	0.00127
Acting P_a on Ta-10W shell (psi)	3020	3210	3600	3110	3030	2875	715	1820	895	1890
Hoop tension in Ta-10W shell (psi)	37,000	39,500	44,100	38,100	46,000	43,700	13,100	33,300	16,400	34,500
Acting P_i on SiC coating (psi)	2495	2930	3260	2970	2400	2700	465	1005	795	1540
Hoop compression in SiC coating (psi)	74,100	21,600	53,400	12,400	57,900	16,500	54,400	55,600	27,100	25,500

(U) Conversely, a higher SiC modulus of elasticity has a deleterious effect on the thermal shock or thermal stress that the coating can sustain without fracture. This arises since the allowable ΔT is inversely proportional to the modulus of elasticity, E. A comparison of relative thermal shock resistances for the subscale and fullscale thrust chambers is presented later in this report.

(U) Returning to the data in Table VII, it should be noted that this is only a presentation of as-assembled component deflections and stresses. The subscale chambers selected for this comparison were; (1) the basic design, (2) S/N 005 which had run for 602 seconds continuous plus 132 seconds in a subsequent run, and (3) S/N 006 which had run for 600 seconds intermittently with five restarts. A comparison of these with the two fullscale configurations shows the basic differences in the initial stressed state of the SiC coatings and the Ta-10W shells.

(U) In the No. 1 fullscale chamber assembly, it can be seen that the hoop compression stresses in the throat section SiC coating are higher than in any of the other throat sections. This is partly because the thickness was below the design range; however, the coating stress would still have been in the 50,000 psi range. In the chamber section of this assembly, the initial SiC stress was in the same range as that in the two highly successful subscale test chambers. The increased thickness of SiC in the No. 2 assembly resulted in a considerable lowering of the initial compression stresses. Although the chamber section coating stress was reduced to about half that in the subscale chamber sections, the stress in the throat-section coating was still higher than in the equivalent subscale throat section. With the present configuration bounds, this is about the minimum acceptable value for a coating assembly stress.

B. 5000 LB THRUST CHAMBER FABRICATION

(U) The basic materials for this chamber were Carbone 2239 graphite for the liner substrate, Ta-10W for the shell and Marquardt's RM-005 silicon carbide for the liner protective coating. Round moulded graphite was purchased in the maximum size available (9.0 OD x 8.25 inches long) and machined to the chamber-nozzle contour. After machining, the graphite liners were coated with SiC by vapor deposition. After coating, the outside diameter and the rear face were finished by grinding to a very fine finish and precise dimensions.

(U) The flanged cylindrical shell of Ta-10W was somewhat more difficult and time-consuming to fabricate. Large-diameter tube or pierced rod was not available in any reasonable length of time, so the starting material was purchased from NRC in the form of 0.3 inch thick plate. The shell assembly was made by the following process:

1. Press-brake-form cylinder from Ta-10W plate (intermediate stress relief).
2. Fit longitudinal joint and E.B. weld.
3. Rough-machine cylinder.
4. Rough-machine forward and aft flanges.
5. E.B. weld flanges to cylinder, X-ray inspect.
6. Finish-machine flanges and cylinder O.D.
7. Finish-machine and grind cylinder I.D.
8. Have Sylcor R512 coating applied.
9. Finish-grind cylinder I.D. and flange seal areas.

After this final clean-up, the shell was ready for assembly with the SiC-coated graphite liner. The Ta-10W exit cone assembly was fabricated by roll-forming the cone from 0.040-inch thick sheet, seam welding, and then final welding to the rear flange. After final machining, this part was also coated with R512 by Sylcor. Attachment of the exit flange to the shell was made with 0.5% Ti-Mo nuts and bolts. These were not available commercially, so they were machined in-house and coated with Durak "B" by the Chromizing Corporation.

(U) Water-cooled steel bolts were fabricated for attachment of the chamber assembly to the Air Force water-cooled chamber extension section. The pressure seal between sections was made by compressing a P.G. gasket between the flange faces. The gasket and flange faces were lapped to an 8 microinch finish. After final assembly of the thrust chamber and chamber extension, it was plugged in the throat and capped at the forward end for a 500 psi pressure check.

(U) Two 5000 lb thrust chamber assemblies were completed for hot-firing evaluation by the Air Force at AFRPL, Edwards, California. A detailed description of the fabrication effort on individual components and assemblies is presented below.

SiC Coated Graphite Liners

(U) Originally, four liners were machined from Carbone 2239 graphite and coated with RM 005 silicon carbide. One of these was an inferior piece of graphite which has visible voids at the internal machined surface. This piece was used only to help set the coating deposition parameters. The second liner coated showed evidence of some surface flaking but was also useful to evaluate O.D. and rear face grinding procedures. The third and fourth liners were coated and finish ground. Both were apparently suitable for test use, even though there was some microcracking and spalling of the coating on the ground surfaces. The interior SiC coated surfaces were of a general high quality. The best one of these (liner S/N 003) was used for the first trial assembly into the Ta-10W shell. A photograph of this liner is presented as Figure 14.

Ta-10W Flanged Shell

(U) The Ta-10W plate was power-brake-formed to a cylindrical shape which could be closure-welded and finish machined to the required inside diameter. End scraps from the plate were then prepared for electron beam (E.B.) weld evaluation. E.B. weld evaluations were first made at the Hughes Research Laboratory with their 3 KW Hamilton-Zeis machine. Narrow specimens ($\sim$ 0.4 inch) were originally welded and looked satisfactory upon initial examination. However, sectioning and metallographic examination (after polishing and etching) showed insufficient penetration and some voids in the weld area. After further trials and metallurgical and chemical examinations, it was determined that the Hughes machine was not powerful enough to weld this thickness of Ta-10W, even with two passes. A two-pass joint had also been designed in which the lower half of the joint would be flush-butt-welded and then the upper half of the joint would be strip-filled before welding. Because of the low-power capacity of the machine, even this method was not completely satisfactory. The Elektron Standard Company was then approached to determine their capability of welding this thickness of Ta-10W.

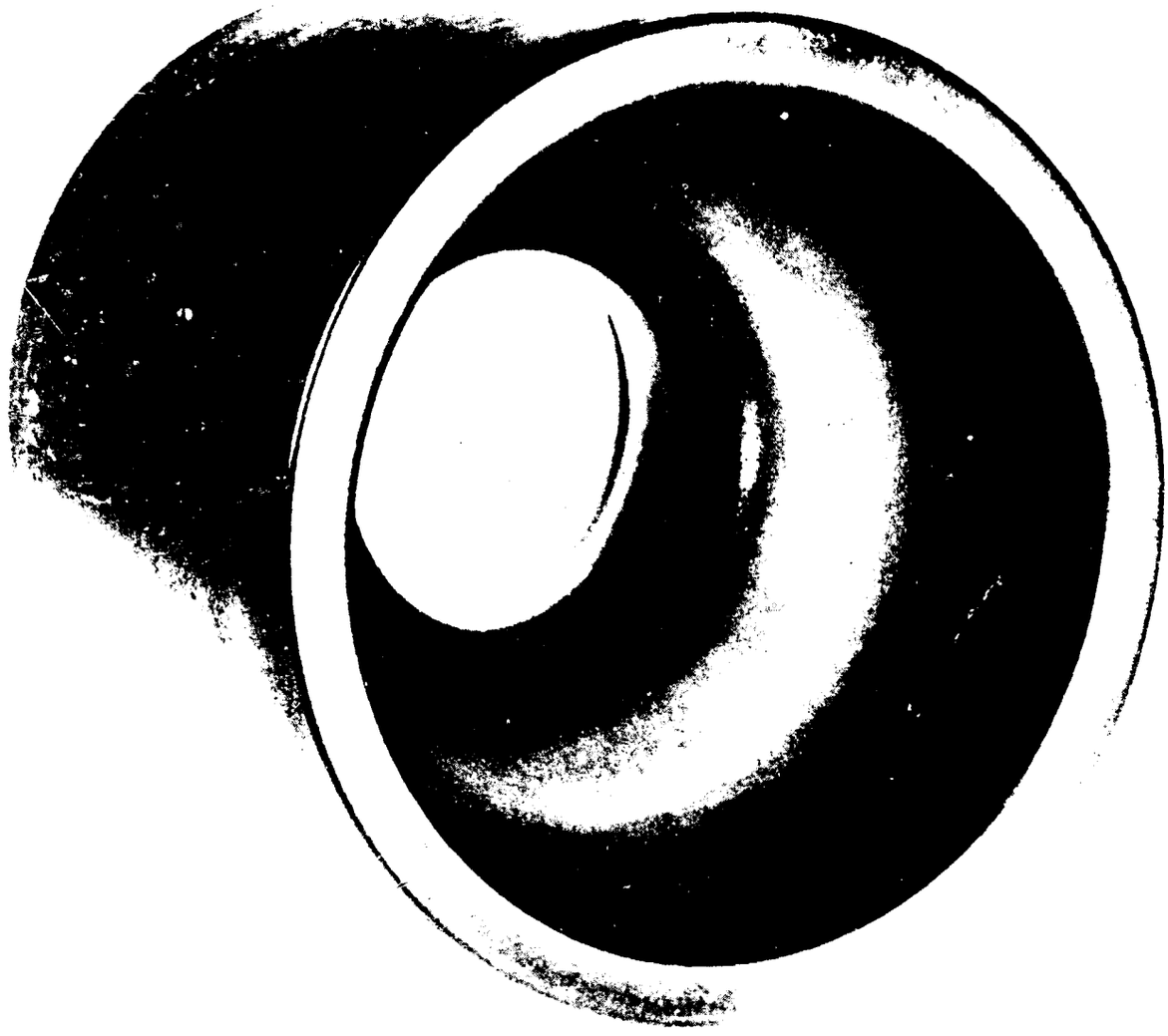

Figure 14

RM-005 SiC COATED GRAPHITE LINER

6 INCH DIAMETER - 5000 POUND THRUST CHAMBER

R-21,946
Neg. 8128-1

(U) After a number of additional trials and weld examinations, electron beam welding of this thick material (0.30 in.) was accomplished at Elektron Standard, with a 6 KW welder. A strip of 0.040-inch thick Ta-10W was used as a backup behind the joint. The beam was set to penetrate through the joint and into the backup strip, but not through it. In this manner, the molten material is contained and full joint material thickness is achieved with little or no undercutting. Without the backup, the weld parameter settings were extremely critical and either insufficient penetration occurred or the beam passed through the material, undercutting at top and bottom.

(U) After the longitudinal seam weld was made, the ends of the cylindrical shell were machined so the flange weld joints could be made. Backup strips were again used to contain the beam. The assembly was then X-ray inspected at a vendor facility with a million-volt unit. The seam weld and the forward flange weld were Class I welds, but the aft flange joint had some minor voids. Since these were minor and the material is ductile, the part was accepted for use. After X-ray inspection, the assembly was ready for final machining on all surfaces. When the machining was completed, the thrust-chamber shell was shipped to Sylcor in New York for application of the R512 oxidation protection coating. Final grinding of the inside diameter and the seal face were accomplished after coating, to ready the flanged chamber for liner installation. Figure 15 shows this unit in the as-coated condition.

Ta-10W Flanged Exit Cone

(U) The exit cone was first roll-formed from 0.040-inch thick Ta-10W sheet and E.B. seam-welded. The cone was trimmed and the flange machined to match the exit diameter of the SiC-coated liner. Then the cone was E.B. welded to the flange, final machined, and shipped out for R512 coating. Figure 16 is a photograph of this assembly after coating.

Attachments and Seals

(U) Water-cooled bolts, coolant distribution manifolds and coolant lines were fabricated using standard processes. The 0.5% Ti-Mo bolts and nuts (for attachment of the exit cone flange to the rear shell flange) were designed and fabricated with a slightly rounded thread form. Because of the brittleness of this material at room temperature, it was difficult to machine to precise dimensions. However, by selective fit

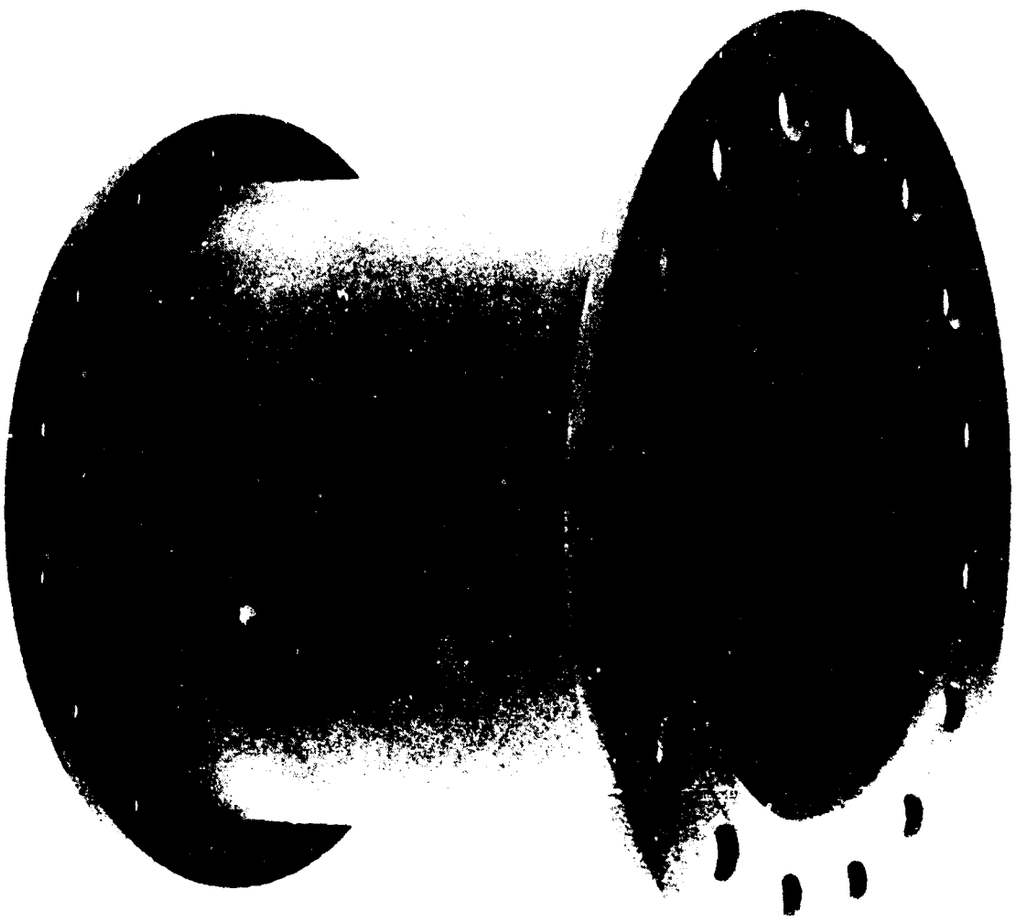

Figure 15

R512 COATED Ta-10W SHELL ASSEMBLY

5000 POUND THRUST CHAMBER

R-21,966
Neg. 8128-4

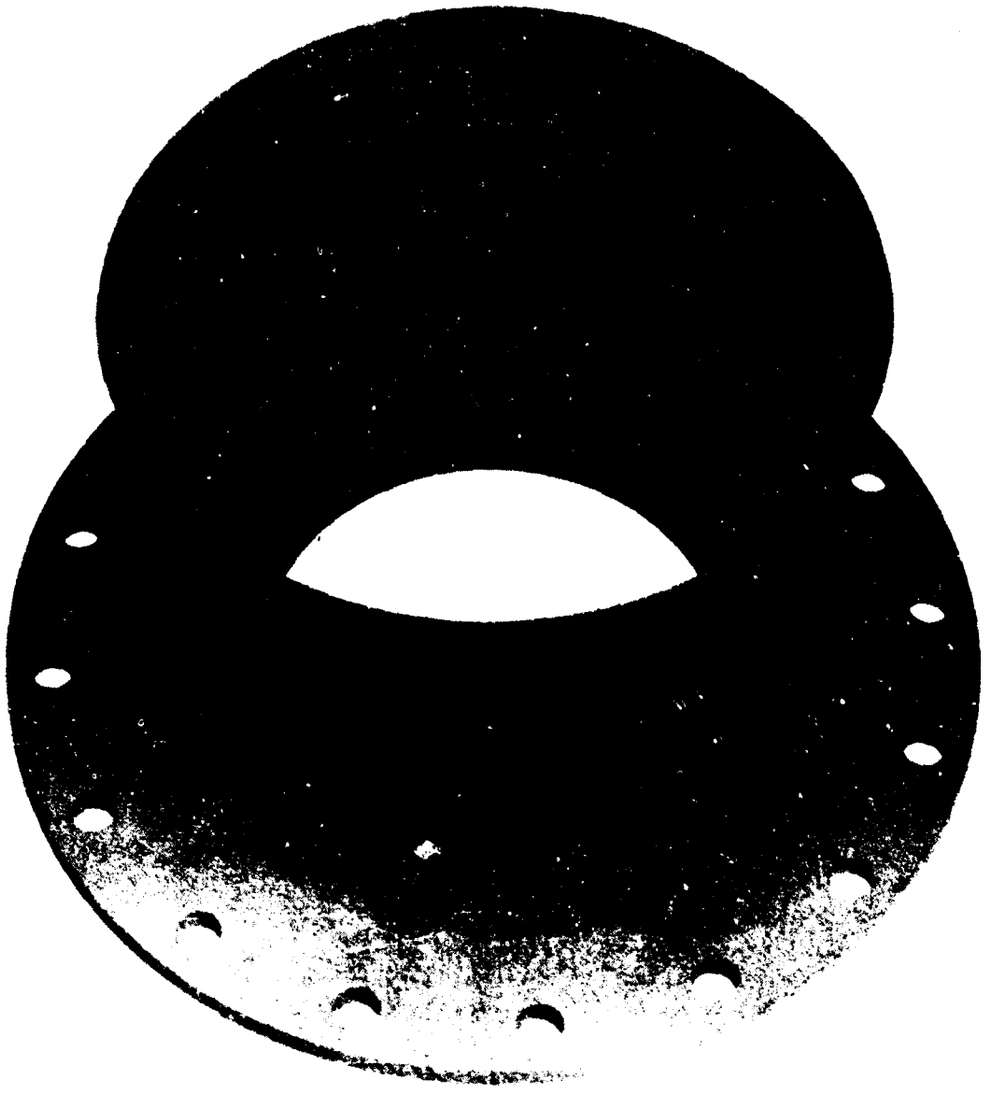

Figure 16

R512 COATED Ta-10W EXIT CONE ASSEMBLY
5000 POUND THRUST CHAMBER

R-21,945
Neg. 8128-3

of the 16 nuts and 16 bolts, the individual tolerance effect was minimized. Only one of the bolts was broken during the few times that the joint was assembled. Light torque loads were used since the joint would tend to tighten up under heating conditions (Ta-10W expansion is greater than 0.5% Ti-Mo).

(U) Pyrolytic graphite washer-type seals were easily machined, and then lapped to a precise thickness dimension and a fine surface finish. The hardware mating surfaces (chamber extension and the coated shell) were also finished to a very smooth, flat surface conditions, so that an effective pressure seal could be easily made.

Shell-Liner Assembly

(U) With the shell fabricated to a smaller diameter than the SiC-coated liner, it was necessary to expand the liner before the assembly could be made. A simple assembly fixture was designed and fabricated to assist the rapid insertion of a SiC-coated liner into the heated shell. Figure 17 is a photograph of the fixture showing the liner attached to the rod of a fast-acting air cylinder. In operation, induction coils are wrapped around the shell below the liner. A heat shield is placed below the liner to keep it cool and unexpanded. When the shell has been inductively heated to the required temperature ($\sim$2500°F), the heat shield is removed and the air cylinder actuated by an electrically operated solenoid valve. Liner insertion is accomplished in less than 0.5 seconds by this method. Thus, the liner can be fully inserted before the shell can cool and contract. The assembly procedure was thoroughly checked out and no problems were encountered during this step of the operation.

(U) The first assembly of a SiC-coated liner into the flanged shell was made with a high radial interference liner. The assembly went as planned; however, some cracking and spalling of the SiC coating in the throat section was evident on cool-down from the assembly heat cycle. The assembly was made on a Friday afternoon, and some additional spalling occurred in the combustion chamber and convergent section at some time during the weekend. Figure 18 is a photograph of the first assembly, showing that the coating has been completely lost in the chamber area and forward edge, except in the one small, light area at the bottom of the picture. Further into the chamber and nozzle convergent section, areas of thin SiC coating can be seen. Four laminations were evident in the remaining coating. Microscopic examination of a full thickness section of coating from the throat

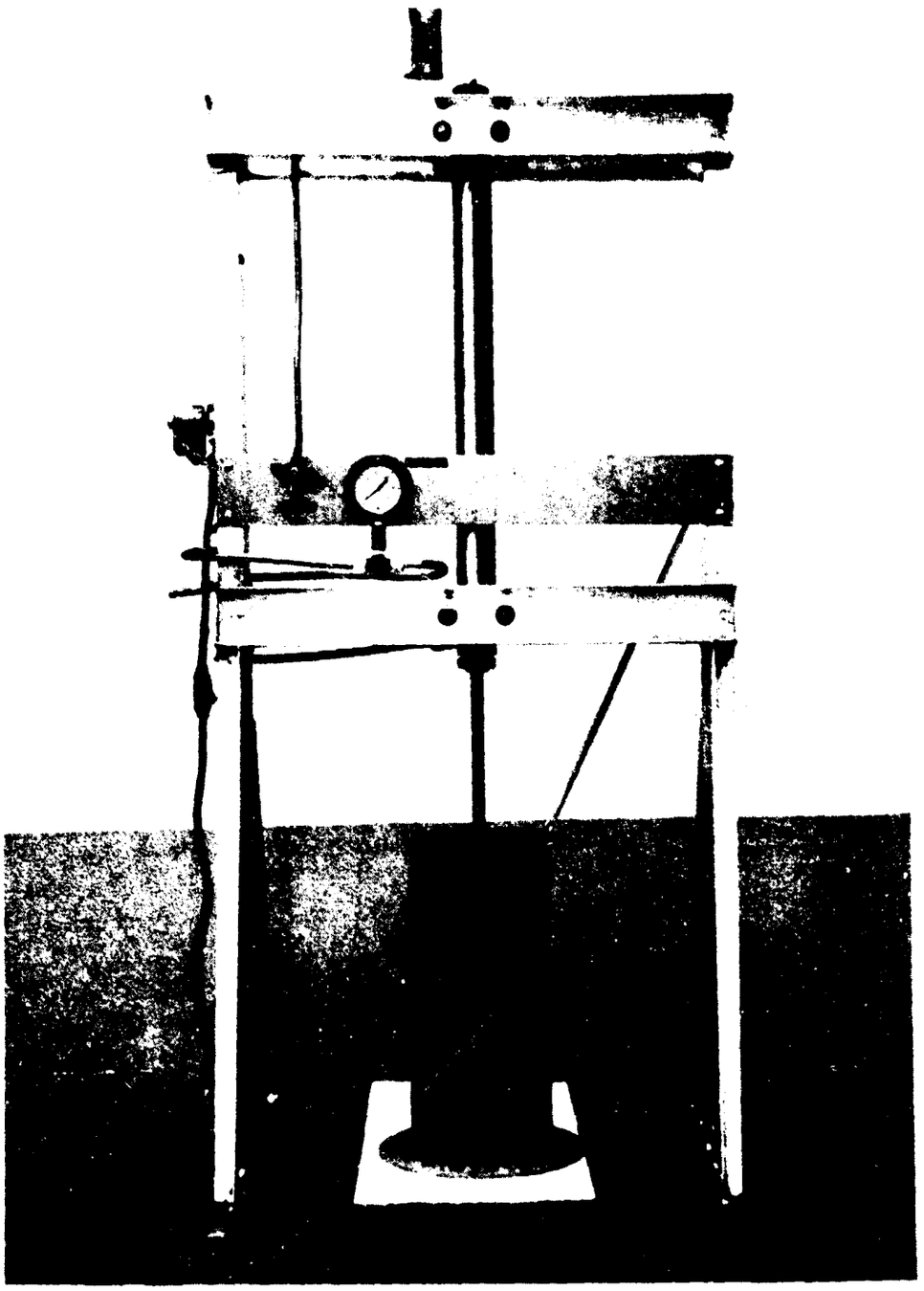

Figure 17

ASSEMBLY FIXTURE

5000 POUND THRUST CHAMBER

R-21,967
Neg. 8128-6

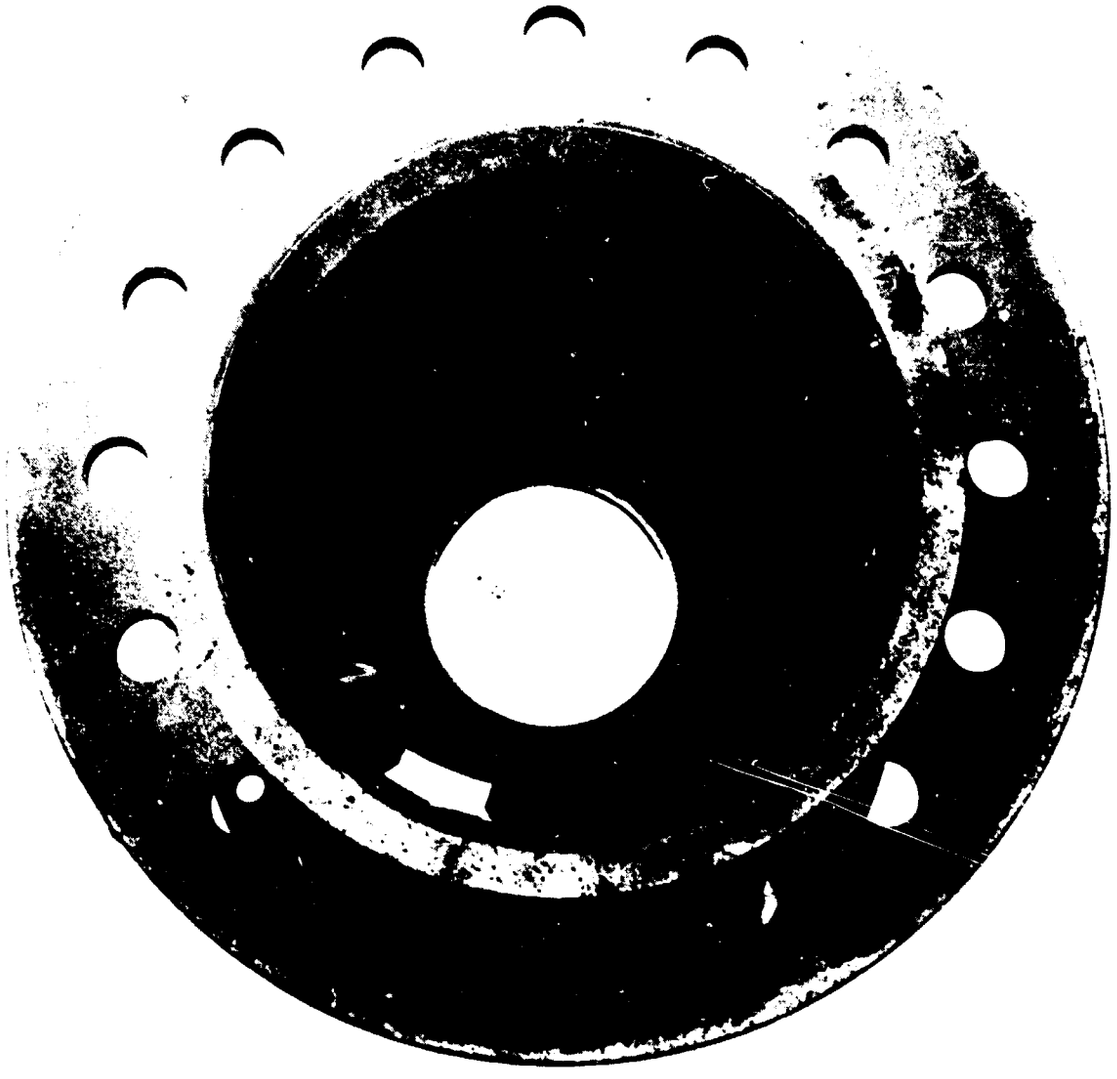

Figure 18

FIRST ASSEMBLY - SiC COATING FLAKED

5000 POUND THRUST CHAMBER

R-22, 336
Neg. 8128-7

area showed at least 9 laminations and a high carbon content in the material. This type of structure is attributed to temperature and/or flow interruptions in the vapor deposition process.

(U) The laminated coating composition resulted in a structure that was unstable under the high compressive loads imposed on it in this assembly. Two possible corrective measures were available, and both were undertaken. First, a new graphite liner was designed to apply a reduced compressive stress to the inner SiC coating. Second, coating deposition variables were re-evaluated and more finely controlled.

(U) This assembly was made without incident. Figure 19 shows this liner-shell assembly which was designated Test Assembly No. 1. The coating composition and appearance were excellent, although the thickness was less than desired. No coating was lost during this assembly, and only minor microcracking of the surface occurred at circumferential areas at the throat and the entrance to the convergent section. Cracking was less pronounced than in the majority of the subscale assemblies.

(U) After attachment of the exit cone, the nonregeneratively cooled thrust chamber was bolted to the water-cooled chamber extension section. The entire assembly was successfully pressure-checked at 500 psi, and then transported to AFRPL for setup and test. The completed assembly is shown in Figure 20.

(U) When this No. 1 test assembly lost the inner SiC coating by mechanical breakup during a 5-second hot-firing run, the entire chamber design was reviewed and some modifications made for the second test assembly. Figure 21 is a cross-section drawing of the second fullscale thrust-chamber assembly. This differs from the first assembly (Figure 13, page 52) in the following respects:

1. The inner RM 005 silicon-carbide coating thickness was increased from a nominal 0.030 to 0.090 inches. The actual change was from 0.026 to 0.094 for the two test assemblies.

2. The SiC-coated graphite liner was shortened on the forward end to allow full radial prestress to the coated liner end. Due to the radius on the I.D.-to-forward face of the Ta-10W shell, the first liner was not loaded in this area, and the liner partially fractured on startup with the resultant loss of coating and substrate protection. (See inset, Figure 13)

3. With the shortening of the liner, a space of less than 0.2 inch was created, which was filled with a pyrolytic

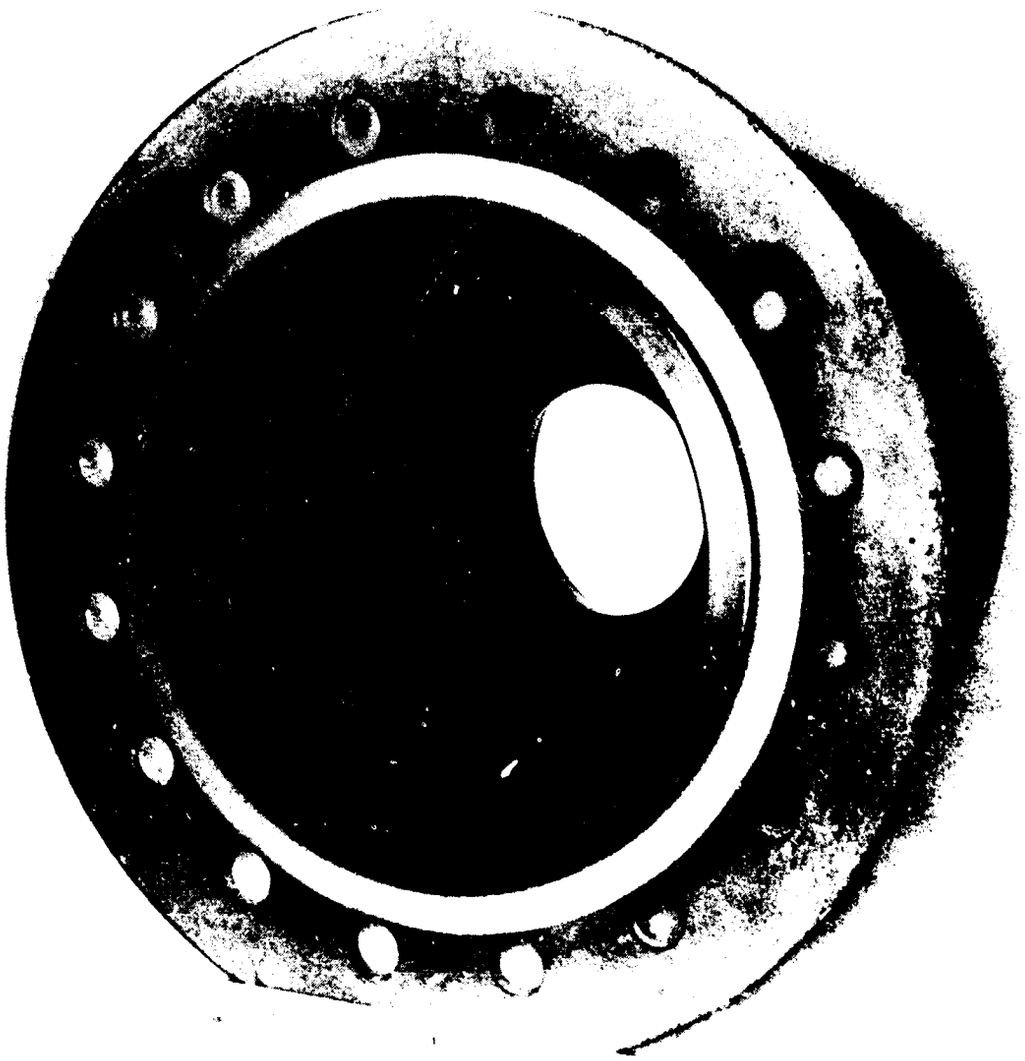

Figure 19

SiC COATED GRAPHITE INSERT
Ta-10W SHELL ASSEMBLY

5000 POUND THRUST CHAMBER

R-22, 337
Neg. 8128-10

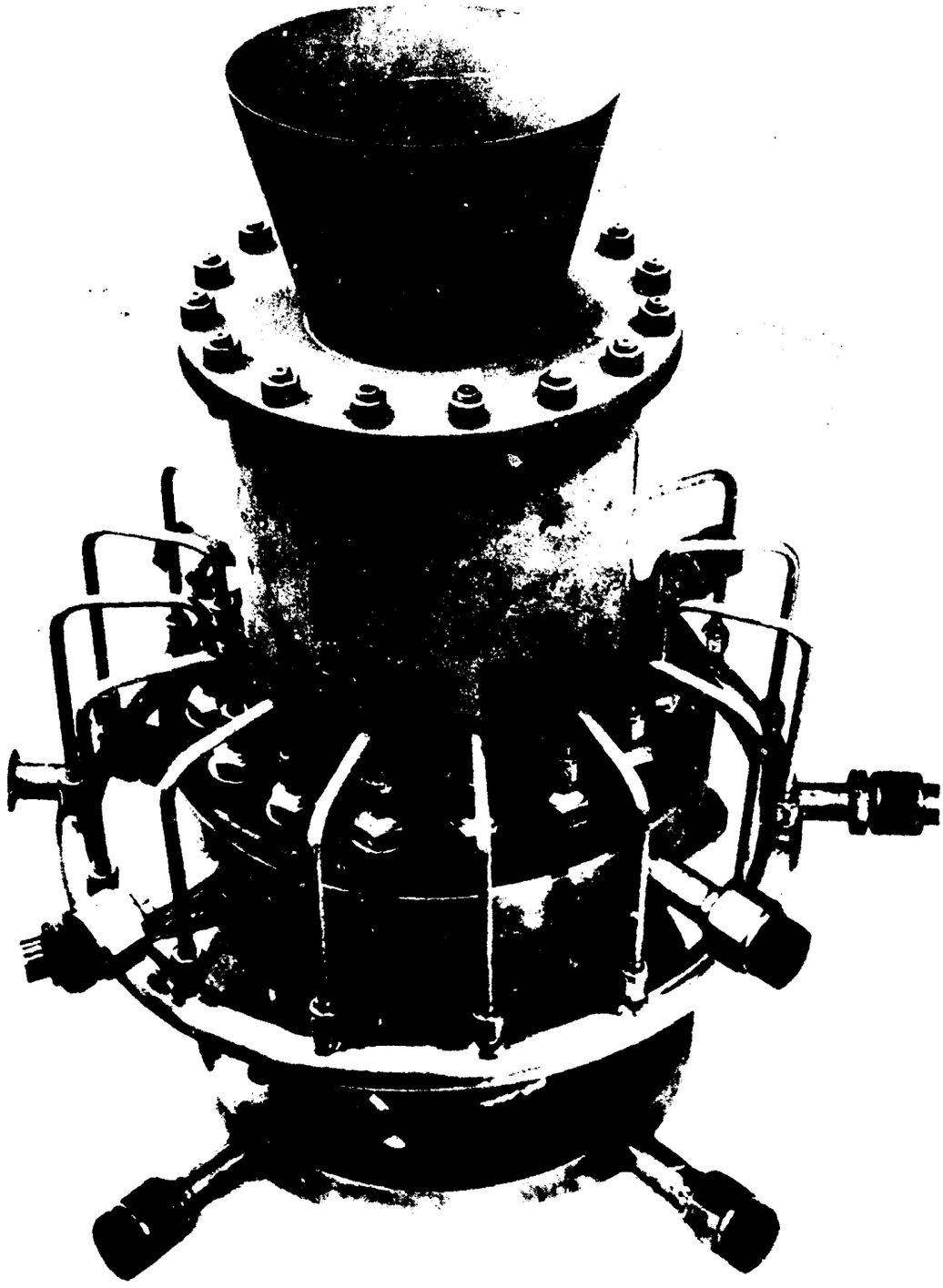

Figure 20
5000 POUND COMPOSITE THRUST CHAMBER ASSEMBLY NO. 1
AS ASSEMBLED

R-22,393
Neg. 8128-14

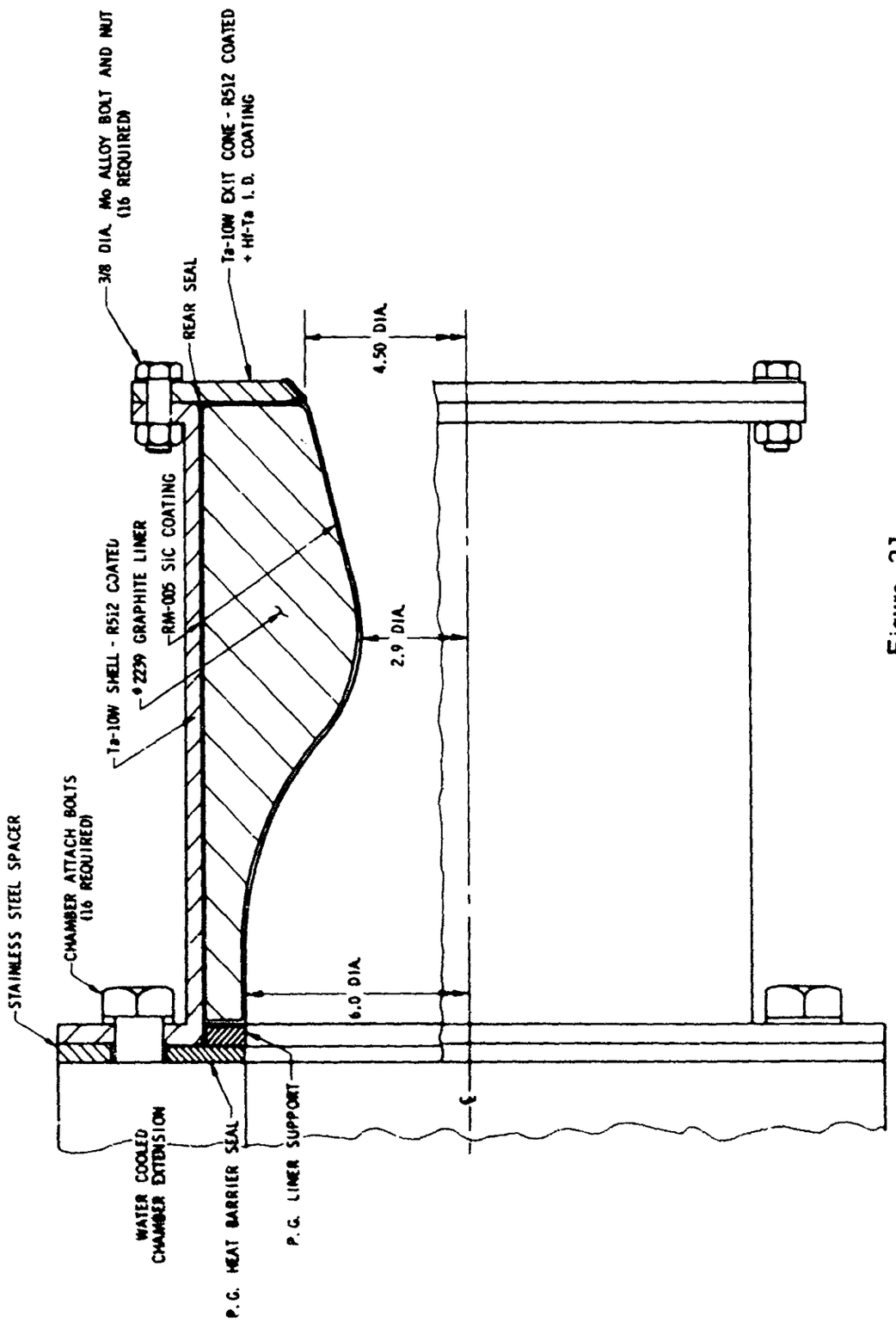

Figure 21

FULL SCALE (5000 POUND) THRUST CHAMBER

graphite ring which was compressed on assembly to preload the forward liner face in the axial direction. This was intended to further reduce the possibility of catastrophic liner break-up on ignition.

4. The most noticeable change is at the exit end of the assembly. During the first test, a thin-wall (0.040-inch) Ta-10W exit-cone extension was used to provide full exhaust gas expansion. This R512-coated cone was badly damaged during the 5-second test, so an exit cone was not used on the second chamber assembly. Instead, a similar flange-plate closure was fabricated from Ta-10W plate and R512-coated on all surfaces except for the I.D. surface on which a thick (0.020 - 0.030-inch) Hf-Ta coating was deposited for higher temperature protection.

(U) The rest of the second assembly was identical to the first test item, and in fact, used the same thrust-chamber shell and assembly hardware. To produce this second assembly, two new graphite liner substrates were machined and SiC-coated. The first of these was coated to a 0.071-inch thickness and the second was coated to 0.094. The forward, rear, and outer surfaces were ground to provide smooth surfaces for the assembly preloading. The 0.094-inch thick coated liner was selected for assembly with the shell, and the assembly was made with no detrimental effects on either component. There were, however, some surface defects in the chamber section of the SiC coating. Some flaking of a very thin inner SiC coating was evident in this area. This thin coating was discontinuous from the homogeneous, full-thickness coating structure, having formed only in a localized area during the terminal phase of the coating deposition process. Due to the possible ineffectiveness of the discontinuous coating, a nominal SiC thickness of 0.090 was used in the stress and failure analysis calculations. Attachment of the rear flange and the chamber extension section concluded the fabrication effort under this program.

V

FULLSCALE THRUST CHAMBER TESTING & EVALUATION

A. FULLSCALE THRUST CHAMBER TESTING

(U) Hot-firing tests of both fullscale thrust chamber assemblies were accomplished by AFRPL facility personnel in Test Area 1-46, AFRPL, Edwards, California. Although specific information is not available, the test instrumentation and controls were extensive and thorough. The thrust chamber assemblies were bolted to the Air Force injector and fired horizontally.

(U) The injector was a multielement type, resulting in high combustion efficiencies. The outer ring of injection points had 24 sets of two fuel jets and two oxidizer jets impinging at a common point. Additional sets of injection points were located across the injector face. The fuel injection holes were in the outer ring, angling inward, and the oxidizer holes were inboard, angling outward. At the O/F ratio of 1.6 used in the No. 2 test, the momentum angle of the oxidizer/fuel exchange was 18° to 19° outboard from the chamber axis (toward the wall). During the No. 1 test, at an O/F ratio of 1.8, it was even higher.

(U) In addition to the customary pressure, temperature, and flow measurements, specific instrumentation for these chamber tests consisted of six high-temperature thermocouples on the outer wall and overall chamber observation by photographic pyrometry and high-speed motion pictures. For the test of the No. 1 assembly, four of the Pt/Pt-10% Rh thermocouples were located on the cylindrical shell and two were on the exit cone. As for the subscale tests, these thermocouples were not attached to the structure, but were held in intimate contact by spring loading. Attachment to the Ta-10W shell would have required grinding away an area of the R512 coating. This could leave an unprotected metal area open to oxidation degradation, since a ceramic potting would have had to be used which might spall off during test.

(U) From the instrumentation standpoint, high-speed motion pictures are only useful for general observations. However, as an aid to failure analysis, they are invaluable since they can show how and when specific events occurred. A new method of temperature measurement that was used in these tests was that of photographic pyrometry. Individual frames of an extended range film were exposed at 2-second intervals during the tests.

This film reacts to temperature in such a manner that a wide range of surface temperatures can be accurately detected. For determination of actual surface temperatures the film color density is compared on a densitometer with the color density from the photograph of a controlled temperature specimen. Temperatures can be correlated as close as 50°F and hot spots can be seen that might not be detected by thermocouples.

1. No. 1 Thrust Chamber Test

(U) The first test was scheduled for a five-second duration. Longer times would have been run later if the first test had been completely successful. The actual firing went very smoothly, taking about 1/2 second to reach maximum chamber pressure of 503 psi, with no pressure spike indicated. No external leaks were evident at any time. Post-test photographs of the assembly are presented as Figures 22 through 25.

(C) The data on the test firing of the No. 1 assembly was as follows:

Propellants: N_2O_4/0.5 N_2H_4 - 0.5 UDMH

	Target Conditions	Test Results[1]
Flow Rate	18.5 lb/second	18.25 lb/second
Mixture ratio, O/F	1.8	1.78
Thrust	4500 pounds	4500 pounds
Chamber pressure	500 psi	503 psi
Run time	5 sec	4.55 sec
C*	5745 ft/sec	5650 ft/sec
C* efficiency		98.5%

[1] At maximum P_c

Performance of Structure During Test

(U) R512 coated Ta-10W exit cone: The exit cone was extensively damaged. The coating had flowed, eroded, crystallized, and failed to protect the substrate. As shown in Figure 25, the inside diameter of the exit-cone flange was partly eroded such that it would not give full axial support to a coated liner in a new assembly. The exit cone was only an expedient, and was not required for proof of the thrust-chamber concept, so it was not used on the next assembly. A similar rear flange, without the cone extension, was fabricated from Ta-10W plate as discussed previously.

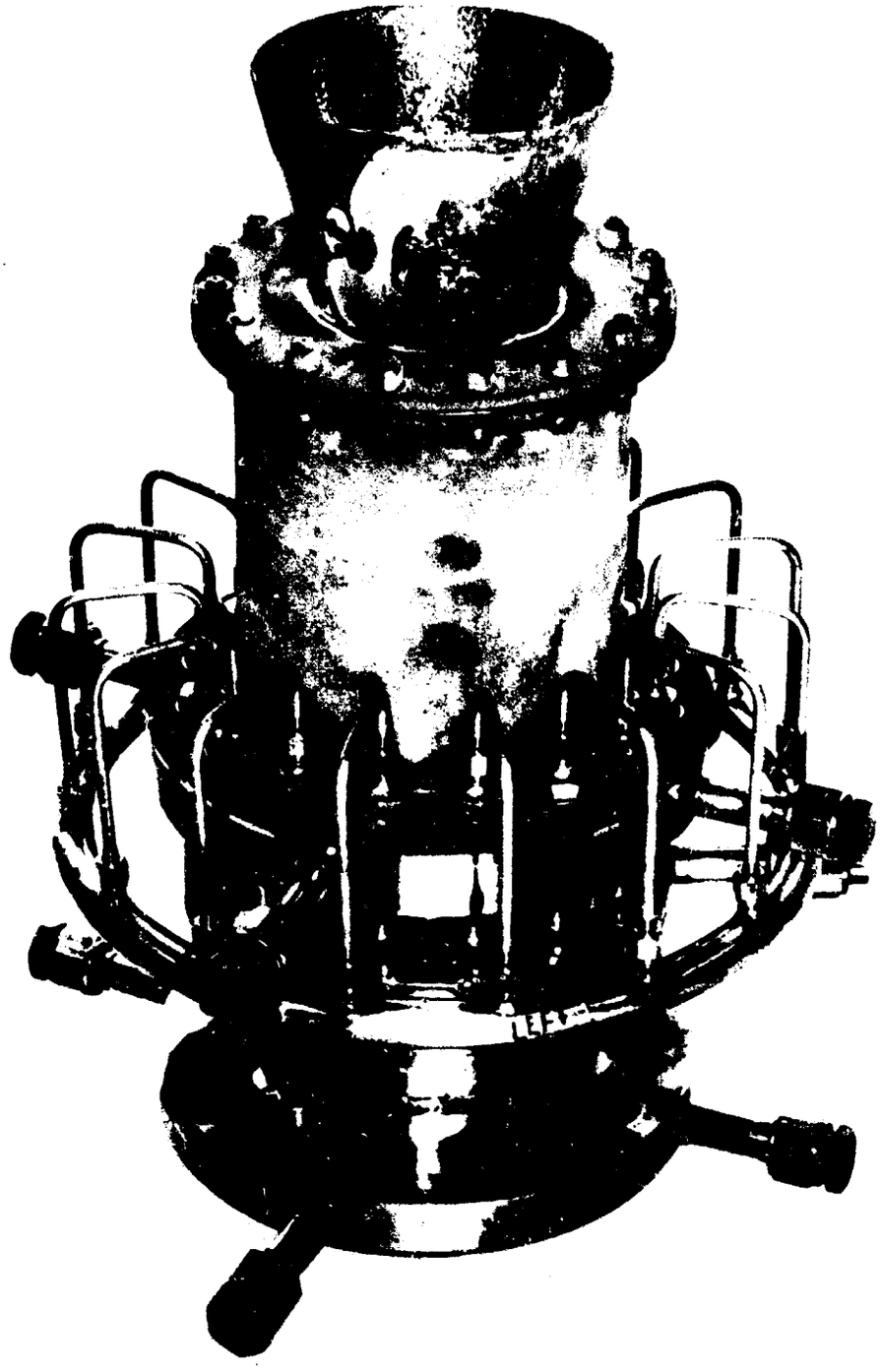

Figure 22
5000 POUND COMPOSITE THRUST CHAMBER ASSEMBLY NO. 1
AFTER 5 SECOND TEST AT AFRPL

R-22,388
Neg. 8i28-15

Figure 23

EXIT CONE DAMAGE - ASSEMBLY NO. 1 AFTER 5 SECOND TEST AT AFRPL

R-22,389
Neg. 8128-16

Figure 24

DIVERGENT SECTION - ASSEMBLY NO. 1 AFTER 5 SECOND TEST AT AFRPL

R-22,390
Neg. 8128-17

Figure 25

EXIT CONE JOINT AREA - ASSEMBLY NO. 1 AFTER 5 SECOND TEST AT AFRPL

R-22,391
Neg. 8128-18

(U) SiC coated graphite liner: Almost all of the 0.026-inch thick SiC coating was lost from the inside of the nozzle liner, apparently by mechanical breakup at the start of the test run. Only a few small areas of coating remained attached to the graphite substrate. Figures 23, 24, and 25 show two of the larger pieces remaining in the nozzle-divergent section and Figure 26 shows one piece remaining near the forward edge of the liner. Inspection of these remaining pieces showed the formation of SiO_2 at the broken edges, but the original I.D. face appeared unchanged, i.e., no erosion or oxide formation.

(U) The fracture mode in this instance was markedly different from that experienced in the subscale thrust-chamber evaluations. In the small chambers, all cracks that occurred were essentially radial, so that a wedge was formed between the substrate and the adjacent SiC sections, which retained all pieces in their original position. In this large chamber, the remaining SiC pieces showed a highly angular break in relation to a radial plane, which allowed the broken pieces to be forced away from the wall.

(U) The forward edge of the SiC-coated graphite liner in this design was not axially supported or radially prestressed over the last quarter-inch, since the pressure seal was made on the flange and not on the coated liner. This condition allowed the SiC to break up at the leading edge and take some of the graphite substrate with it. As a matter of fact, a number of small pieces of unoxidized SiC and graphite were found in the desert sand, 100 to 400 feet from the chamber exit. This substantiated the theory of mechanical coating removal rather than removal by oxidation and erosion. Metallographic, spectrographic and X-ray diffraction analyses were made of residue samples from the chamber and nozzle wall to assist the final evaluation of the failure mode. These analyses showed the SiC to be reasonably homogenous and of a high quality. Oxide formation (SiO_2) occurred generally at the broken edges where the SiC was excessively heated.

(U) Other test hardware: None of the other items in the test setup were damaged during the test run. The R512 coated Ta-10W shell was suitable for use in the second thrust-chamber assembly with no rework required. The forward and rear seals, and all manifolds and bolts were reuseable. The Air Force chamber-extension section shows an injector burning pattern (Figure 26) but this does not affect the utility of the part.

Figure 26
CHAMBER AREA - ASSEMBLY NO. 1 AFTER 5 SECOND TEST AT AFRPL

R-22,392
Neg. 8128-19

(U) Temperature measurements: The aft thermocouple on the exit cone (1.85 inches from flange face) reached an indicated temperature of 3100°F after 4-seconds and was still above 2000°F 2-seconds later. The other exit cone thermocouple was inoperative. Throat wall and chamber wall temperatures only increased from 10 to 370°F over ambient due to the heat-sink capacity of the composite wall. The pyrometry film data from the test was developed and compared with control specimen readings. The control specimen (emissivity type had been heated and photographed at 50°F intervals through the range of 1600°F to >3300°F where the R512 coating failed. The comparison showed final exit cone temperatures above the control specimen temperature of 3300°F. This was consistent with the condition of the failed coating as shown in Figures 22, 23, and 24.

(U) On the side of the exit cone viewed, six temperature streaks are visible in the first pyrometry photograph which was taken between 1 and 2 seconds after the start of the run. Temperature variations are greater than 200°F but are difficult to read precisely due to the small film size and the relatively large viewing spot on the densitometer. More accurate methods of reading the variations are being developed, but were not completed during the term of this program. If temperature variations of this magnitude were present throughout the thrust chamber length they could have a significant effect on the stresses developed in the brittle inner SiC coating, and may have contributed to the coating breakup during test.

(U) Review of the high speed motion pictures of the test run showed that pieces of the SiC coating were expelled intermittently, from less than a second after the run started until near the end. Some indications of uneven heating of the exit cone are also evident on this film record.

2. No. 2 Thrust Chamber Test

(C) The modified chamber assembly with the 0.090 inch thick SiC coating was set-up and instrumented for test similar to the first assembly. All six spring loaded thermocouples were located on the chamber shell since there was no exit cone on this test item. As for the No. 1 assembly, a 5-second test was scheduled and run. Test conditions were essentially as programmed: An O/F ratio of 1.64 to 1.61 at a $\dot{w}$ of 19.7 lb/sec, aP_c maximum of 508 degrading to 455 psia, and a η_c* increasing from 94.4% to 100% at the end of the run. The thick inner SiC coating was almost completely lost by mechanical breakup during the run. The thick

coating had been applied to the graphite substrate in an effort to achieve a straight, radial-break type of fracture, in which the SiC pieces would be contained by the wedge effect of the cylindrical contour if cracking should occur. Although some of the coating fractures were essentially radial, others were along an angular plane allowing them to be dislodged.

(U) Post-test photographs are presented as Figures 27 through 30. Figure 27 shows the entire chamber assembly wherein its appearance is identical to its pre-test condition, except for the inner lining surface. Figure 28 shows a closer view of the exit cone - rear flange area. The inner diameter surface of the rear flange had a Hf-Ta coating which was unaffected by the test. The three large, dark areas near the exit plane are pieces of the SiC coating which remained attached to the graphite substrate. The white material at the upstream edges of the SiC pieces is SiO_2 which formed when the edge was overheated by the impinging gas stream.

(U) Figure 29 is a view of the combustion chamber-nozzle entrance area. The numbers on this figure locate the areas where specimens were taken for spectrographic and X-ray diffraction analysis. The white material from areas 1, 2, 3, and 4 was found by X-ray analysis to have an amorphous structure (non-crystalline) typical of glassy-phase SiO_2. All specimens (1 - 4) were found by spectrographic analysis to have Si as the major element, with only slight percentages of other elements indicated. One of the other elements present was Al which was detected in amounts up to 0.5% in specimens 2 and 3. This aluminum probably came from the Al_2O_3 coating on the Air Force water cooled chamber extension section. Figure 29 also shows gouges in the graphite substrate, where part of it was torn out by the SiC coating when it fractured and was expelled. The large gray area in the throat convergent section (left of points 3 and 4) is the graphite substrate at essentially its original surface contour. The SiC coating evidently stayed on this section until late in the test run.

(U) Figure 30 is a close-up view of the forward edge of the chamber assembly where it mated to the chamber extension section. On the left side, all of the SiC coating has broken away from the inner surface, while just right of center it has fractured at the corner yet retains its original surface condition. Farther right, the SiC has a white, oxidized surface. The fracture pattern in the remaining SiC coating is typical of that noted on the small pieces of SiC which were found in the desert sand downstream from the test setup. The forward edge of the SiC coated graphite

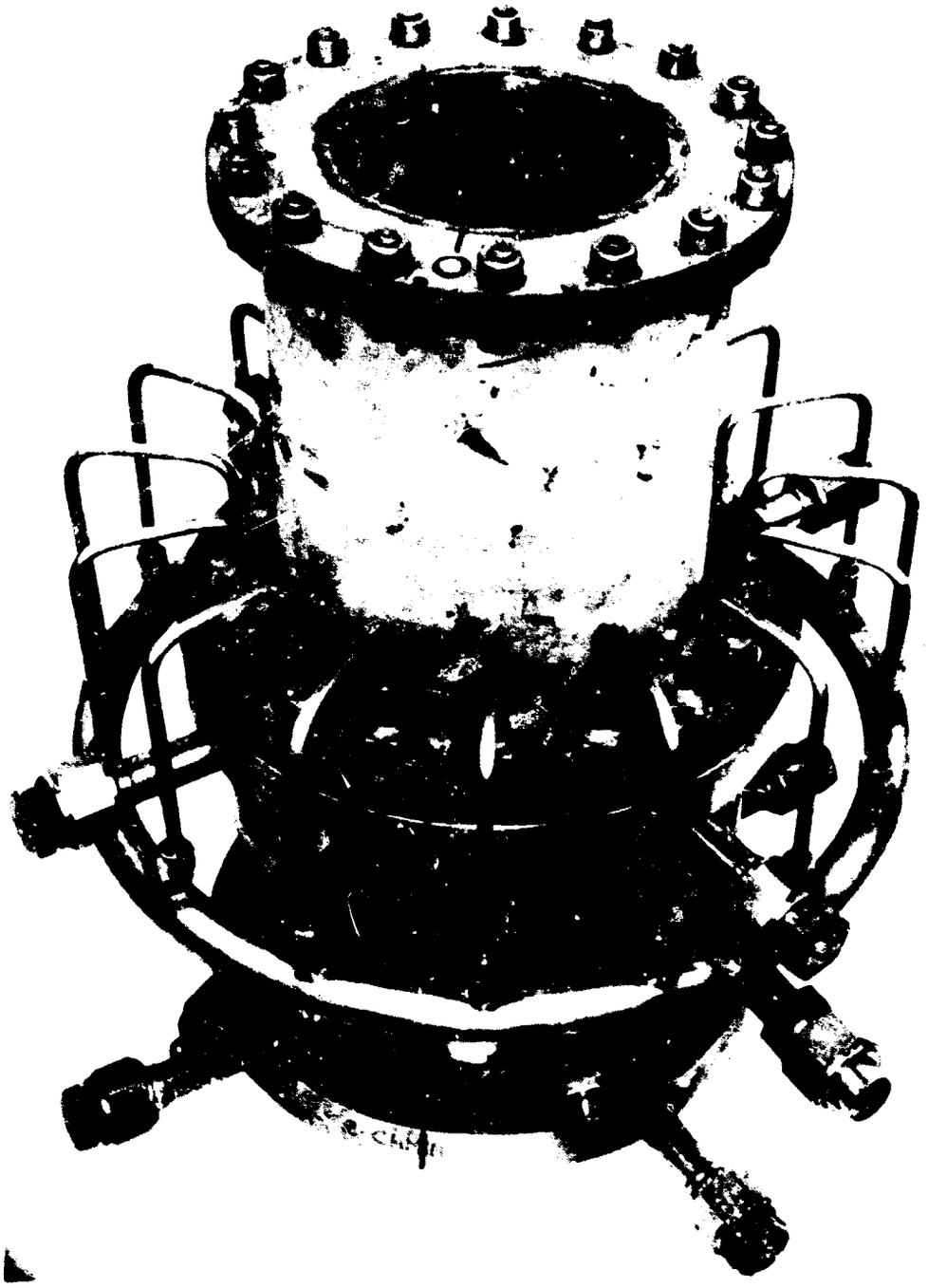

Figure 27
THRUST CHAMBER - ASSEMBLY NUMBER 2
AFTER TEST

R-21,146
Neg. 8128-32

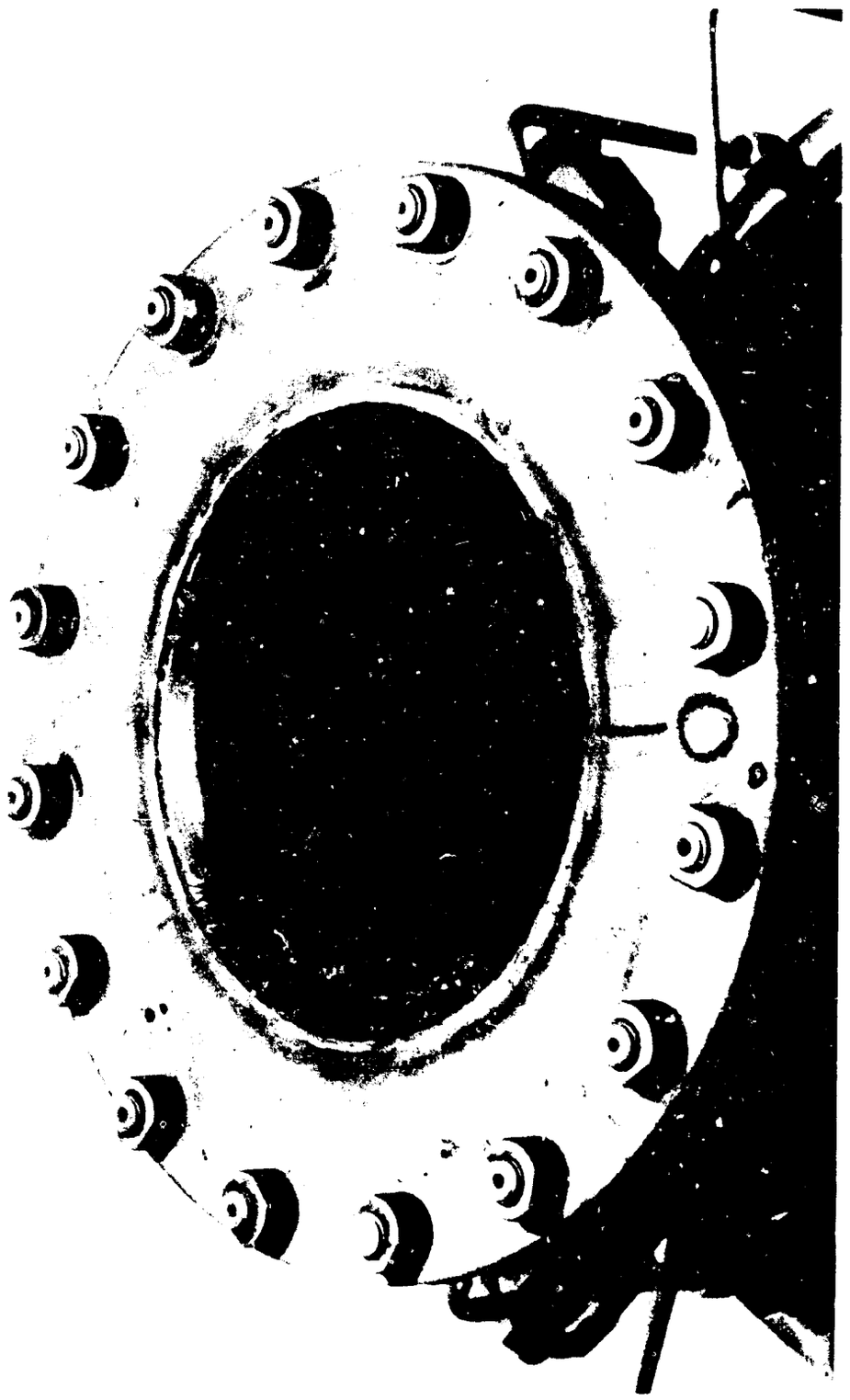

Figure 28
EXIT VIEW - ASSEMBLY NUMBER 2
AFTER TEST

R-21,149
Neg. 8128-31

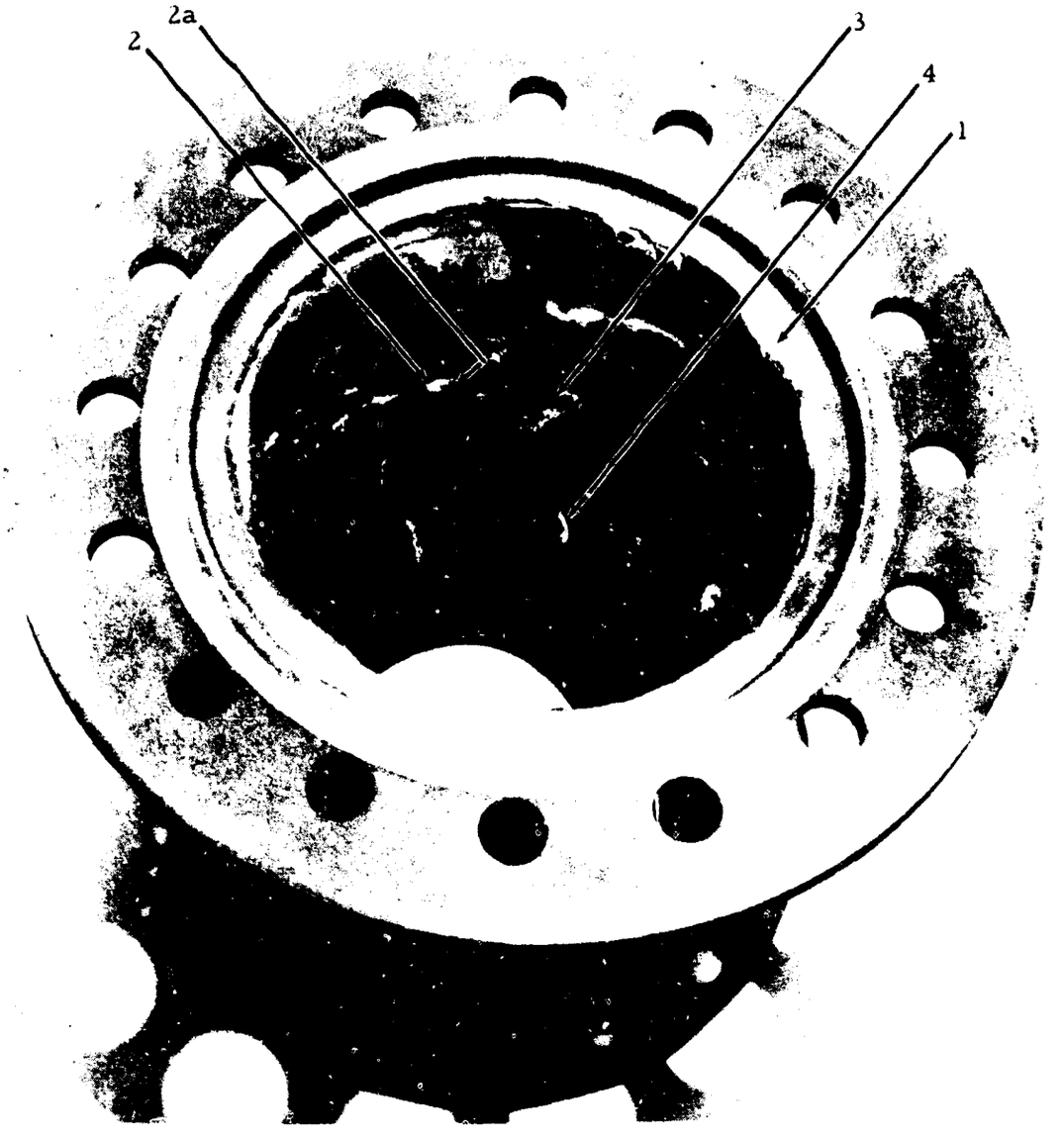

Figure 29

FORWARD CHAMBER VIEW - ASSEMBLY NUMBER 2
AFTER TEST

R-21,147
Neg. 8128-33

Figure 30

FORWARD EDGE - ASSEMBLY NUMBER 2
AFTER TEST

R-21,148
Neg. 8128-34

chamber was ground to provide an even surface for axial preload, which accounts for its relatively smooth but streaked surface. The nodular appearance of the unoxidized SiC on the inner chamber surface is typical of the as-deposited surface. Even though the axial preloading in this second chamber was effective in containing the forward edge SiC coating, it did not prevent the circumferential cracking of the graphite substrate. Two graphite crack lines can be seen in Figure 30. Graphite cracking, however, was less pronounced in this assembly than in the first one.

(U) As shown in the photographs and by other post-test observations, there is some conflicting evidence which has not been resolved concerning the oxidation resistance of silicon carbide in this application. Most of the small areas of SiC which remained in the chamber were oxidized on the edges, and some on the surfaces. This can be explained by the fact that a small piece with sharp edges exposed to the hot gas stream is subjected to a more severe heating environment than a similar section of a full, internal surface. However, there are a few pieces, such as shown in Figure 24, which are oxidized at one point and unaffected in an adjacent area. This suggests a possible inconsistent injector heating pattern that was initially noticed in the uneven heating of the thin exit cone extension during the test of the first 5000 lb thrust chamber.

(U) Motion pictures were also taken of this test firing. An individual frame inspection of the Marquardt film (128 frames/second) showed that the SiC coating loss began at about 0.2 seconds after ignition and occurred intermittently thereafter until just prior to the end of the 5-second run. On the film these were usually seen as bright streaks exiting from the rocket exhaust, but in at least one frame the SiC pieces are large enough (or moving slow enough) to be positively identified. Air Force movies (taken at 200 frames/second) confirmed the intermittent loss of small pieces of SiC coating during the run.

(U) The hot-firing of assembly No. 2 completed the fullscale thrust chamber testing planned for this program. However, a major problem still remained - that of establishing why the fullscale thrust chamber wall could not be kept intact.

B. ANALYSIS OF RESULTS

(U) In order to determine why the fullscale chambers did not perform satisfactorily, a review was made of all certain, probable, and possible factors that affect the performance of the SiC coating. This review encompassed the factors of geometric configuration, allowable strengths, and loading intensity. The effect of these factors on the magnitude and distribution of component stresses was evaluated on an absolute basis when possible, and on a sub- to full-scale comparative basis.

(U) The geometric configuration factors are:

1. Radius of curvature (diameter).
2. Material volume and surface area.
3. Contraction ratio (chamber dia./throat dia.).
4. Section stiffness.

(U) The allowable strength factors as affected by increased size are:

1. Reduced tensile strength.
2. Reduced compressive stability.
3. Reduced thermal shock resistance.

(U) The loading intensity factors are:

1. Prestress interference.
2. Pressure loads.
3. Heat loads.

(U) To view these factors in the proper context, a brief review of the thrust-chamber designs and the test results should be made. Looking first at the subscale thrust chambers, it is seen that this was not a sophisticated design. The chambers were made up basically of a SiC-coated graphite liner in a simple, cylindrical metal shell. They were externally supported with the coated liner compressed axially. During test, cracking of the inner SiC coating was prevalent in the convergent throat and divergent nozzle areas, but no coating was lost, and even the throat surface was not eroded or oxidized during firing durations of more than 10 minutes. The Apollo type injector that was used for these subscale tests had been specifically designed and developed for use with a radiation-cooled, coated molybdenum wall thrust chamber which has a low temperature brittleness problem as

does silicon carbide, so there were no undesirable wall heating effects. However, even this comparatively simple design results in a structurally complicated configuration that was analytically indeterminate, yet experimentally sound.

(U) In designing the fullscale thrust chambers, it was soon evident that there were additional problems, over and above those encountered in the subscale phase. There were the obvious size effects of: (1) reduced stability to radial compressive loads [$(t/D)^3$ function], (2) the potential loss of SiC tensile strength (critical flaw function), (3) pressure stress on the shell ($\frac{Pr}{t}$), and (4) the differential thermal expansion between liner and shell (radial and axial), with no external support or restraint. However, there was also a theoretical reduction in wall heating rate due to the increased diameter ($q \sim 1/D^{0.2}$), which could result in a lower surface temperature. This effect was initially discounted, though, since the subscale chambers had reached equilibrium temperatures considerably below theoretical. The unknown quantity of injector effects on wall heating was felt to be of such a magnitude that the design temperatures could not possibly be taken as any lower than those of thermal Model 1-C (page 23). Any actual reduction occurring during test would be accepted as an increased capability function.

(U) The fullscale thrust chambers were thus seen to be considerably more complicated, and with less experimental variability allowed (only two test items) and less design analysis scheduled (short-time fabrication schedule). Obviously, in either the large or the small thrust chambers, it was desirable to have an inner SiC coating that would not fracture during operation, since there would be less opportunity for subcoating leakage. However, the subscale chamber tests had proven, in that configuration, that cracking of the coating was not critical if the pieces were not displaced. The basic problem with the fullscale thrust chambers was that the SiC coating fractured, broke away from the wall, and was expelled, leaving the graphite substrate unprotected. The analysis of performance factor effects is directed toward resolving the problem of mechanical loss of the SiC coating in the fullscale chambers.

Geometric Factors

(U) The first of the geometric configuration factors investigated is that of the radius of curvature (diameter). In tension, a large-diameter cylinder has a simple radius ratio increase in hoop stress over that of a small-diameter cylinder of the same thickness ($\sigma_t = \frac{Pr}{t}$). Under a

compressive load (external pressure), the same ratio holds for acting stress, σ_c, however, the allowable pressure for elastic buckling is considerably reduced for a larger diameter cylinder.

(U) The significance of the thickness/diameter ratios can be appreciated by considering the elastic stability equation for thin, circular cylinders under external pressure loads. In References 7 and 8, Timoshenko develops equations for elastic buckling of thin-walled circular cylinders, accounting for various end conditions on long and short cylinders. (These analyses account for stretching of the shell middle surface and assume the loads in the circumferential direction are the major loads.) This analysis results in an equation for the critical buckling pressure which, if simplified (by neglecting the effects of the L/r ratio), gives

$$P_{cr} = \frac{E\,t^3\,(N^2 - 1)}{12r^3\,(1 - \nu^2)}$$ (a first-order approximation for long cylinders)

where

E = modulus of elasticity

t = shell wall thickness

N = number of nodes in buckled shell

r = mean radius of shell

ν = Poisson's ratio

P_{cr} = critical pressure

An analysis-design type approach was taken by R. G. Sturm Reference 9 (with the following assumptions: the cylinder is initially round and of uniform thickness; the material is elastic; the cylinder is thin-walled, and the displacements experienced prior to buckling are small). In conjunction with his analysis, Sturm carried out an extensive testing program and the final equations published were verified experimentally. The results of this work were presented as charts for cylinders with various end conditions showing the interrelationship of L/r and D/t. The resultant equation for P_{cr} is a function of the modulus of elasticity E, a geometric constant, and $(t/D)^3$.

(U) In checking the difference between the sub- and full-scale configurations, both sets of equations discussed above, and the L/r modification of Reference 8, were used. As a preliminary check, the equations for long cylinders were evaluated for a typical small-diameter cylinder (S/N 005, with D/t = 46), and both the thick SiC-coated (D/t = 67) and thin SiC-coated (D/t = 230) large-engine configurations. These calculations showed that both the radial elastic deflection and the critical collapse pressure for the small cylinder were 10 to 20 times greater than for the large cylinder with the thin, SiC coating, and 3 to 5 times greater than for the large chamber with the thick SiC coating. The final check utilized equations which accounted for the length-to-radius ratio of the cylinder under consideration. In this case, the large-diameter cylinder with thin SiC coating showed low critical collapse pressures, one lower and one higher than the effective pressure of 465 psi caused by assembly. The large-diameter cylinder with a thick SiC coating indicated a critical collapse pressure higher than that calculated for the small cylinder in each case. The results of all calculations are shown in Table VIII. An E_{SiC} of 30×10^6 psi was used for these calculations. An effective modulus of 60 would double the allowable pressures; however, the comparison of sub- and full-scale chambers is valid in either case.

(U) Comparing the results for short cylinders, which are the most realistic, the last values of P_{cr} in the table show the effect that was anticipated in the No. 2 test assembly, but not realized. If the failure mode in the No. 1 test assembly had been purely buckling instability, the 30 times greater allowable collapse pressure in the No. 2 assembly should have alleviated the problem. Theoretically, at least, the compressive stability was restored.

Allowable Material Stress

(U) In terms of brittle material strength, the effect of going from a small section to a large section is to reduce the allowable tensile stress that can be carried by the coating without fracture. SiC has been shown to be thickness-strength conscious, which is a typical volume-area effect for brittle materials (Weibull type critical flaw probability function). The large diameter chambers have a greater volume of SiC under stress, even with the same coating thickness. In the No. 2 chamber, the greater coating thickness reduced the allowable operating tensile strength to about one-third that in the No. 1 chamber. The compressive strengths are not appreciably reduced, and in the 0.090-inch thick SiC, they are 50 to 100 times as great as the tensile strength (~200,000 psi compared to 2,000 to 4,000 psi in tension).

TABLE VIII

CRITICAL COLLAPSE PRESSURES OF SiC SHELLS

Small Diameter Cylinders D/t	Small Diameter Cylinders P_{cr}	Large Diameter Cylinders D/t	Large Diameter Cylinders P_{cr}	Cylinder Length Assumptions
46	5000	230	290	Relative deflection of long cylinders only (1)
		67	1000	
46	5050	230	43	Long cylinders only (2)
		67	1740	
46	9120	230	527	Short cylinders (3)
		67	17,500	
46	6720	230*	237	Short cylinders (4)
		67**	7140	

(1) Elastic Deflection of a Long Thin Shell, Reference 7.

(2) Critical Collapse Pressure of a Long Thin Shell, Reference 8.

(3) Critical Collapse Pressure of a Short Thin Shell, Reference 8.

(4) Critical Collapse Pressure of a Short Thin Shell, Reference 9.

*combustion chamber section - Assembly No. 1

**combustion chamber section - Assembly No. 2

(U) The fracture mode experienced in these two fullscale assemblies (catastrophic breakup) is more typical of a compressive-type SiC failure than a tensile type. With the initial compressive loading on the SiC coating, there will be a high value of stored elastic energy. This will be further increased by the heating at the start of a test run, which produces additional compression at the inner surface of the coating. The material factors which affect the fracture behavior of brittle materials under conditions of thermal shock consist of:

1. The elastic energy stored at fracture, which provides the driving force for crack propagation.

2. The effective surface energy required to create the new fracture surfaces.

3. Possible dispersion and attenuation of the stress waves accompanying the propagating crack and of any other stress waves nucleated at the time of fracture.

The total elastic energy stored in a brittle material subjected to thermal shock at the time of fracture will depend on the material properties of the body, on size and shape, and on the temperature and stress distribution.

(U) The following equation, developed by Crandall and Ging, (Ref. 10) gives the maximum temperature difference to which a ceramic body of simple geometric shape can be subjected without fracturing.

$$\Delta T = \frac{K F_t (1 - \nu)}{\alpha E} \left(1 + \frac{2}{\beta} \right)$$

where: ΔT is the maximum difference between the two ambient temperatures between which the ceramic body can be transferred without fracturing.

K - is a shape constant (2.0 for a cylinder)

E - is the Young's modulus

F_t - is the tensile strength

α - is the coefficient of expansion

ν - is Poisson's ratio

β - is Biot's modulus = $\frac{rh}{k}$

r - is the radius of the cylinder

h - is the surface heat transfer coefficient

k - is the thermal conductivity

It should be noted that this equation is the sum of two terms. The first is simply a rearrangement of the formula for the thermal stress through a cylindrical wall ($\sigma = \frac{\Delta T \ \alpha E}{2(1-\nu)}$), and gives the maximum temperature difference that can be supported without fracture (acting σ = allowable F_t). The second term gives the partial temperature difference to which the wall can be subjected during the period of heat transfer without having the internal temperature difference exceed the temperature difference given by the first term. The first term depends on material properties only whereas the second term includes the size of the body and the magnitude of the thermal shock.

(U) In evaluating the difference in thermal shock resistance between the SiC coatings in the large and small thrust chambers it is necessary first to investigate the Biot's modulus. In the throat sections there is an increase in r from 0.26 to 1.45 inches, and in the chamber section an increase from 0.88 to 3.03 inches. The heat transfer coefficient, h, is directly effected by the mass flow rate per unit area, $\dot{w}/A$, and inversely as the section diameter, D, from the Bartz equations for heat transfer rates. (Reference 2)

$$h \sim \frac{(\dot{w}/A)^{0.8}}{D^{0.2}}$$

(U) The other term in the modulus is the thermal conductivity of the material, k_{SiC}. SiC is an excellent low-temperature conductor whose conductivity decreases with temperature. At 200°F, its k is 1200 Btu-in/ft^2-hr-°F, 800 at 1000°F and continuing down to 100 at 3000°F (Reference 1, page 30). To evaluate the initial thermal shock, a value of 1200 was used. Table IX lists the data and calculations made. Item 14 gives the reduction in allowable ΔT for a large-size chamber compared to a subscale throat section and chamber section. This comparison is based on an identical allowable thermal stress for the comparative configurations. This is not precise since SiC undergoes a reduction in allowable strength, F_t, with increased thickness, and therefore a reduction in allowable ΔT with increased thickness. A knowledge of the precise material strength was not a primary factor since both thin and thick coatings were fractured.

(U) Assuming the transient wall temperature distribution of Thermal Model 1-C accurately described the SiC wall ΔT for a typical subscale chamber, the acting stresses and allowable differential temperatures could be calculated and compared from this arbitrary base. If this base were a valid thermal stress fracture point and the total stress pattern in the coating were known, an exact comparison of actual and allowable stresses for the relative chamber sections could be made. However, the base is not this accurate or reliable, recalling that the subscale chambers cracked through the nozzle region (where the ΔT_{SiC} is high and the interference compressive stress is low) but did not crack in the cylindrical chamber section (where the ΔT_{SiC} is low and the interference compressive stress is high). The base point fracture stress is somewhere between these two bounds. From the original thermal analysis for the subscale chambers, the maximum ΔT_{SiC} at the throat was 750°F (0.030-inch thick coating, 15 seconds after start-up), while in the chamber section it was less than 100°F. Coupled with these wide bounds is the other unknown, actual material stress state. For these reasons, the calculation of allowable ΔT's was not pursued any further.

(U) There are, however, a few more points that should be noted on the subject of allowable ΔT for thermal shock. First, the No. 1 fullscale thrust chamber had a thin coating (0.026 inch thick) which would make its allowable ΔT slightly higher than indicated. Second, the No. 2 assembly had a very thick (0.090 inch) SiC coating which would markedly lower its allowable ΔT. Third, the period of thermal shock probably lasts for the first 5 - 10 seconds of operation. Wall temperatures at the throat would be approaching 3000°F at the end of this period, with the consequent reduction in the thermal conductivity of SiC. As k_{SiC} is reduced, the Biot's

TABLE IX

HEAT TRANSFER - SIZE EFFECTS ON ALLOWABLE ΔT FOR SiC SHELLS

	Item	Subscale Throat	Subscale Chamber	Fullscale Throat	Fullscale Chamber
1.	Mass Flow, $\dot{w}$ (lb/sec)	0.40	0.40	19.0	19.0
2.	Diameter, D (in.)	0.414	1.75	2.90	6.05
3.	Flow Area, A ($in.^2$)	0.135	2.40	6.6	28.7
4.	$\dot{w}/A$ ($lb/in.^2$-sec)	2.96	0.167	2.88	0.66
5.	$(\dot{w}/A)^{0.8}$	2.37	0.24	2.33	0.72
6.	$D^{0.2}$	0.838	1.118	1.237	1.433
7.	Heat trans. coeff. proportionality $\frac{(5)}{(6)}$	2.83	0.215	1.89	0.502
8.	Heat transfer coefficient, h $\left(\frac{Btu}{ft^2\text{-hr-}^oF}\right)$	2440	185	1620	430
9.	Radius, r = D/2 (in.)	0.20	0.88	1.45	3.03
10.	rh	490	163	2350	1300
11.	Coefficient of thermal conductivity for SiC, k $\left(\frac{Btu - in.}{ft^2\text{-hr-}^oF}\right)$	1200	1200	1200	1200
12.	Biot's modulus modifier, $\frac{2k}{rh}$	4.9	14.7	1.0	1.85
13.	1.0 + (12)	5.9	15.7	2.0	2.85
14.	Reduction in allowable ΔT,				
	a. compared to subscale throat			66%	52%
	b. compared to subscale chamber			87%	82%

modulus modifier (Item 12 in Table IX) approaches zero, which means that at increased temperatures the SiC has a very low tolerance for thermal shock loads. This is a property of the material itself, independent of configuration, although the actual allowable ΔT is a function of configuration as previously discussed. The last point is that this heat transfer - size effect evaluation is based on a uniform circumferential temperature distribution and comparable wall heating rates and effective gas temperatures. The theoretical effects of mass flow/unit area and section size have been included, but the actual wall heating rates, effective gas temperature and their uniformity are unknown quantities which can only be approximated by test data and post-test conditional observations.

(U) From the test results of small and large thrust chambers it can be concluded that there was definitely a difference in the wall heating loads. Theoretical wall temperatures were not reached in the subscale tests, even at steady-state conditions with high combustion efficiencies, and there was no erosion or oxide formation on the SiC coating. Conversely, in the fullscale tests, some surface oxide formations were generated at the full chamber diameter during only 5 seconds of operation. These were not consistent circumferentially, but then, neither was the remaining coating. According to a transient thermal analysis, wall temperatures of 3100°F (required for significant SiO_2 formation) should not have occurred during a 5-second test, even in the throat section. Oxide formation temperatures must have been generated by the loss of a suitable heat conduction path after the breakup and expulsion of the adjacent coating. It was postulated, at the conclusion of the subscale chamber evaluations, that the thrust chambers were operating cooler than predicted due to boundary layer and flow profile effects along the internal wall. Similar effects were evidently not present in the fullscale tests. The probability of severe wall boundary-layer gas temperature and the possibility of unsymmetrical temperatures with the fullscale test operations, coupled with the test results, shows the desirability of having low-intensity, consistent wall gas conditions. Historically, this has been found to be a make-or-break effect for brittle wall (metal or ceramic) thrust chambers.

Fracture Modes

(U) When the SiC coating under compression and thermal shock loadings is fractured, the elastic energy stored at fracture is transformed into various other forms of energy, among which are acoustic, kinetic, and the effective surface energy required for the creation of the new crack surfaces. The major crack propagation energy dissipator is anelastic deformation at the tip of the propagating crack. It is postulated that the SiC

cracking in the subscale thrust chamber throat areas was due to thermally induced critical tensile stress at the SiC-graphite interface. In order for a thermal shock fracture to take place non-catastrophically, a major part of the energy stored at fracture must have been absorbed by the propagation of nucleated cracks.

(U) The criterion for failure by thermal shock to be non-catastrophic is that the area over which the cracks will propagate (calculated from the elastic energy stored at fracture, divided by the effective surface energy required for crack propagation) is less than the cross-sectional area of the body multiplied by the number of cracks nucleated at the time of fracture. If this condition is not satisfied, additional energy is still available, even after the cracks have traversed the body completely. This additional energy will probably be imparted to the fragments in the form of kinetic energy, with the result that the body will fracture explosively, scattering the fragments. It should be noted that the energy required for crack propagation under conditions of thermal shock is supplied by the elastic energy stored in the body, and no external force is necessary. However, in this thrust-chamber design, there is also an additional force provided by the compressive preload.

(U) It is highly probable that the SiC coating in the fullscale chambers failed catastrophically by the thermal shock load in conjunction with the initial prestress. Whether or not they would have failed catastrophically if the preload were lower, or if the heating loads were reduced cannot be accurately determined at this time. The complexity of the stress patterns and the number of unresolved variables contributing to the stress-temperature distribution are such that a considerable amount of further analysis and laboratory experimentation would be required before the problems were accurately solved. In conclusion, it appears that the low thermal-shock capability of the large thrust chamber coatings had the greatest probability of being responsible for the in-test performance failures.

(U) The stress distribution in the SiC coating is visualized as follows: a thin wall SiC cylinder, initially under a uniform, external compression load is subjected to a relatively low internal tension load (chamber pressure) and a high heat load. On start-up, the chamber pressure P_c, reduces the compression stress only slightly. The heat load ($<5000^{\circ}F$ combustion gas) is felt as a ΔT through the wall which causes a compressive stress at the inner wall surface and a tensile stress at the outer wall surface (SiC-graphite interface). When the tensile stress exceeds the allowable

(which is quite low compared to the compression stress allowable) a crack is started which propagates inward until it reaches a point where the compressive stresses stop its radial progression. The composite wall restrains the SiC coating from the outward motion (expansion) that it would experience if unrestrained. This increases the compressive stress in the reduced effective thickness of coating to a value which can no longer be tolerated, resulting in a compressive/shear-type fracture. The SiC coating has a high value of stored energy with its modulus of 30 - 60 x 10^6 psi at a compressive stress approaching 200,000 psi. This energy propagates the tensile-induced cracks and imparts motion to the fractured sections of coating. Stress patterns after the partial loss of coating are even more difficult to visualize, but any free edges of SiC would be highly stressed and fracture-prone.

(U) The solution to the coating loss problem is not immediately apparent, but it is recognized that the size-effects must be minimized. Possibly a segmented or a pre-cracked chamber design would be effective. Further analysis and laboratory effort would be required to optimize the composite wall concept for utilization of silicon carbide in large diameter rocket thrust chambers.

VI

CONCLUSIONS AND RECOMMENDATIONS

(U) Subscale rocket thrust chambers (100 lb thrust) were successfully tested for continuous and intermittent firing durations exceeding 600 seconds. During these tests, the inner SiC coating experienced some non-critical cracking in the contoured nozzle section. The coating did not oxidize or erode, and none of the fractured pieces were displaced, so the original wall contour was retained. However, in the hot-firing tests of both fullscale thrust chambers (5000 lb thrust) the inner SiC coating was almost completely lost by catastrophic breakup during the initial 5-second test run.

(U) The coating failures in the two 5000 lb thrust-chamber assemblies demonstrate a probable basic design limit on size/configuration using a silicon-carbide continuous coating on graphite. This is a conditional conclusion based on the apparent impracticability of providing a trade-off between precompression loading to resist tensile failure, and compressive/shear resistance of the coating. Sufficient prestress to eliminate tensile failure results in excessive buckling pressure on the coating when thermal compression is added.

(U) No evidence has been established which would indicate that the RM-005 SiC coating is not entirely acceptable from the aspect of environmental resistance. In the environment of N_2O_4/50-50 propellants, this material remains unsurpassed in its erosion resistance at chamber pressures up to 500 psi for long-duration firings without regenerative cooling.

(U) Therefore, if justification exists for a high-pressure, long duty-cycle thrust chamber with the N_2O_4/50-50 propellant system, further structural design evaluation of SiC liner concepts is warranted. Such concepts should be oriented toward circumventing the critical size limitation. Potential design approaches include segmenting, precracking, or reinforcing the liner. Further analysis and experimental effort will be required to optimize the composite wall concept for large scale rocket thrust chambers.

REFERENCES

1. Taylor, R. J., Evaluation of Advanced Non-Regeneratively Cooled Rocket Thrust Chamber Concepts, Technical Report AFRPL-TR-66-69, The Marquardt Corporation Report No. 25, 189, February 1966, Contract AF 04(611)-10917. CONFIDENTIAL (Title-Unclassified)

2. Bartz, D. R., "A Simple Equation for the Rapid Estimation of Rocket Nozzle Convective Heat Transfer Coefficients", Jet Propulsion, Vol. 27, No. 1, January 1957.

3. Timoshenko, S., Strength of Materials, Part II, 3rd Edition, 1956, D. Van Nostrand Co., Inc., Princeton, N.J.

4. Roark, R. J., Formulas for Stress and Strain, 3rd Edition, 1954, McGraw-Hill Book Co., Inc., New York.

5. Chang, Chieh-Chien, Chu, Wen-Hwa., "Stresses in a Metal Tube Under Both High Radial Temperature Variation and Internal Pressure", Journal of Applied Mechanics, pg. 101-108, June 1954.

6. Johnson, C. A., Campbell, J. R., Summary Report on the CY 1961 Contributing Engineering Program, The Marquardt Corporation Report 25, 045, Volume IV of IV, February 1962, Contract AF 33(600)-42621. UNCLASSIFIED

7. Timoshenko and Woinowsky-Krieger, Plates and Shells, McGraw-Hill, 1959.

8. Timoshenko and Gere, Theory of Elastic Stability, McGraw-Hill, 1961.

9. Sturm, R. G., Study of the Collapsing Pressure of Thin Walled Cylinders, University of Illinois, Bulletin #329, 1941.

10. Crandall, W. B., and Ging, J., "Thermal Shock Analysis of Spherical Shapes," J. Amer. Ceram. Soc., 38, 44 (1955).

UNCLASSIFIED
Security Classification

DOCUMENT CONTROL DATA - R&D
(Security classification of title, body of abstract and indexing annotation must be entered when the overall report is classified)

1. ORIGINATING ACTIVITY (Corporate author)	2a. REPORT SECURITY CLASSIFICATION
The Marquardt Corporation 16555 Saticoy Street Van Nuys, California 91409	CONFIDENTIAL
	2b. GROUP IV

3. REPORT TITLE (UNCLASSIFIED)

Evaluation of an Advanced Non-Regeneratively Cooled Rocket Thrust Chamber Concept

4. DESCRIPTIVE NOTES (Type of report and inclusive dates)
Final Report - 1 June 1965 - 30 November 1966

5. AUTHOR(S) (Last name, first name, initial)
Taylor, Ronald J.

6. REPORT DATE	7a. TOTAL NO. OF PAGES	7b. NO. OF REFS
January 1967	110	10

8a. CONTRACT OR GRANT NO.	9a. ORIGINATOR'S REPORT NUMBER(S)
AF 04(611)-10917 b. PROJECT NO. 3058522 c. d.	Marquardt Report No. 25,211 9b. OTHER REPORT NO(S) (Any other numbers that may be assigned this report) AFRPL-TR-67-89

10. AVAILABILITY/LIMITATION NOTICES

"In addition to security requirements which must be met, this document is subject to special export controls and each transmittal to foreign governments or foreign nationals may be made only with prior approval of AFRPL (RPPR-STINFO), Edwards, California 93523."

11. SUPPLEMENTARY NOTES	12. SPONSORING MILITARY ACTIVITY
	Air Force Rocket Propulsion Laboratory Edwards Air Force Base, California

13. ABSTRACT

(U) Subscale (100-lb) and fullscale (5000-lb) rocket thrust chambers of an advanced nonregeneratively cooled concept were designed, fabricated, and tested for durability at 500 psi chamber pressure, using N_2O_4/0.5 N_2H_4-0.5 UDMH propellants. The concept employs a silicon carbide-coated graphite thrust-chamber liner prestressed in compression by a refractory metal outer shell. The subscale units were successfully tested for continuous and intermittent firing durations exceeding 600 seconds. In the subscale tests, the inner SiC coatings were cracked through the nozzle region, but did not oxidize or erode. In both fullscale rocket thrust-chamber tests, the SiC coating fractured catastrophically during a 5-second test, leaving the graphite substrate unprotected. Test results and failure analyses indicate that a practical size/configuration limit was exceeded for this structural design concept in progressing from the 1.75-inch diameter chambers to the 6.0-inch diameter chambers. Since the silicon-carbide coating is highly efficient from the environmental resistance aspect, new design concepts should be developed to circumvent the critical size limitation. (U)

DD FORM 1 JAN 64 1473 0101-807-6800

UNCLASSIFIED
Security Classification

UNCLASSIFIED
Security Classification

14. KEY WORDS	LINK A		LINK B		LINK C	
	ROLE	WT	ROLE	WT	ROLE	WT
100 and 5000 lb Rocket Thrust Chamber Eval. Radiation - Heat Sink Cooled Prestressed Composite Wall Silicon-Carbide Coating N_2O_4/50-50 at P_c = 500 psia						

INSTRUCTIONS

1. ORIGINATING ACTIVITY: Enter the name and address of the contractor, subcontractor, grantee, Department of Defense activity or other organization *(corporate author)* issuing the report.

2a. REPORT SECURITY CLASSIFICATION: Enter the overall security classification of the report. Indicate whether "Restricted Data" is included. Marking is to be in accordance with appropriate security regulations.

2b. GROUP: Automatic downgrading is specified in DoD Directive 5200.10 and Armed Forces Industrial Manual. Enter the group number. Also, when applicable, show that optional markings have been used for Group 3 and Group 4 as authorized.

3. REPORT TITLE: Enter the complete report title in all capital letters. Titles in all cases should be unclassified. If a meaningful title cannot be selected without classification, show title classification in all capitals in parenthesis immediately following the title.

4. DESCRIPTIVE NOTES: If appropriate, enter the type of report, e.g., interim, progress, summary, annual, or final. Give the inclusive dates when a specific reporting period is covered.

5. AUTHOR(S): Enter the name(s) of author(s) as shown on or in the report. Enter last name, first name, middle initial. If military, show rank and branch of service. The name of the principal author is an absolute minimum requirement.

6. REPORT DATE: Enter the date of the report as day, month, year; or month, year. If more than one date appears on the report, use date of publication.

7a. TOTAL NUMBER OF PAGES: The total page count should follow normal pagination procedures, i.e., enter the number of pages containing information.

7b. NUMBER OF REFERENCES: Enter the total number of references cited in the report.

8a. CONTRACT OR GRANT NUMBER: If appropriate, enter the applicable number of the contract or grant under which the report was written.

8b, 8c, & 8d. PROJECT NUMBER: Enter the appropriate military department identification, such as project number, subproject number, system numbers, task number, etc.

9a. ORIGINATOR'S REPORT NUMBER(S): Enter the official report number by which the document will be identified and controlled by the originating activity. This number must be unique to this report.

9b. OTHER REPORT NUMBER(S): If the report has been assigned any other report numbers *(either by the originator or by the sponsor)*, also enter this number(s).

10. AVAILABILITY/LIMITATION NOTICES: Enter any limitations on further dissemination of the report, other than those imposed by security classification, using standard statements such as:

(1) "Qualified requesters may obtain copies of this report from DDC."

(2) "Foreign announcement and dissemination of this report by DDC is not authorized."

(3) "U. S. Government agencies may obtain copies of this report directly from DDC. Other qualified DDC users shall request through _____."

(4) "U. S. military agencies may obtain copies of this report directly from DDC. Other qualified users shall request through _____."

(5) "All distribution of this report is controlled. Qualified DDC users shall request through _____."

If the report has been furnished to the Office of Technical Services, Department of Commerce, for sale to the public, indicate this fact and enter the price, if known.

11. SUPPLEMENTARY NOTES: Use for additional explanatory notes.

12. SPONSORING MILITARY ACTIVITY: Enter the name of the departmental project office or laboratory sponsoring *(paying for)* the research and development. Include address.

13. ABSTRACT: Enter an abstract giving a brief and factual summary of the document indicative of the report, even though it may also appear elsewhere in the body of the technical report. If additional space is required, a continuation sheet shall be attached.

It is highly desirable that the abstract of classified reports be unclassified. Each paragraph of the abstract shall end with an indication of the military security classification of the information in the paragraph, represented as (TS), (S), (C), or (U).

There is no limitation on the length of the abstract. However, the suggested length is from 150 to 225 words.

14. KEY WORDS: Key words are technically meaningful terms or short phrases that characterize a report and may be used as index entries for cataloging the report. Key words must be selected so that no security classification is required. Identifiers, such as equipment model designation, trade name, military project code name, geographic location, may be used as key words but will be followed by an indication of technical context. The assignment of links, roles, and weights is optional.

UNCLASSIFIED
Security Classification